Development of Sustainable Lightweight Green Building Panels

Final Year Project

Submitted by

Fazal Hussain	311114
Shayan Ali khan	305069
Ameer Hamza	294681
Fazal Rehman	304573

BACHELOR'S IN CIVIL ENGINEERING

Session 2019-2023

Project Advisor:

Associate Prof. Dr. Rao Arsalan Khushnood

Co-Advisor:

Assistant Prof. Dr. Fawad Ahmed Najam

NUST Institute of Civil Engineering (NICE)

School of Civil and Environmental Engineering (SCEE)

National University of Sciences and Technology (NUST),

Islamabad, Pakistan

This to certify that the

Thesis Titled

“Development of Sustainable Lightweight Green Building Panels”

Submitted by

Fazal Hussain	311114
Shayan Ali khan	305069
Ameer Hamza	294681
Fazal Rehman	304573

has been accepted towards the requirements

for the undergraduate degree in

CIVIL ENGINEERING

_____

(Dr. Rao Arsalan Khushnood)

Associate Professor of Structural Engineering

Head of Department of Research

Department NUST Institute of Civil Engineering

School Civil and Environmental Engineering

Acknowledgements

In the name of Allah, the most Beneficent, the most Merciful, and peace and blessings upon Prophet Muhammad, His servant, and final messenger. We begin our acknowledgments by expressing our deepest gratitude to Allah Almighty for enabling us to complete our research project. Without His guidance and blessings, we could not have imagined accomplishing such an enormous task.

We would like to extend our sincere thanks and appreciation to our thesis supervisor, Dr. Rao Arsalan Khushnood, for his invaluable support, guidance, and encouragement throughout the research process. Your insightful comments, constructive criticism, and constant motivation have been a source of inspiration for us.

Our heartfelt thanks also go to our families and friends for their unwavering love, support, and encouragement throughout our academic journey. Their prayers and encouragement have been a constant source of motivation for us.

We also express our gratitude to the faculty members and staff of NUST Institute of Civil Engineering (NICE) at National University of Science and Technology (NUST) for providing us with the necessary resources and facilities for carrying out our research. The support and encouragement we received from our colleagues has been instrumental in shaping our ideas and improving the quality of our work.

We would also like to express our gratitude to the Military College of Engineering (MCE), Risalpur, for providing us with essential resources, including the electric furnace and other necessary equipment, for carrying out our research work. Without their support, it would have been challenging to complete this project successfully. The facilities and resources provided by MCE have been crucial in achieving our research objectives. We are grateful to MCE for their support and cooperation.

We would like to further extend our sincere appreciation to the staff of School of Chemical and Materials Engineering (SCME) and U.S.-Pakistan Center for Advanced Studies in Energy (USPCAS-E) at the National University of Sciences and Technology (NUST), for providing us with their advanced testing facilities such as XRD, SEM, TGA, XRF, Compression testing machine, Furnace, etc. These testing facilities were crucial in conducting various tests and analyses during our research work. The expertise and guidance provided by the staff at these facilities have been invaluable, and we could not have achieved the level of accuracy and precision without their support. We are extremely grateful to SCME and USPCAS-E at NUST for their assistance, which has been fundamental in the successful completion of our research project.

Lastly, we would like to acknowledge the valuable contributions of all the participants who participated in our research study. Without their cooperation and willingness to share their experiences and insights, this research would not have been possible.

Funding Acknowledgements

We would like to extend our sincere gratitude to the Pakistan Engineering Council (PEC) for their generous funding of our final year project, titled "Development of Sustainable Lightweight Green Building Panels." This project was conducted under the expert guidance of Dr. Rao Arsalan Khushnood in the Structural Engineering Lab at NUST and the Structural Dynamics Lab at the Military College of Engineering, Risalpur, NUST. The support provided by Dr. Rao Arsalan Khushnood and the financial assistance from PEC's Annual Award of Final Year Design Projects (FYDPs) were instrumental in the successful completion of our research endeavor.

Development of Sustainable lightweight Green Building Panels

Abstract

Nowadays, lightweight aggregate concrete is becoming more popular due to its versatile properties. It mainly helps to reduce the dead loads of the structure, which ultimately reduces design load requirements. The widespread use of lightweight aggregate concrete in Pakistan poses a significant challenge in identifying an optimized mix that meets the necessary requirements while keeping costs manageable. As the concrete matrix typically comprises 50 to 60% aggregate, we opted to replace the traditional natural aggregate with artificial lightweight expanded clay aggregate to improve the performance of the concrete. To achieve this, we selected five prominent and largely untapped clay fields in Pakistan. The selected clay fields include Nandipur, Multan, Mirpur, Sibbi, and DIK. After essential geotechnical characterization, the collected soil samples of chosen fields were chemically analyzed using X-ray diffraction and X-ray fluorescence tests, whereas thermal stability was assessed using thermogravimetric analysis. The characterized soil was used in the synthesis of ALECA through 120 different mixes recipes designed by varying pellet sizes, and the dose of admixed fly ash and kerosene oil. Nandipur clay turned out to be ideal for bloating, with a bloating index of 33.33% and a loose bulk density of 0.39 g/cm^3. To solve the problem of mix design for lightweight concrete, a Machine learning-based application was developed and tested on a dataset of 420 data points. The application reduced the need for time-consuming experimental trials and allowed for the selection of the three lightest mixes. The suitability of these mixes for non-structural panels was tested according to ASTM guidelines and they met all requirements specified by ASTM. Finally, a cost comparison study was conducted on a selected building using ALECA infill panels versus brick infill. The results showed that using ALECA infill panels reduced overall construction costs by 16% compared to a building constructed with brick infill. Furthermore, BIM-based modeling was performed to evaluate the heating and cooling load demands and environmental performance of the building. The results

revealed that the use of ALECA infill panels not only provided a cost-effective solution but also resulted in sustainable environmental performance.

TABLE OF CONTENT

LIST OF FIGURES

LIST OF TABLES

LIST OF ABBREVIATIONS:

LWA	Lightweight aggregate
ALECA	Artificial lightweight expanded clay aggregate
XRF	X-ray fluorescence
XRD	x-ray diffraction
TGA	Thermogravimetric analysis
LL	Liquid limit
PL	Plastic limit
PI	Plastic Index
SL	Shrinkage limit
W_{op}	Optimal water content
T_{max}	Maximum toughness
SEM	Scanning electron microscope
LOI	Loss on Ignition
BI	Bloating Index
S	Compressive strength
ρ_A	Particle density
PS	Pellet size
WA_{24}	Water absorption after 24 h immersion

LWA	Lightweight Concrete
BIM	Building Information Modeling
PBD	Performance Based Design

LWAC	Lightweight aggregate concrete
LWA	Lightweight aggregate
AI	Artificial Intelligence
ML	Machine Learning
SVM	Support vector machine
DT	Decision Tree
XGBoost	Extreme gradient boosting tree

GPR	Gaussian process of regression
ANN	Artificial neural network
R2	Coefficient of determination
RMSE	Root mean square error
MSE	Mean square error
MAE	Mean absolute error
SD	Standard derivation
R	Pearson correlation coefficient
c/c	Cement-to-cement ratio
s/c	Sand-to-cement ratio
w/c	Water-to-cement-ratio
LWA/c	Lightweight aggregate-to-cement ratio
FA/c	Fly ash-to-cement ratio
Normal Agg/c	Normal aggregate-to-cement ratio

Chapter 1

INTRODUCTION

1.1 General

Over the years, concrete technology has progressed significantly, with new advancements being made in materials science, structural engineering, and construction techniques. Today, modern concrete is made by mixing cement, water, and aggregates like sand and gravel. Reinforced concrete, which incorporates steel bars or fibers for added strength, is widely used in construction for its high strength, durability, and fire resistance. Despite its many benefits, conventional concrete also has some drawbacks, including its weight. The high density of traditional concrete makes it a poor choice for structures where weight is a concern, such as high-rise buildings or bridges. To address this issue, lightweight concrete was developed, which has a lower density and weight than traditional concrete.

The need for lightweight concrete arose from the limitations of conventional concrete. In many construction projects, the weight of the structure is a critical factor, especially in high-rise buildings or bridges, where the weight of the structure can affect the foundation and overall stability. By reducing the weight of the structure, builders can reduce the load on the foundation, resulting in cost savings and improved structural performance. The history of lightweight concrete can be traced back to the early 20th century when it was first used for insulation purposes. In the 1920s, the first lightweight concrete blocks were introduced, which were made from sawdust and cement. These blocks were used mainly for insulation, but they soon found use in load-bearing applications due to their lightweight and fire-resistant properties.

In the 1950s, a new type of lightweight concrete, known as cellular or aerated concrete, was developed. This type of concrete is made by adding air bubbles to the concrete mixture, resulting in a lower density material. Cellular concrete is widely used today in construction for its insulation properties, fire resistance, and lightweight. In the 1960s, lightweight aggregate concrete was introduced, which is made by replacing traditional aggregates like sand and gravel with lightweight materials like expanded clay or shale. This type of concrete has a lower density and weight than traditional concrete, making it ideal for use in high-rise buildings and bridges.

In recent years, advances in lightweight concrete technology have continued, with new materials and construction techniques being developed to further improve its properties. Today, lightweight concrete is widely used in construction for its many benefits, including improved structural performance, reduced weight, and cost savings. In the context of Pakistan, traditional brick construction is prevalent due to the abundance of locally available raw materials such as clay and

sand. However, the limitations of traditional brick construction such as poor thermal insulation, high material consumption, and inadequate seismic resistance have paved the way for alternative construction materials such as lightweight concrete.

In recent years, rapid urbanization and industrialization have led to a surge in construction activities in Pakistan. The construction industry has been growing at an unprecedented rate of 9% per annum, contributing significantly to the country's GDP. However, this rapid expansion has put a strain on the country's natural resources, resulting in a shortage of materials such as cement, steel, and aggregates. Lightweight concrete has significant applications in the context of Pakistan as infill panels for construction. The use of lightweight concrete infill panels can lead to reduced structural loads, increased thermal insulation, and improved seismic resistance. The implementation of lightweight concrete in construction projects can lead to cost savings, improved efficiency, and reduced environmental impact.

1.2 Problem Statement

The problem at hand is that Pakistan lacks a reserve of lightweight aggregate, which poses a challenge in the production of lightweight concrete. As a result, there is a need to develop locally sourced lightweight aggregates that are abundant and cost-effective. Additionally, there is a need to automate the mix design process for such concrete to improve its quality and efficiency. To ensure the concrete's structural integrity, a strut width formula needs to be developed to study its interaction with the structure. Furthermore, there is a need to investigate the environmental impact of concrete and its insulation properties to promote sustainability and energy efficiency. Addressing these challenges will pave the way for the production of lightweight concrete that is affordable, structurally sound, environmentally friendly, and has excellent insulation properties.

1.3 Research Objectives

The project aims to develop lightweight concrete panels using expanded clay aggregates made clay available in various regions of Pakistan. The lack of reserves of other lightweight aggregates and their high cost makes the use of locally available clay an ideal solution. The mix design of

lightweight concrete is currently manual, leading to inconsistencies and inefficiencies. Therefore, the project also aims to automate the mix design process using machine learning-based graphic user interface. Furthermore, to study the interaction of lightweight concrete panels with the structure, a strut width formula will be developed. The formula will enable the determination of the width of the concrete strut to be used for structural analysis, ensuring the safety of the structure. Finally, the environmental aspects of lightweight concrete, such as its insulation properties and life cycle analysis, will also be studied to ensure that the solution is environmentally sustainable.

1.4 Organization Report

This thesis consists of 9 well-structured chapters that aim to explore and analyze Lightweight Aggregate Concrete (LWA) comprehensively. Chapter 1 serves as an introduction to the topic, highlighting the significance of LWA, and outlining the research objectives. The Chapter 2 provides an overview of the basic concepts related to LWA and a review of the relevant literature. This chapter sets the foundation for the research methodology, which is discussed in detail in the third chapter. The methodology adopted for the research is thoroughly explained in Chapter 3, which helps readers understand the research process in-depth. Chapter 4 delves into the first research objective, while the Chapters 5, 6, 7 & 8 discuss the subsequent research objectives. The conclusions derived from the research findings are presented in Chapter 9, along with recommendations for future studies. This chapter summarizes the key points of the thesis and provides valuable insights into the field of LWA.

Chapter 2

LITERATURE REVIEW

2.1 Lightweight Concrete for Infill Panels: The Conceptual Basis

Lightweight concrete is widely regarded as the best material for making lightweight infill walls due to its availability and durability as compared to other products. The evolution of lightweight concrete dates back to the early 1900s when the need for materials that could provide enhanced performance and lower weight than traditional concrete became apparent. The emergence of lightweight concrete can be traced back to the use of lightweight aggregates, such as expanded clay, shale, and slate, that are processed to reduce their weight while maintaining their strength and durability.

The motivation behind the use of lightweight concrete was driven by the need to reduce the dead load of concrete structures while maintaining their mechanical properties. Two types of lightweight concrete emerged: lightweight aggregate concrete and lightweight matrix concrete. Lightweight aggregate concrete is composed of lightweight aggregates that mixed with Portland cement and water to form a hardened material. On the other hand, lightweight matrix concrete is a material that consists of a low-density matrix that is reinforced with fibers or aggregates to provide enhanced strength.

Various types of lightweight aggregates have been developed over the years, including expanded clay, shale, slate, perlite, and vermiculite. These aggregates have different properties, such as particle size, shape, density, and strength, that make them suitable for specific applications. Among these aggregates, expanded clay aggregate (ECA) has gained popularity due to its excellent thermal insulation, low density, and good mechanical properties, which utilizes ECA as the primary aggregate material, has proven to be superior to other lightweight aggregates due to its high porosity, low thermal conductivity, and excellent mechanical properties. It has found extensive use in building construction, road construction, and bridge construction due to its outstanding properties. Therefore, the combination of lightweight concrete with expanded clay aggregate has become a popular choice for the construction of lightweight infill walls due to its durability, availability, and versatility.

2.2 Morphology and texture of Expanded clay aggregate

Expanded clay aggregate (ECA) is an ideal material for making lightweight concrete due to its unique properties. ECA is a lightweight, porous ceramic material that is produced by expanding clay in a rotary kiln. The porous nature of ECA makes it an ideal material for lightweight concrete,

as it allows the mixture to achieve a lower density while maintaining the required strength and durability. ECA's high porosity results in lower thermal conductivity, providing excellent thermal insulation properties. Additionally, the porous structure allows the material to absorb and retain moisture, providing an excellent humidity control solution. Furthermore, ECA's spherical shape and smooth surface texture result in better workability of the concrete mixture and lower water absorption, which leads to better bonding with cement paste.

2.3 Bloating mechanism

The bloating mechanism of expanded clay aggregate (ECA) is based on the release of gases during the firing process in a rotary kiln. Clay particles contain adsorbed water and chemically bound water, which, upon heating, start to evaporate, generating a large number of gas bubbles inside the particle. As the temperature increases, the gases are released and expand, causing the clay particle to bloat and resulting in a significant increase in volume. The high temperature also causes the clay particles to fuse together, creating a strong, lightweight, and porous structure. This bloating mechanism results in ECA's unique properties, such as high porosity, low thermal conductivity, and excellent mechanical strength.

2.4 Strength and density requirement

Concrete made with lightweight expanded clay aggregate (ECA) is an excellent choice for applications that require both lightweight construction and adequate compressive strength. The porosity of the ECA provides the concrete with a lower density while still maintaining the required mechanical properties. ECA concrete has a density range of 800 to 1,200 kg/m^3, which is much lower than traditional concrete, making it a preferred choice for lightweight construction. Moreover, the spherical shape and smooth surface texture of ECA provide better workability of the concrete mixture, resulting in an improved bond with cement paste. The ECA structure provides sufficient compressive strength of up to 14 MPa, to the concrete, making it suitable for a wide range of applications in the construction industry, including in the production of prefabricated elements, lightweight slabs, and lightweight infill panels.

2.5 Literature review

Ayati et al. [1] asserted that naturally available clays are promising raw materials for manufacturing artificial lightweight aggregates due to their abundant availability in urban areas. The utilization of clays and clayey-rich wastes for producing lightweight aggregates and their bloating mechanism have been extensively examined by Loutou and Hajjaji, Anan and Abd El-Wahed, and Kanari et al. [2-3]. Furthermore, studies suggest that the plasticity of clay plays a crucial role in facilitating palletizing, whereas the particle size of clay governs the extent of bloating and expansion of aggregates [4-5]. Riley made a significant contribution to the field by proposing that the decomposition of some organic and mineral species, such as dolomite, phyllosilicate, chlorides, or ferrous minerals, results in a porous internal structure of the aggregate [6]. In addition, Lee et al. [7] investigated the bloating mechanism of artificial lightweight aggregates by modifying their surface with coal ash, while Bernhardt et al. [8] studied the impact of different additives, including Na_2CO_3, SiO_2, Fe_2O_3, and Fe, on the production of artificial lightweight aggregates.

References

[1] A. V. Rodrigues and S. R. Braganç, "An evaluation of the increased expansion of clayaggregates fired at 1300°C to maximize lightnessfor non-structural concrete," *Boletin de la Sociedad Espanola de Ceramica y Vidrio*, 2021, doi: 10.1016/j.bsecv.2021.11.003.

[2] N. Kanari, F. Diot, C. Gauthier, and J. Yvon, "Use of residual materials for synthesis of lightweight granulates by thermal treatment process," *Appl Clay Sci*, vol. 123, pp. 259–271, Apr. 2016, doi: 10.1016/j.clay.2015.12.027.

[3] M. Loutou and M. Hajjaji, "Clayey wastes-based lightweight aggregates: Heating transformations and physical/mechanical properties," *Appl Clay Sci*, vol. 150, pp. 56–62, Dec. 2017, doi: 10.1016/j.clay.2017.09.011.

[4] "Standard Test Method for Shrinkage Factors of Soils by the Mercury Method 1." [Online]. Available: www.astm.org,

[5] A. International and files indexed by mero, "Standard Test Methods for Liquid Limit, Plastic Limit, and Plasticity Index of Soils 1."

[6] C. M. Riley, "Relation of Chemical Properties to the Bloating of Clays."

[7] K. G. Lee and K. G. Lee, "Bloating Mechanism for Artificial Light Weight Aggregate of Surface Modification with Coal ash," *Journal of the Korean Ceramic Society*, vol. 52, no. 2, p. 159, Mar. 2015, doi: 10.4191/KCERS.2015.52.2.159.

[8] M. Bernhardt, H. Justnes, H. Tellesbø, and K. Wiik, "The effect of additives on the properties of lightweight aggregates produced from clay," *Cem Concr Compos*, vol. 53, pp. 233–238, Oct. 2014, doi: 10.1016/J.CEMCONCOMP.2014.07.005.

Chapter 3

METHODOLOGY

The methodology used in this research involved several steps to develop a lightweight concrete panel using locally available materials, with the aim of optimizing its cost while ensuring good performance. To achieve the research objectives, the work was divided into five distinct modules, each with its own focus and goals.

1) **Module I** focused on developing artificial lightweight expanded clay aggregates (ALECA) using Pakistani clays. Five zones were selected for clay sourcing, and after testing 400 mixes with varying fly ash, kerosene oil percentages and temperature ranges, the 120 best mixes for both structural and non-structural concrete were proposed.
2) **Module II** involved the development of a machine learning-based application for optimized mix design of lightweight aggregate concrete. This application helped to determine the most appropriate mix design for the concrete panel based on the properties of the locally available materials.
3) **Module III** focused on the development of lightweight concrete panels using artificial expanded clay aggregates. The mechanical, physical, and thermal properties of the panels were measured and compared with existing lightweight concrete panels. The results showed that the developed panels met the desired performance criteria and were cost-effective.
4) **Module IV** involved a case study of a 23-story building to evaluate the cost comparison and performance of the ALECA (Artificial Lightweight Expanded Clay Aggregate) infill lightweight concrete panels compared to traditional bricks. The study found that constructing the building using ALECA-based lightweight concrete panels resulted in a 16% reduction in overall building costs compared to a building constructed with brick infill. The cost savings were mainly due to the reduced weight of the ALECA-based panels resulted in lower design demands which ultimately reduces 13 – 15% reinforcement demands, and handling costs compared to traditional bricks.
5) **Module V**, finally in this module thermal performance and CO_2 emissions were calculated using Building Information Modeling (BIM). The results were compared with other commonly used building materials, including EPS panels and AAC blocks, as well as traditional bricks. The findings indicated that the developed lightweight concrete panel had lower CO2 emissions and better thermal performance than other materials.

Through these five modules, the research team successfully developed a cost-effective and high-performing lightweight concrete panel that could be produced using locally available materials. The systematic approach provided by the methodology allowed for effective collaboration and efficient progress towards the research objectives.

Chapter 4

MODULE-1

Study of physical and mechanical behavior of artificial lightweight aggregate made of Pakistani clays

Abstract:

This study aims to unravel the potential of Pakistan in the domain of artificial lightweight expanded clay aggregates (ALECA) and investigate the influence of pellets size, firing temperature, and admixture doses on the mechanical properties of ALECA. The five prominent and unfathomed clay fields in Pakistan were chosen. The selected clay fields include Nandipur, Multan, Mirpur, Sibbi, and DIK. After essential geotechnical characterization, the collected soil samples of chosen fields were chemically analyzed using X-ray diffraction and X-ray fluorescence tests, whereas thermal stability was assessed using thermogravimetric analysis. The characterized soil was used in the synthesis of ALECA through 120 different mixes recipes designed by varying pellet sizes, and the dose of admixed fly ash and kerosene oil. The addition of fly ash and kerosene allowed the development of a well-distributed-porous core surrounded by a very thin shell. Nandipur clay turned out to be ideal for bloating, with a bloating index of 33.33% and a loose bulk density of 0.39 g/cm^3. These lightweight aggregates will not only help preserve natural mountain reserves but also significantly impact the lifecycle costing of structures.

4.1 Introduction

The aggregate industry is the largest provider of raw materials for building construction and infrastructures, being also fundamental in other industrial sectors. The annual requirements for aggregates in the global building market have reached 55 billion tons in 2020. The amount would double in the next decade if the consumption rates remained [1]. The situation results in a shortage of natural aggregates which will be an inevitable problem for building construction in the near future. Also, the growing global interest in the sustainable economy of raw materials and the savings in transport costs, associated with the reduction of the weight of materials, has stimulated attention to the use of lightweight concrete, which should be produced preferably closer to the consumption centers [2]. Aggregate has been an urgent issue in the background of large-scale concrete forest construction. The selection of construction materials with a low carbon footprint is one of the most valuable strategies for achieving sustainable construction. The utilization of suitable construction materials may reduce CO_2 emissions by up to 30% [3].

The 17 SDGs (sustainable development goals) proposed by G-20 countries and the 2030 agenda envisioned by the UN emphasize innovation in infrastructure and a shift towards greener construction. Since the whole world is shifting to sustainable and readily available raw materials, a new horizon has opened for lightweight aggregates (LWA). The porous structure of LWA not only enhances their acoustic and thermal insulation but also results in load reduction of the building. Reduction in dead load minimizes the transport and handling costs of precast units along with construction costs and sizes of cross sections, i.e., foundations [4], [5]. These financial and operational advantages validate diverse and countless applications of LWA's in the construction sector. LWAs have been used to construct precast bridge girders, roofing, flooring, filter material in the water treatment process, insulating material under salt tank foundations in solar thermal energy plants, skyscrapers, offshore structures, concrete reinforced vessel buildings, etc. [4]–[6].

Romans were the first to use lightweight aggregates such as pumice, scoria, volcanic cinder, and vesiculated lava with gray lime as cementing material, commonly known as Roman cement, to form the first lightweight concrete. Apart from these natural lightweight aggregates, various industrial outlets such as blast furnace slag, coal ashes, and numerous other residues were also used to synthesize artificial lightweight aggregates [7]. Waste tire rubber, bottom ash, crushed glass, and other recycled lightweight aggregates are alternatives [8], [9] [10].

The biggest concern related to the feasibility of lightweight aggregates as a replacement of conventional aggregates is the availability of the raw material for manufacturing LWA. The transport cost associated with transferring these raw materials to consumption centers was also an issue. The advent of lightweight expanded clay aggregates has addressed this issue as well. The attention drawn by artificial lightweight expanded clay aggregate (ALECA) is all due to the abundance of clay worldwide and the possibility of easily setting up a manufacturing plant [11]. The synthesis of ALECA for the first-time dates back to 1917, Kansas, Missouri, under the patent name of Heydites since Heyde made them [5]. The ALECA based products, such as concrete blocks and slabs, are extremely light, highly fire resistant, good acoustic and thermal insulators, and non-decomposable when exposed to acidic or alkaline substances. ALECA has an edge over conventional aggregates since they can save up to 10 to 15% on steel and 50% on heating and cooling expenses [4]. The inert character, high porosity, satisfactory mechanical strength, and low density of ALECA make it the future aggregate.

Ayati et al. [12] believed that naturally available clays have the highest potential to be used as raw materials for artificial lightweight aggregates since they are abundantly available near citified areas. A detailed study about the use of clays and clayey-rich wastes in making lightweight aggregates and their bloating mechanism has been performed by Loutou and Hajjaji**,** Anan and Abd El-Wahed and Kanari et al. [13]–[15]. Furthermore, studies also propose that the plasticity of clay is the key feature that governs the ease in palletizing, and particle size of clay, on the other hand, governs the extent of bloating and expansion of aggregates [16], [17]. A colossal contribution has been made by Riley and the processes he indicated sixty years earlier still govern the theory that explains bloating [18]. He proposed that the decomposition of some organic and mineral species such as dolomite, phyllosilicate, chlorides or ferrous minerals, and others, results in a porous internal structure of aggregate. Furthermore, Lee et al. [19] studied the bloating mechanism for artificial lightweight aggregate of surface modification with coal ash. Bernhardt et al. [20] experimented the effect of the different additives including Na_2CO_3, SiO_2, Fe_2O_3, and Fe with various percentages on artificial lightweight aggregate.

Commercially, ALECA is manufactured by sintering clay in a rotary kiln at a temperature range of 900 - 1300ºC [21]. The kiln is further divided into three distinct temperature zones. The preheating zone is characterized by losing 80% of gases within 3 minutes, whereas the temperature remains below 1175ºC. The next one is the transition zone which starts at 1175ºC, and finally, the bloating zone, where significant volumetric expansion causes the aggregates to swell 5, 6 folds. The temperature in this phase hikes up to 1300ºC. Other than bloating temperature, the key determinants which impact bloating are the mineral composition of clays, amount of water added to clay, type of kiln, and additives utilized. Still, a significant amount of research is going on to add various additives to make ALECA as light as possible with sufficient strength [6], [17], [22]**.**

Pakistan’s construction industry accounts for 2.5% percent of its GDP and provides employment to nearly 7% of Pakistanis, which is expected to increase [23]. As mentioned above, most of the used aggregate comes from the country's mountain reserves. The aggregate plants nibble away mountains chunk by chunk, and this seems to be an alarming situation for an already at-risk country like Pakistan. More importantly, the special health risk of dusk exposure for laborers is also associated with aggregate plants [24]. The aggregate crushing plants also contribute significantly to worsening air, and noise pollution's already deteriorating condition [24]. Due to all these reasons

crushed plants across Pakistan are facing backlash, and the operational plants are unable to meet the country's needs. Therefore, it is pertinent that the diverse variety of clay deposits found in Pakistan must be commercialized in terms of ALECA so that the mountain reserves of the country are saved, and the transport cost associated are reduced.

This study aims to unravel the potential of Pakistan to launch ALECA as an alternative to conventional aggregates. After the 2005 earthquake in Pakistan, people's interest in reinforced concrete construction surged tremendously. Increased RC structures manifest increased demand for natural aggregates, which depletes natural mountain reserves [25]. Therefore, this study suggests an integrated green technology framework to revolutionize the construction industry by introducing locally made and highly sustainable aggregates. Since Pakistan's geography is a blend of mountains, plateaus, deserts, and beaches, a variety of clays are spread throughout Pakistan [26]**.** Firstly, the noteworthy clay deposits of Pakistan are identified and classified according to standards. Secondly, their elemental composition and crystalline structures are also studied with the help of XRF and XRD, respectively. The thermogravimetric analysis (TGA) helped us identify the fraction of volatile components and the thermal stability of clays. Finally, 120 recipes with varying proportions of kerosene and fly ash with clay were bloated at 1100 – 1300 ^{o}C and analyzed. After bloating, the crushing strength, water absorption, loss on ignition, bloating index, and density were analyzed. The ultimate goal of this study is to determine the most bloatable clay and its recipe in order to create readily available, lightweight aggregates for structural and non-structural uses. Additionally, the clays' individual properties as well as the stated post-bloating findings can be valuable in a variety of construction and research projects.

4.2. Materials and Methodology

4.2.1 Clay sample

A detailed study was carried out to find the clay deposits in Pakistan. Five areas were investigated in this study where expanded clay aggregates can be manufactured. To analyze the bloating mechanism of expanded clay aggregates, different samples were collected from five distinct clay fields in Pakistan **Fig. 1**. The clay samples used in this study were collected from Nandipur, Multan, DIK, Mirpur (Azad Jammu and Kashmir), and Sibbi. To extract the pure clay without organic matter or other impurities, the samples were collected from 3 to 4ft in depth [27].

Fig. 1. Map of Pakistan showing the study locations.

4.2.2 Geotechnical investigation

It is important to know the basic geotechnical properties before making the expanded clay aggregates to have an idea of how much water content should be added and the shrinkage potential of that soil [16], [28]. The amount of water at which soil behaves as a liquid material is known as the liquid limit. The plastic limit is the amount of water content in which soil shifts its behavior from solid to semi-solid. Ellipsoidal-sized soil mass rolling test was performed to find the plastic limit. The liquid limit (LL), plastic limit (PL), and plastic index (PI) of the clays were found, which were used in this study according to ASTM D-4318 [16]. The clays' shrinkage limit (SL) was found according to ASTM D-427 [17]. The moisture content at which no further volume changes occur with further reduction in moisture content is known as the shrinkage limit.

The theoretical optimal moisture content (W_{op}, %) was evaluated using the relationship PL x 1.234 to achieve the best workability of clay for molding clay pellets. Manuel Moreno-Maroto and Jacinto Alonso-Azcárate have developed an equation to find the maximum toughness T_{max} (KJ/m^3) that clay offers with PI and LL [22]. Casagrande (1932) studied the relationship of the plasticity index to the liquid limit of a wide range of natural soils and proposed a relationship. Using the relationship of LL and PI proposed by Casagrande, we have determined the texture of clays. The properties of clays in this study are presented in **Table 1.**

$$T_{max} = [(PI/LL)-0.3397]/0.0077 \quad (1)$$

$$PI=LL - PL \quad (2)$$

$$SL = \left(\frac{m_1 - m_2}{m_2} \right)(100) - \left[\frac{(V_i - V_f)\rho_w}{m_2} \right](100) \quad (3)$$

Table. 1

LL = Liquid limit, PL = Plastic limit, PI = Plastic index, T_{max} = Maximum toughness, SL = Shrinkage limit

W_{op} = Optimum water content.

Clay name	**LL (%)**	**PL (%)**	**PI (%)**	**PI/LL**	**SL (%)**	**T_{max} (kJ/m^3)**	**W_{op} (%)**	**Texture**
Nandipur	48.6	23.90	24.70	0.51	8.19	21.9	29.5	Highly plastic clay
Multan	34	19.79	14.21	0.42	17.94	10.2	24.4	Medium plastic clay
DIK	36	18.08	17.92	0.49	24.37	20.5	22.3	Medium plastic clay
Mirpur	27	14.28	12.71	0.47	16.22	17.0	17.6	low plastic clay
Sibbi	40	15.43	24.57	0.61	8.95	35.6	19.0	Low Plastic clay

4.2.3 Lightweight aggregate manufacturing

There are two main stages in the formation of artificial lightweight expanded clay aggregate (ALECA) i.e., granular formation and sintering. In the granular formation stage, clay is first converted into fine particles, then optimum water content is added so that clay comes in a plastic state. When clay is in plastic form, it is molded by hand into small granules with desired aggregate sizes. Once the moist aggregate has been air-dried for 24 hours, it is placed at a temperature ranging between 1100 to 1300 ^oC after drying. **Fig. 2.** illustrates the typical steps involved in the production of expanded clay aggregate.

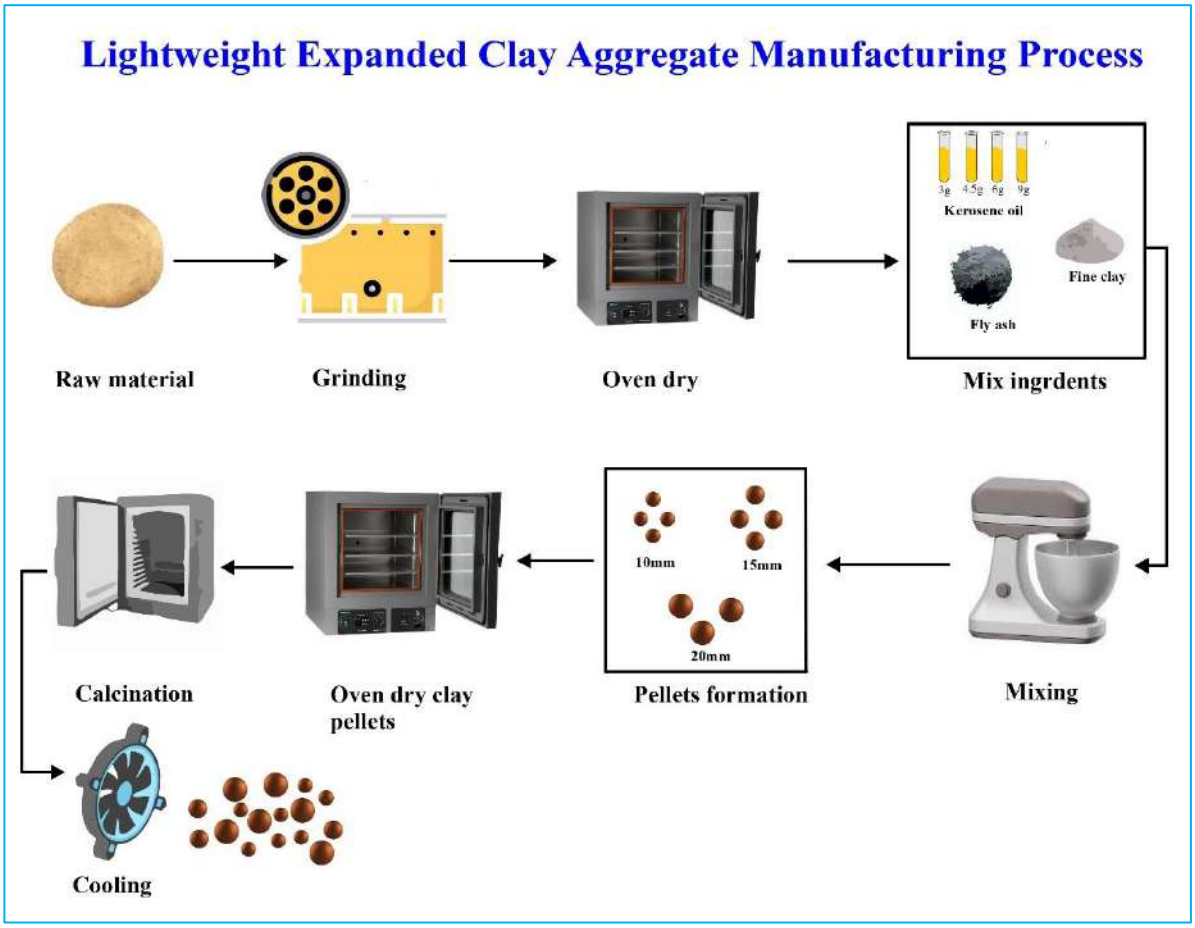

Fig. 2. The manufacturing process of artificial lightweight expanded clay aggregate.

4.2.3.1 Clay grinding

The clay grain size directly affects the bloating of expanded clay aggregate. A. Ozguven et al. [5] reported that decreasing the size of clay grain size positively affects aggregate expansion. The more clay fines result in more gases escaping from pores and increasing aggregate expansion. Before grinding the clay samples, the first oven dries the clay samples for 24 hrs at 110^{o}C. To make the clay fine grinding is done and sieved through 200 sieves so that the particle distribution of clays remains uniform **Fig. 3.**

Mirpur clay Nandipur clay Multani clay DIK clay Sibbi clay

Fig. 3. Types of clay studied in this research.

4.2.3.2 Mix proportion with varying percentages of fly ash

In Pakistan 21.65 million tons fly ash per year is produced which is a huge amount. Fly ash cannot be disposed-off in the open field because it pollutes the air, soil, and ground water [29]. Considering the massive production and associated disposal challenges of fly ash in Pakistan, we have decided to utilize it in production of lightweight aggregate which can further benefits by decreasing the density due to its low specific gravity. For this research, fly ash was collected from power coal-fired electric generating plant of Kohinoor Textile Mill, Rawalpindi. To prepare economical lightweight aggregate, fly ash was used by a power coal-fired electric generating plant. To achieve lightweight expanded clay aggregate, we have prepared 120 mix recipes having representations of eight from each selected clay by varying the percentage of fly ash by 0%, 5%, 10%, and 15% by the weight of clay.

4.2.3.3 Molding of pellets

The expansion of aggregate increases with an increase in aggregate size [30]. If the aggregate density requirement is low, select a suitable pellet size closer to the optimum point [31]. Because appropriate heat cannot be delivered to the core of the aggregate if the aggregate is too large, there will be insufficient expansion, and the weight of the pellet will drop [5]. Samples from five distinct fields with the same size distribution were prepared for this study in three different pellet sizes. To prepare pellets, we firstly prepared clay in the plastic state by adding the water content between the plastic and liquid limit. The pellets were made by hand in three sizes, 10mm, 15mm, and 20mm. After several trials, we selected the optimum pellet size of 10mm, 15mm, and 20mm. The pellets were shaped by hand and kept these pellets in the oven at 110^{o}C for 48hrs until the weight became

constant. When aggregate weight becomes constant, the diameter and weight of aggregates were measured.

4.2.3.4 Bloating Agent

Typical lightweight aggregate is formed by the black coring phenomenon caused by the reduction of Fe_2O_3 [32]. Kerosene oil was used as a bloating agent to achieve the lightweight aggregate. During the burning process, kerosene oil acts as fuel, which helps the internal gases escape easily by reducing the partial pressure of oxygen inside the aggregate and expanding internal pores, which helps the gases escape outside the aggregate core. During the burning process of aggregates following reactions take place [21]:

$$\mathbf{3Fe_2O_3 \longrightarrow 2Fe_3O_4 + 0.5O_2}$$

$$\mathbf{Fe_3O_4 \longrightarrow 3FeO + 0.5O_2}$$

Increasing the percentage of kerosene density, the strength of aggregates decreases due to increases in porosity. On exceeding the threshold of 6% kerosene oil by weight of clay, the bursting of aggregate occurs [33]. The selected percentage of kerosene oil tested in this work is 2%, 3%, 4%, and 6% by weight of clay. To see the microstructure of aggregates, we have used Scanning Electron Microscope (SEM) model JSM-6490A, having a magnification from 5x to 300000x. Fig. 6 pertains to Nandipur clay pellet with 0% (a), 3% (b) and 6% (c) addition of kerosene oil. Five different magnifications scales have been selected to visualize the internal porous structure of aggregate on increasing dose of kerosene oil. Their scanning electron microscopic images are shown in **Fig. 5**, which shows that as the percentage of kerosene increases, the porosity increases due to the expansion of pellets.

4.2.3.5 Bloating Mechanism

Bloating mechanism of expanded clay aggregate consists of three stages a) Preheating zone, b) Intermediate zone, and c) Bloating zone [34]. During the burning process of aggregates, an increase in the temperature cause softening of clay pellets known as sintering. A rise in temperature during the aggregate burning process causes clay pellets to soften and consequently the clay particles come closer, this process is also known as sintering.[35]. The gas pressure inside the pores increases as the temperature increases; due to this, gases rapidly escape, increasing the pores' size

and distribution [36]. The increase in temperature leads to a reduction in aggregate density and an increase in bloating potential. The pellets were placed in the Muffle Furnace and were bloated at different temperature rates, and after conducting several trials, an optimum temperature rate of 20 ^{o}C/min was found. After modeling pellets, the clay pellets were air dried and then fired at a temperature of 1100 to 1300 ^{o}C, and finally allowed to cool as shown in **Fig.4.** The temperature at which the material must be heated to create lightweight aggregates is an additional factor to consider because greater temperatures result in higher energy, financial, and environmental expenses. Generally, the firing temperatures range between 1100 ^{o}C and 1300 ^{o}C. The factor which controls the bloating temperature of clay aggregate is ratio of $SiO_2/\sum$ Flux. The clay which has higher ratio of $SiO_2/\sum$ Flux needs more temperature for bloating as compared to clay which has lower ratio.

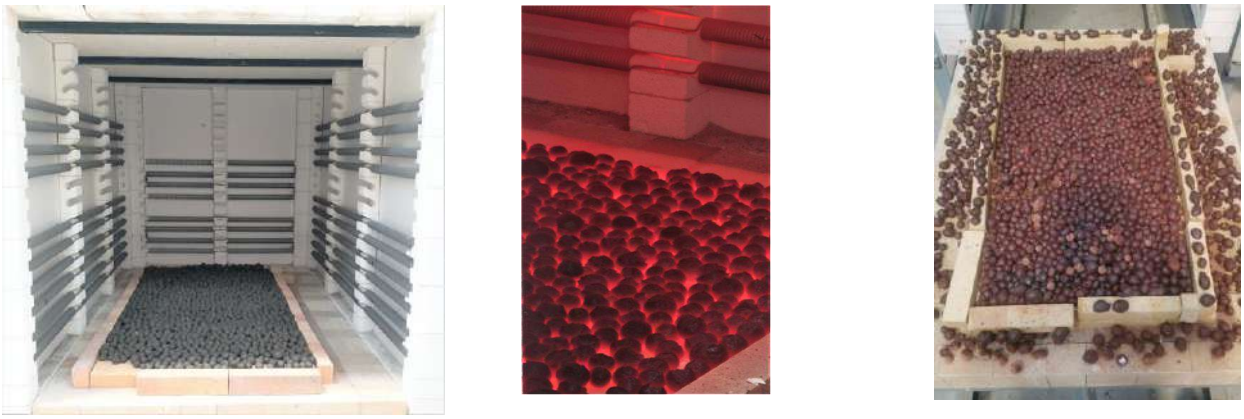

Air drying Calcination Cooling of pellets

Fig. 4. Formation of artificial lightweight expended clay aggregate.

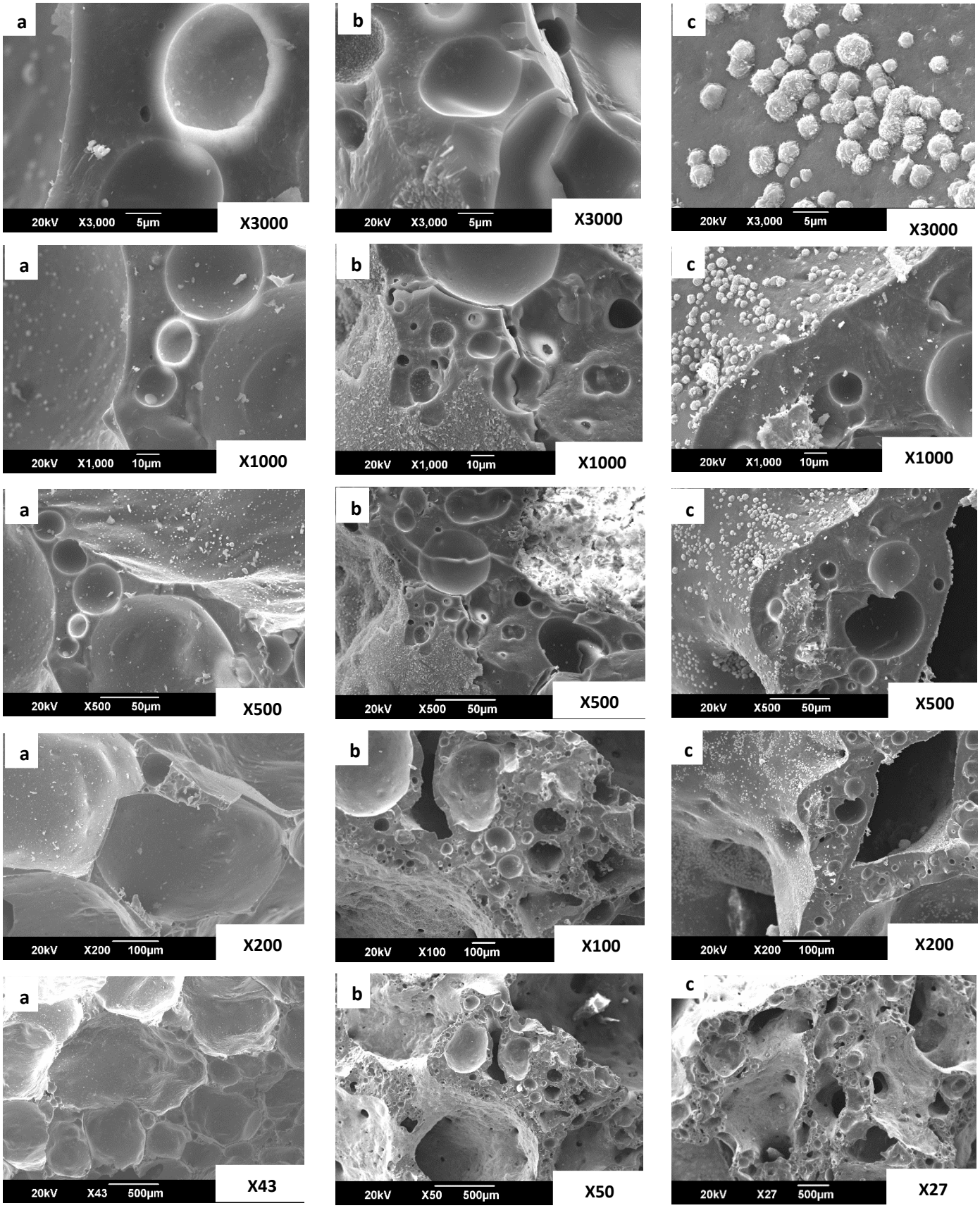

Fig. 5. a) Nandipur pellets with 0% kerosene **b)** Nandipur pellets with 3% kerosene **c)** Nandipur pellets with 6% kerosene

4.2.4 Structure of expanded clay aggregate

The schematic structure of the artificial expanded clay aggregate is shown in **Fig. 6.** An external non-porous dark brown surface surrounds the expanded clay aggregate, and the internal structure is porous. A suitable heating rate is required to achieve the uniform porous structure of aggregate. As the temperature increases, the aggregate phase changes from solid to liquid phase due to the excessive gas generated inside the aggregate, increasing total porosity and producing a continuous porous structure [37]. The heating rate also affects the microstructure of expanded clay aggregates. If the heating rate is slow, no sufficient aggregate bloating will occur. In addition, if cooling is fast, micro-cracks may form between the shell and core of lightweight aggregate, which ultimately reduces aggregate strength [12].

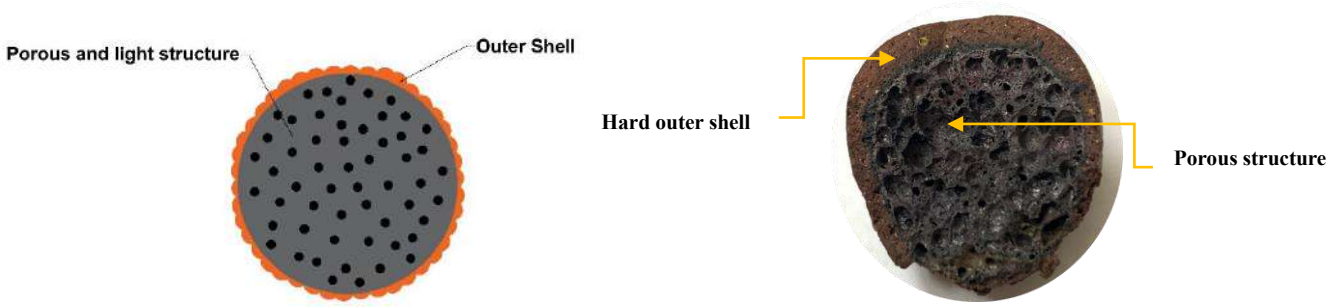

Fig. 6. a) Ideal porous structure of ALECA b) Typical porous structure of ALECA.

4.2.5 Sintered aggregate characterization

It is important to know the crushing strength of individual lightweight expanded clay aggregates for commercial use. According to Gonzalez-Corrochano et al. [38] structural lightweight aggregate material can be used if a single aggregate strength is greater than 3MPa because a commercially available aggregate's single aggregate crushing strength is 3 MPa. The single aggregate crushing strength (S, MPa) was determined in a series of 25 samples from each variety using a Nannetti FM 96 press [39]. To find the strength of a single aggregate, the following formula has been used where F (N) is failure load, and D (mm) is the diameter of a single aggregate [40], [41].

$$S = (2.8 \times F) / (\pi \times D^2) \quad (4)$$

The weight is measured before and after burning, and the difference between the weight loss measured before and after firing is shown in the percentage of loss on ignition (LOI). The procedure followed before heating the aggregate in the furnace until the end of the burning process determines the value of bloating index (BI). The molded aggregates were dried at 110ºC in the oven until the weight and diameter became constant [21]. To know the percentage of loss on ignition (LOI) and bloating index (BI) of expanded clay aggregates, twenty-five granules were used from each type of mix [42].

$$LOI = (w_i - w_f) / w_i \quad (5)$$

$$BI = [(d_2 - d_1)/d_1] \times 100 \quad (6)$$

4.3. Results and discussion

4.3.1 Characterization of raw materials

4.3.1.1 Chemical composition

The mineralogy of collected clay samples was studied by X-ray diffraction (XRD). The XRD patterns of the collected samples from the field are shown in **Fig. 7,** and the results obtained from x-ray diffraction are seen in **Table 2.** The XRD analysis aims to find which types of minerals exist in the clay and check which mineral is dominant. A non-destructive analytical technique used to identify the elemental composition of materials is called X-ray fluorescence (XRF). The XRF of clay samples was found to check which oxides dominate in clay and significantly influence the bloating mechanism. The XRF results of collected samples are seen in **Table 3**.

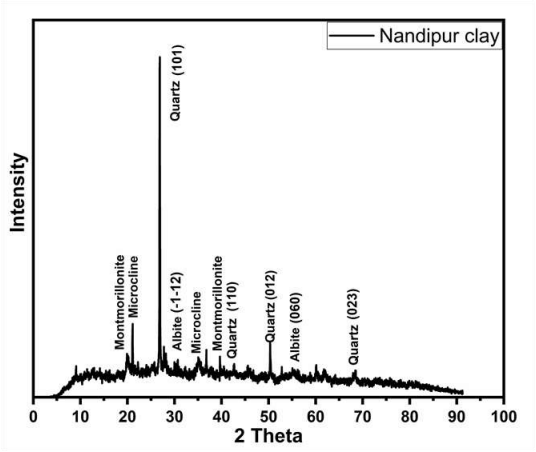

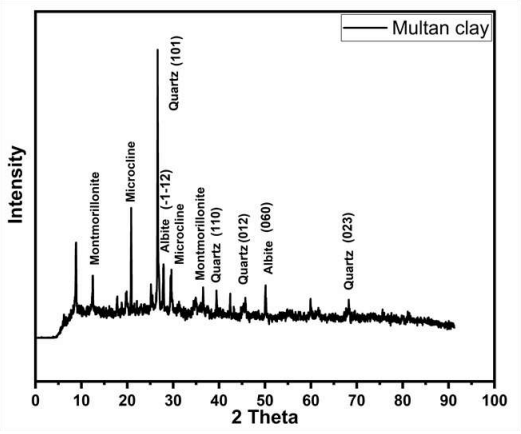

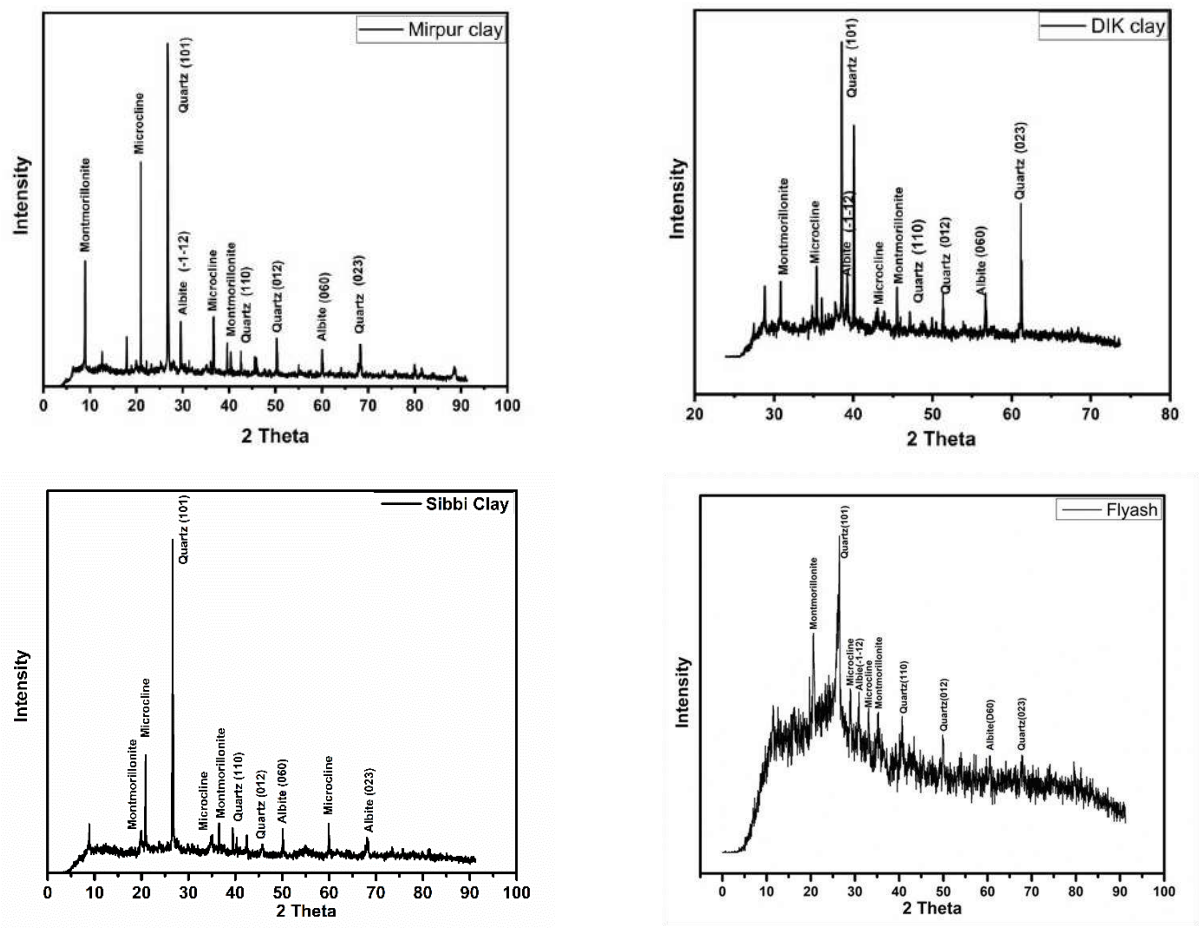

Fig. 7. X-ray diffraction results of clays and fly ash used in this study.

Table 2

Clays under study	Minerals
Multan	Quartz (101) or Rose Quartz, Montmorillonite ($Al_2H_2O_{12}Si_4$), Microcline or feldspar, Albite (-1-12) or pigeon stone, Quartz (110), Albite (060), Quartz (023), Quartz(012)
Nandipur	Quartz (101) or Rose Quartz, Montmorillonite, Microcline or feldspar, Albite (-1-12), Quartz (110) or pigeon stone, Albite (060), Quartz (023), Quartz (012)
Sibbi	Quartz (101) or Rose Quartz, Montmorillonite, Microcline or feldspar, Albite (-1-12), Quartz (110) or pigeon stone, Albite (060), Quartz (023), Quartz (012)
DIK	Quartz (101) or Rose Quartz, Montmorillonite, Microcline or feldspar, Albite (-1-12), Quartz (110) or pigeon stone, Albite (060), Quartz (023), Quartz (012)
Mirpur	Quartz (101) or Rose Quartz, Montmorillonite, Microcline or feldspar, Albite (-1-12), Quartz (110) or pigeon stone, Albite (060), Quartz (023), Quartz (012)

Table. 3

Investigation of chemical composition of samples using XRF, (oxides, %)

[a]Fluxing oxides

Sample name	Chemical composition									
	SiO_2	**Al_20_3**	**Fe_2O_3+FeO[a]**	**Na_2O[a]**	**K_2O[a]**	**MgO[a]**	**CaO[a]**	**TiO_2**	**SO_3**	**SiO_2/∑ Flux**
Nandipur	58.57	17.69	6.90	0.56	3.04	2.88	1.32	0.81	0.00	3.98
Multan	53.57	16.58	6.95	1.14	3.49	3.62	4.81	0.76	0.13	2.68
Mirpur	55.32	18.70	5.91	0.48	2.79	2.61	4.88	0.68	0.15	3.32
DIK	53.44	16.89	6.16	1.40	2.51	3.31	6.08	0.74	0.05	2.75
Sibbi	58.67	18.69	7.29	0.11	2.75	2.09	0.95	0.98	0.00	4.45
Fly ash	51.53	22.43	8.84	0.23	0.39	3.18	4.84	1.62	2.75	2.95

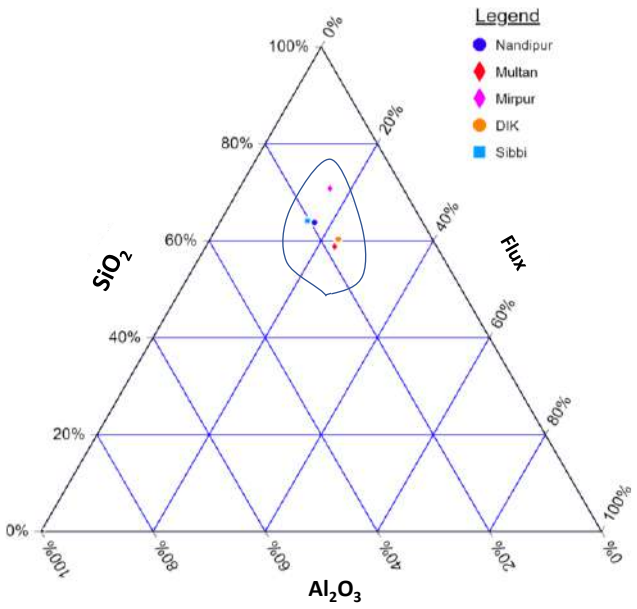

Fig. 8. Representation of the clays studied in the Riley Diagram [18].

4.3.1.2 Thermogravimetric Analysis (TGA)

Thermogravimetric analysis is a method used to measure the loss of mass as the temperature changes over time. The weight of the material is plotted against temperature to determine where the maximum weight loss occurs on the curve. This test aimed to find the temperature range at

which major mass loss occurs and decide the initial bloating temperature. The test conditions were around 20mg of sample in a platinum crucible, air atmosphere, and a 20°C/min heating rate up to 900°C [10]. The major mass loss occurs between 400 and 800ºC after 800ºC the mass loss is almost the same as represented in **Fig. 9**.

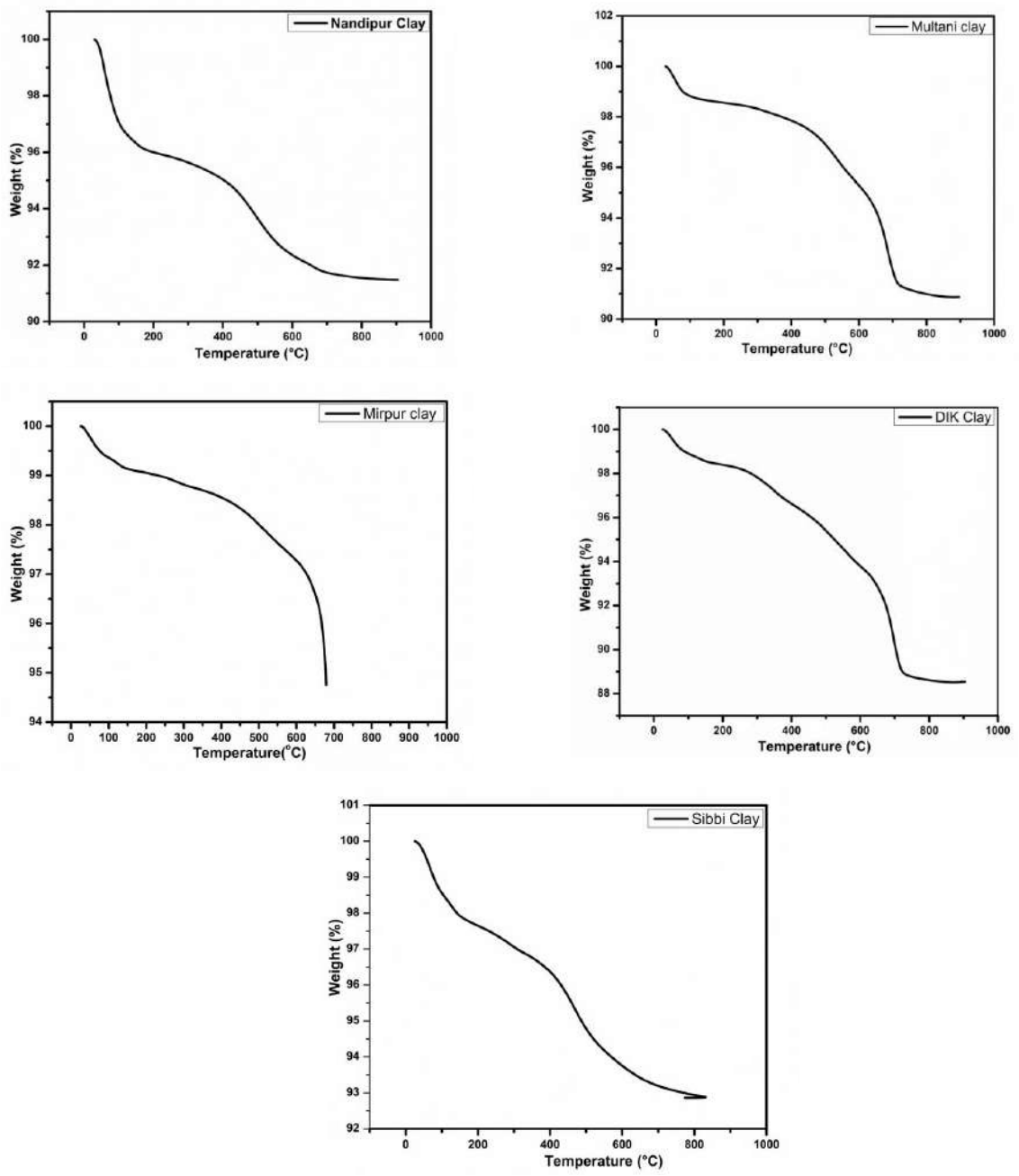

Fig. 9. Thermogravimetric analysis graphs of the clays

4.3.2 Firing temperature

Generally, the firing temperatures range between 1100ºC (DIK-1150 ºC) and 1300ºC (Nandipur-1200ºC, Multan-1200ºC, and Mirpur-1200ºC). However, a significantly higher temperature was required for Sibbi clay at 1250ºC. The XRF results in **Table. 2** show that the value of $SiO_2/\sum$ Flux of Sibbi clay is 4.45, which is significantly higher than other clays. The factor behind that why Sibbi clay required higher temperature as compared to other clays was the higher ratio of $SiO_2/\sum$ Flux as compared to other clays [39]. The value of SiO2/∑ Flux of DIK clay is 2.75 which is lower than Sibbi clay hence therefore it needs a lower temperature for bloating. According to A. Ozguven, the clay grain size affects the bloating mechanism of expanded clay aggregates [39]. The grain size of DIK clay is finer as compared to the other four clays and the grain size of Sibbi clay is comparatively large as presented in **Fig.10.** The other three clays have almost the same grain size and their $SiO_2/\sum$ Flux ratio is between 2.5 to 4 therefore these clays bloated at 1200ºC. There are no discernible variations between the clays under study in terms of weight loss when the thermogravimetric analysis graphs in **Fig. 9** are observed up to 200ºC, which is the approximate average temperature achieved in the preheating zone of the kiln. The following processes, listed in ascending order of temperature **Fig. 9**, cause mass losses up to this temperature of approximately 4-7 % in all cases: loss of hygroscopic water (up to 150 ºC) and interlayer water in illite and smectite (100-200ºC), loss of bound water in palygorskite (between 200-600 ºC) [43], decomposition of organic matter (between 200-550 ºC), and dehydroxylation of illite (400-550 ºC) [44]. All the clays Nandipur, Multan, Mirpur, Sibbi, and DIK also lie in the expansion zone as can be observed when plotted in the triangle of Riley **Fig. 8** [18].

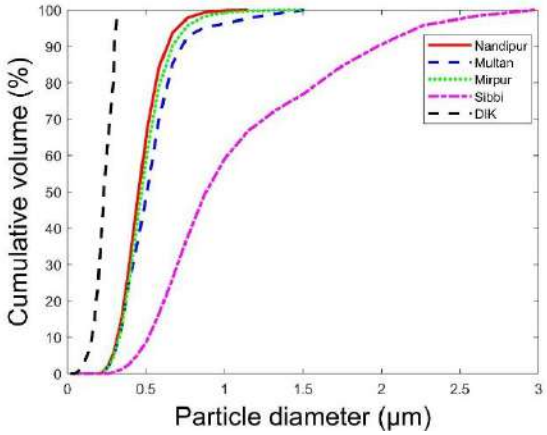

Fig. 10. Particle size distribution of the clays.

4.3.3 Characteristics of ALECA

4.3.3.1 Loss on ignition & Bloating index

The **Fig. 11** shows that as the percentage of fly ash increases, the percentage of loss on ignition increases. The LOI is maximum when the percentage of fly ash is 15%, and on further increasing the percentage of fly ash, aggregates' strength decreases, and aggregates bursting occurs. The LOI percentage of Sibbi clay pellets was low as compared to Nandipur clay because of the higher sand content. It was observed that as the percentage of kerosene oil increases, the pellets' bloating increases. The bloating of pellets was maximum when kerosene oil was 6%. Beyond 6%, the pellets were busted, as previously reported [33].

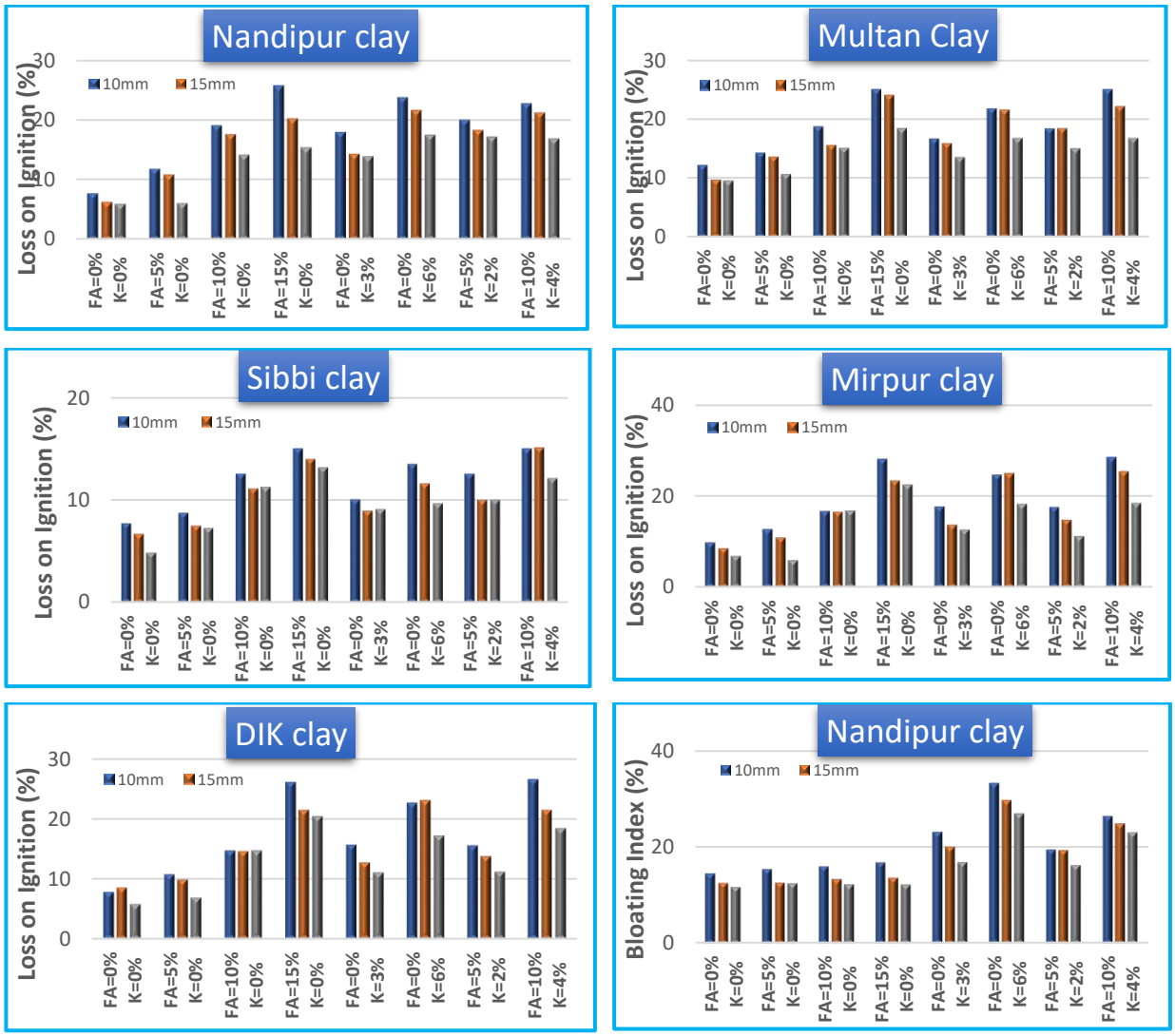

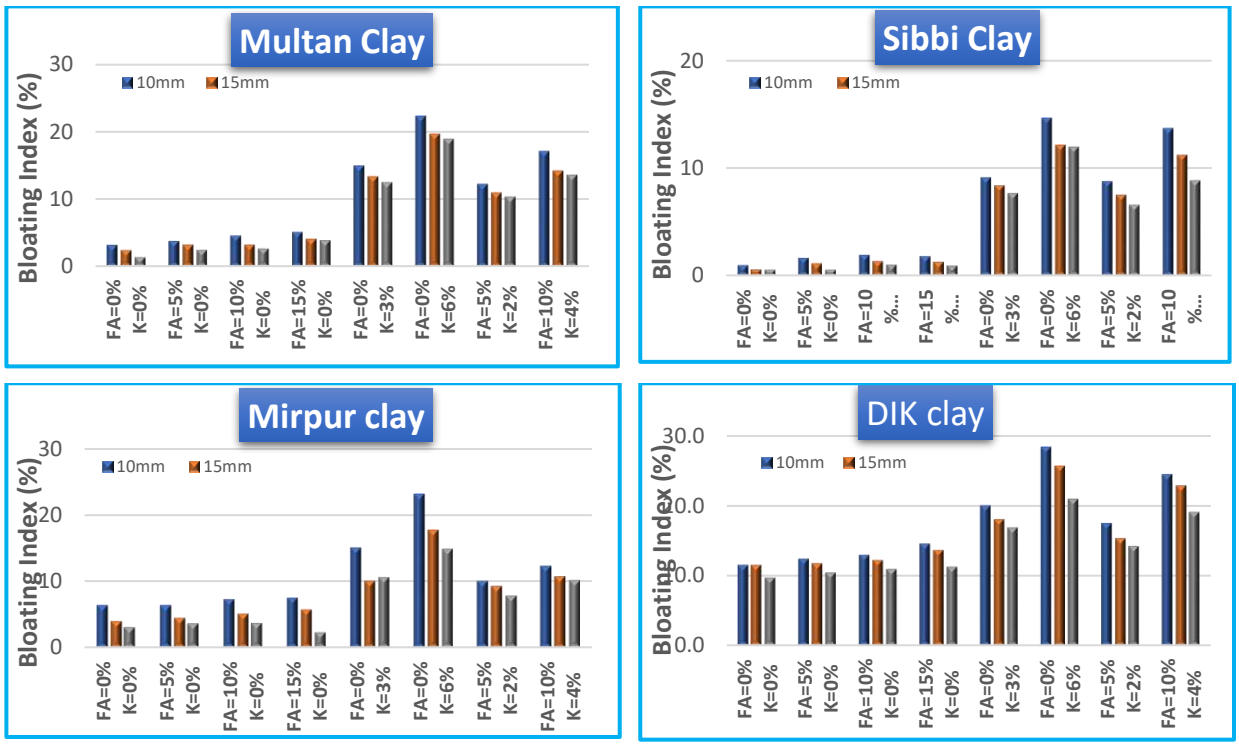

Fig. 11. Loss on ignition (LOI, %) and Bloating index (BI, %)

4.3.3.2 Effect of pellets size

The bloating process in lightweight aggregate is caused by the release of gases, which makes the internal structure of aggregate porous. The smaller the pellet size, the greater the bloating will occur due to uniform temperature distribution [30]. By increasing the size of aggregate, bloating decreases, which was observed in **Fig. 11** that as the size of the pellet increases from 10 mm to 20 mm, the bloating of aggregate decreases. The reason is that as the size of the pellet increases, the temperature does not reach the core, causing it to remain unfired.

4.3.3.3 Mechanical strength

According to **Table 4**, the crushing strength of a single aggregate range from 0.33 to 30 MPa. The lightweight expanded clay aggregates with a strength lesser than 3MPa can be used for non-structural purposes like manufacturing lightweight blocks and panels [45]. The strength of Sibbi clay aggregates is comparatively higher than the other clays aggregate due to the higher density of pellets. As the density of pellets increases, the porosity of aggregates decreases, which ultimately increases the aggregates' strength.

4.3.3.4 Density

Since the ultimate purpose of synthesizing expanded clay aggregates is to produce lightweight and sustainable aggregates, the foremost property we needed to find was the density. Regarding how the fly ash acts, in **Table 4,** it is observed that the particle density (ρ_A) tends to decrease with an increased percentage of fly ash. The drop in ρ_A is directly connected with a rise in total porosity (PT), which is more noticeable when the FA percentage is 15%. Most aggregate particle density ranges between 0.43 and 1.9 g/cm^3 and according to European standard EN-13055-1 [46] enforces that those aggregates of particles density less than 2 g/cm^3 are considered lightweight aggregate, so nearly all the aggregates under consideration fall in this range except few samples. Nandipur aggregate seems to comply completely with this code. The increase in both fly ash and kerosene doses resulted in a decrease in density. As far as fly ash is concerned, its density is already lesser than the clays we used, resulting in aggregates of lesser density. On the other hand, Kerosene increased the gasification inside the pallets, which caused enhanced swelling of aggregates. On the contrary, an increase in pallet size reduced the aggregates' bloating ability. The reason behind this mechanism is with the increase in particle size, the distribution of heat throughout the aggregate becomes non-uniform, and neither the core burns nor the gasification occurs.

4.3.3.5 Water absorption

The water absorption of lightweight expanded clay aggregates was measured according to EN 1097-6:2000 [47]. According to **Table 4,** water absorption value increases as aggregates' density decreases. By decreasing the density of aggregates, the porosity of aggregates increases; due to this reason, water absorption increases [36]. Increasing the percentage of fly ash decreases the density of pellets, and the porosity increases, adding to the water absorption value. During the burning process, kerosene oil acts as fuel, and the combustion of which helps the internal gases escape easily. Increasing the percentage of kerosene oil increases the porosity of pellets, which ultimately increases the water absorption of pellets. Hence, the density and porosity of lightweight expanded clay aggregates are key factors controlling water absorption. The water absorption of lightweight expanded clay aggregates of Nandipur clay is high compared to Sibbi clay because, in Sibbi clay pellets, there was no significant porous structure found; due to this density of Sibbi clay pellets was high as compared to Nandipur.

Table 4

FA= Fly ash (%), K= kerosene oil (%), PS = Pellet size (mm), WA_{24} = Water absorption (%), S = Compression strength of single pellet (MPa), ρ_A = Particle density (g/cm^3),

Clay quantity (g)	FA	K	Nandipur clay-1200ºC													
			PS	ρ_A	WA_{24}	S	S/ρ_A	PS	ρ_A	WA_{24}	S	S/ρ_A	PS	ρ_A	WA_{24}	S	S/ρ_A
150	0	0	10	0.83	9.51	5.36	6.46	15	0.88	6.91	1.73	1.97	20	0.88	14.61	2.51	2.85
150	5	0	10	0.95	5.93	3.02	3.18	15	0.83	8.62	1.68	2.02	20	0.82	12.12	1.57	1.91
150	10	0	10	0.91	4.30	2.50	2.75	15	0.66	6.13	1.85	2.80	20	0.52	7.00	0.48	0.92
150	15	0	10	0.85	5.30	1.96	2.31	15	0.60	10.50	0.82	1.37	20	0.44	10.81	0.33	0.75
150	0	3	10	0.91	14.31	4.29	4.71	15	0.61	12.50	1.27	2.08	20	0.55	14.12	3.14	5.71
150	0	6	10	0.64	14.31	3.69	5.77	15	0.53	12.50	2.48	4.68	20	0.43	20.83	2.62	6.09
150	5	2	10	0.88	9.72	5.71	6.49	15	0.60	9.12	6.84	11.40	20	0.59	9.54	3.33	5.64
150	10	4	10	0.80	15.6	8.53	10.66	15	0.59	9.34	10.82	18.34	20	0.46	6.77	4.91	10.67

Clay quantity (g)	FA	K	Multan clay-1200ºC													
			PS	ρ_A	WA_{24}	S	S/ρ_A	PS	ρ_A	WA_{24}	S	S/ρ_A	PS	ρ_A	WA_{24}	S	S/ρ_A
150	0	0	10	1.62	0.60	10.90	5.14	15	1.77	5.26	8.00	4.52	20	1.61	1.25	5.59	3.47
150	5	0	10	1.30	2.51	5.00	3.85	15	1.28	4.26	4.85	3.79	20	1.25	5.21	3.56	2.85
150	10	0	10	0.94	3.16	3.71	3.95	15	1.25	3.44	3.71	2.97	20	1.35	1.89	3.32	2.46
150	15	0	10	0.94	10.00	4.77	5.07	15	1.10	5.33	2.74	2.49	20	1.14	4.33	2.57	2.25
150	0	3	10	0.89	3.85	4.79	5.38	15	1.08	4.34	5.42	5.02	20	1.00	2.17	4.82	4.82
150	0	6	10	0.76	10.32	4.35	5.72	15	0.74	6.41	7.75	10.47	20	0.76	5.71	6.52	8.58
150	5	2	10	0.83	7.22	5.90	7.11	15	0.90	8.62	4.71	5.23	20	1.1	12.27	8.38	7.62
150	10	4	10	0.72	8.82	4.16	5.78	15	0.81	5.00	5.77	7.12	20	0.83	3.27	6.41	7.72

Clay quantity (g)	FA	K	Mirpur clay-1200ºC													
			PS	ρ_A	WA_{24}	S	S/ρ_A	PS	ρ_A	WA_{24}	S	S/ρ_A	PS	ρ_A	WA_{24}	S	S/ρ_A
150	0	0	10	1.43	0.67	9.00	6.29	15	1.65	1.31	10.54	6.39	20	2.02	0.99	5.29	2.62
150	5	0	10	1.31	0.99	6.95	5.31	15	1.42	3.32	8.24	5.80	20	1.55	1.12	8.94	5.77
150	10	0	10	1.29	0.35	6.71	5.20	15	1.38	2.32	7.28	5.28	20	1.44	1.32	6.77	4.70
150	15	0	10	1.21	22.2	5.11	4.22	15	1.27	2.84	6.78	5.34	20	0.99	2.53	8.32	8.40
150	0	3	10	1.00	0.43	7.89	7.89	15	1.22	0.93	7.90	6.48	20	1.28	1.14	6.24	4.88
150	0	6	10	0.89	5.62	8.29	9.31	15	1.00	3.86	7.33	7.33	20	0.82	1.15	9.90	12.07
150	5	2	10	1.04	0.24	9.12	8.77	15	1.32	5.32	9.82	7.44	20	1.17	1.60	7.6	6.50
150	10	4	10	0.92	0.89	6.21	6.75	15	1.01	0.22	9.14	9.05	20	1.12	0.56	17.36	15.50

Clay quantity (g)	FA	K	Sibbi clay-1250ºC													
			PS	ρ_A	WA_{24}	S	S/ρ_A	PS	ρ_A	WA_{24}	S	S/ρ_A	PS	ρ_A	WA_{24}	S	S/ρ_A
150	0	0	10	2.13	0.54	26.42	12.40	15	1.96	1.61	30.22	15.42	20	2.10	1.24	20.50	10.68
150	5	0	10	2.12	0.34	21.31	10.05	15	1.74	0.43	13.12	7.54	20	1.79	0.88	14.18	7.92
150	10	0	10	2.05	0.77	29.92	14.60	15	1.72	1.50	14.00	8.14	20	1.64	1.70	15.76	9.61
150	15	0	10	1.82	6.42	25.24	13.87	15	1.68	2.21	16.45	9.79	20	1.49	2.30	18.15	12.18
150	0	3	10	1.69	0.44	14.35	8.49	15	1.51	1.56	13.86	9.18	20	1.28	0.98	10.46	8.17
150	0	6	10	1.00	5.56	15.68	15.68	15	1.40	1.81	18.98	24.03	20	1.89	1.79	11.44	6.05
150	5	2	10	1.71	0.65	18.30	10.70	15	1.31	2.72	10.26	7.83	20	1.35	0.98	6.22	4.61
150	10	4	10	1.66	0.54	17.40	10.48	15	1.45	2.76	13.47	17.05	20	1.19	2.25	12.20	10.25

Clay quantity (g)	FA	K	DIK clay-1150ºC													
			PS	ρ_A	WA_{24}	S	S/ρ_A	PS	ρ_A	WA_{24}	S	S/ρ_A	PS	ρ_A	WA_{24}	S	S/ρ_A
150	0	0	10	1.51	8.51	2.12	1.40	15	2.12	4.92	2.00	0.94	20	1.11	12.61	0.89	0.80
150	5	0	10	1.31	4.11	3.04	2.32	15	1.99	3.63	2.34	1.18	20	0.92	8.11	1.21	1.32
150	10	0	10	1.21	5.23	2.57	2.12	15	1.51	5.01	1.89	1.25	20	0.52	9.39	0.51	0.98
150	15	0	10	1.11	6.23	1.50	1.35	15	1.31	10.01	0.99	0.76	20	0.56	10.28	0.42	0.75
150	0	3	10	0.91	12.09	3.72	4.09	15	1.12	11.05	1.27	1.13	20	0.55	8.41	2.12	3.85
150	0	6	10	0.64	13.03	6.67	10.42	15	0.74	11.51	3.21	4.34	20	0.42	11.18	1.62	3.86
150	5	2	10	1.21	9.47	9.92	8.20	15	0.99	9.12	7.89	7.97	20	0.59	9.50	3.33	5.64
150	10	4	10	1.32	12.45	13.98	10.59	15	0.99	9.87	11.76	11.88	20	0.46	9.99	5.92	12.87

4.3.3.6 Color and surface morphology of ALECA

Fig. 12. illustrates the comparison of bloated aggregates from the selected clay samples under investigation. It is apparent from the figures that Nandipur clay showed the best bloating. If we look at the appearance of the bloated aggregates individually, the Nandipur clay aggregate are deep brown (rusty) in color and the texture is rough. Multan clay aggregates on the other hand manifest a pitch-dark and glassy appearance. Due to lesser gasification and glassification, only small pores are visible on the surface of the aggregates. Mirpur clay aggregates resemble with Multan aggregates to a greater extent. Mirpur aggregates also undergo comparatively less glassification and the color is brownish. The Sibbi clay aggregates are reddish brown, and the texture is unwrinkled due to least bloating. Finally, the DIK aggregates showed the second-best bloating, and the texture is also rough and uneven. The color of the DIK clay is rosy, darkish red. The physical appearance also governs the porosity of the aggregates. Nandipur and DIK aggregates turned out to be the lightest and most porous aggregates.

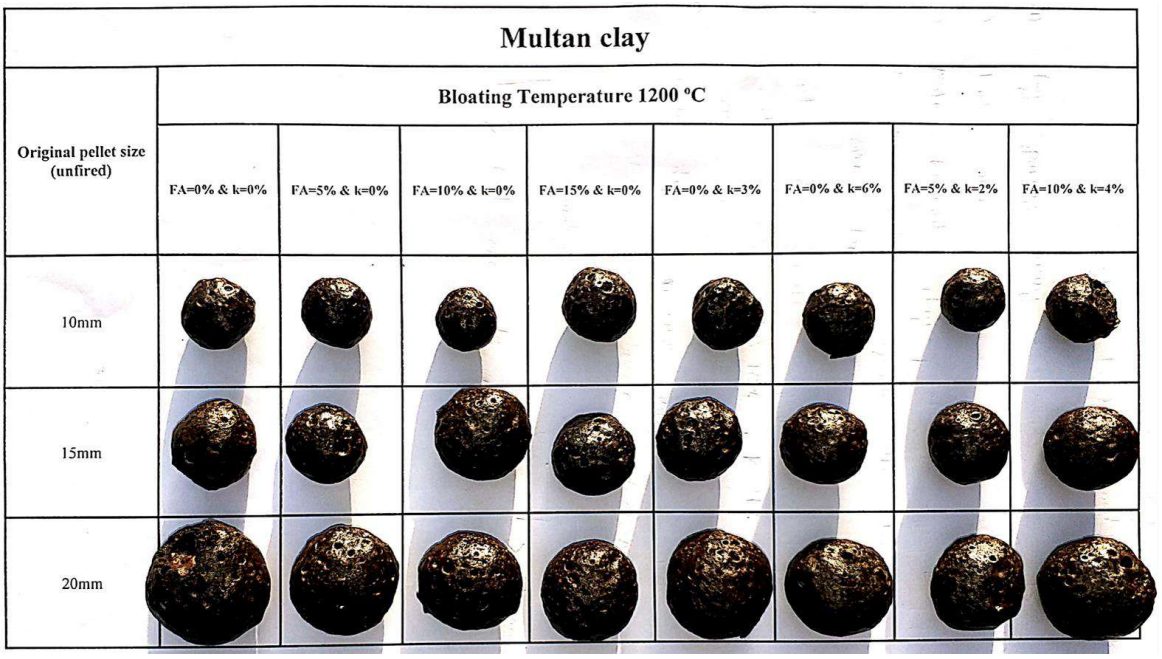

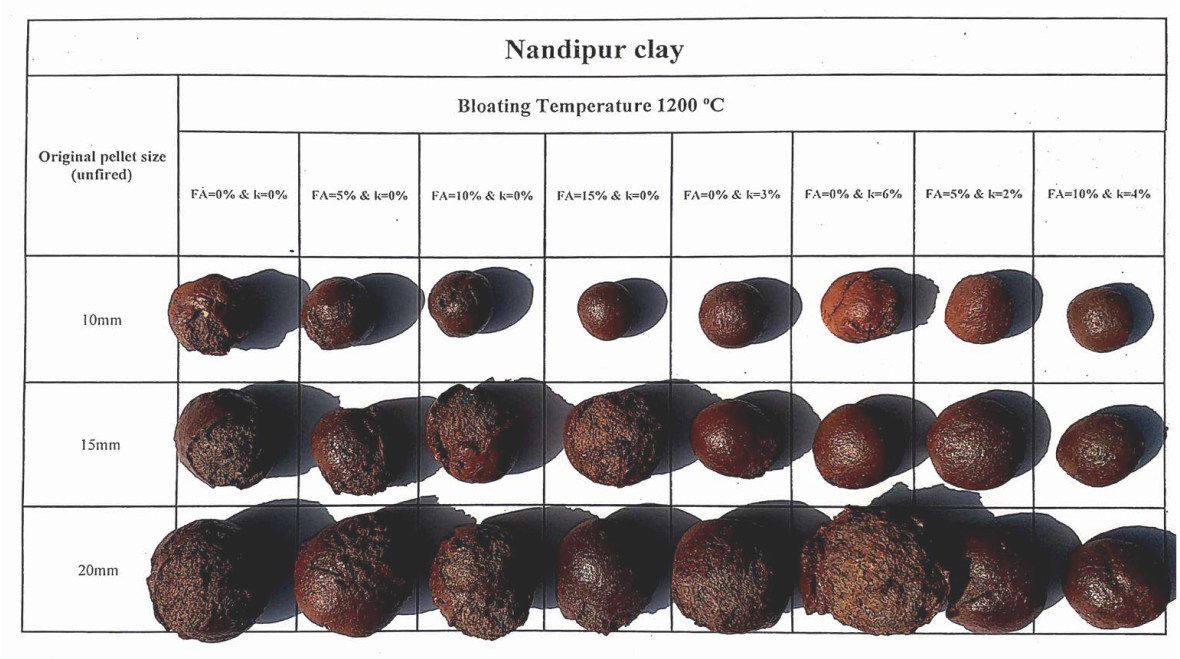
Nandipur clay
Bloating Temperature 1200 °C
Original pellet size (unfired)
FA=0% & k=0%
FA=5% & k=0%
FA=10% & k=0%
FA=15% & k=0%
FA=0% & k=3%
FA=0% & k=6%
FA=5% & k=2%
FA=10% & k=4%
10mm
15mm
20mm

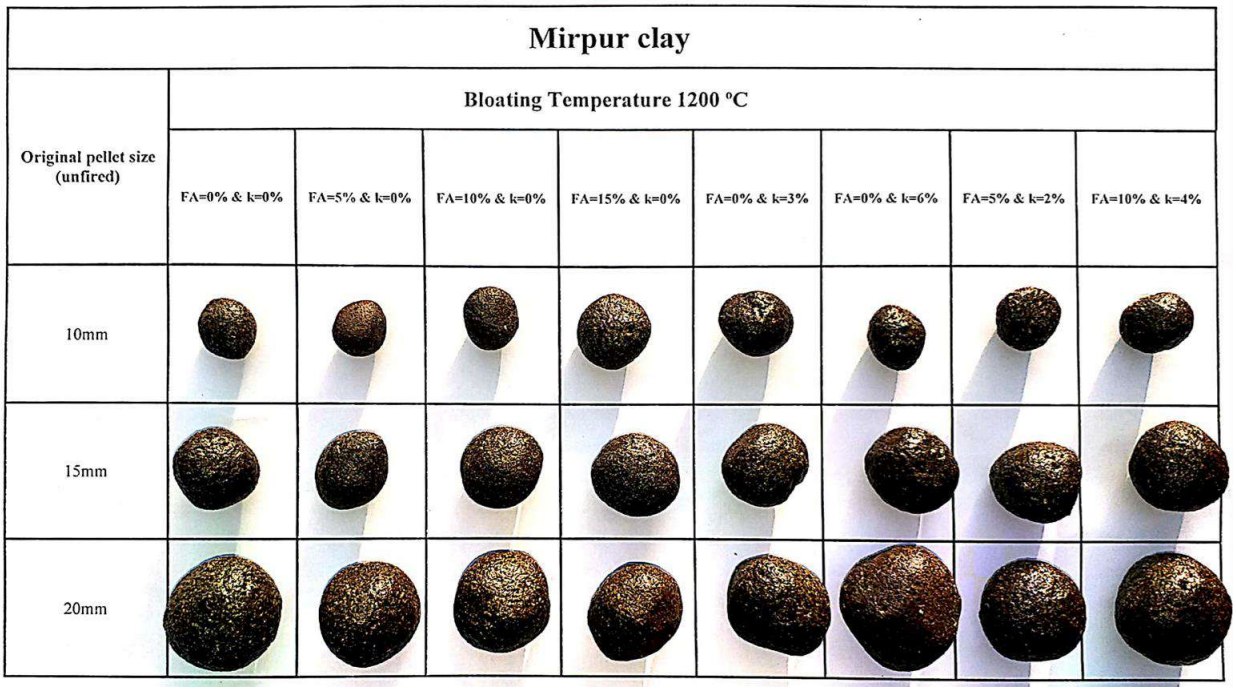
Mirpur clay
Bloating Temperature 1200 °C
Original pellet size (unfired)
FA=0% & k=0%
FA=5% & k=0%
FA=10% & k=0%
FA=15% & k=0%
FA=0% & k=3%
FA=0% & k=6%
FA=5% & k=2%
FA=10% & k=4%
10mm
15mm
20mm

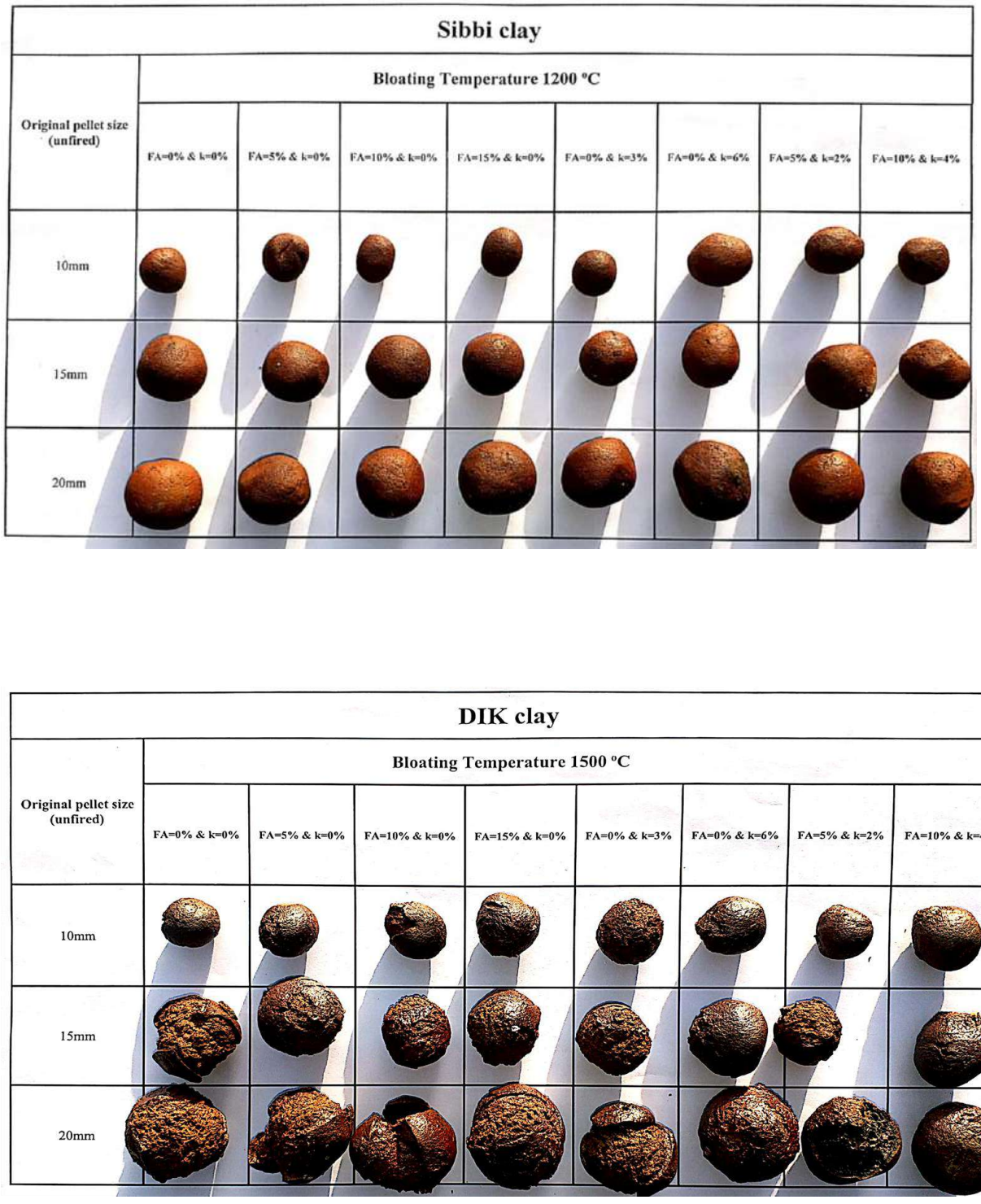

Fig. 12. Pictures of the sintered aggregates regarding the different doses and different size of pellets

4.3.4 Suitability for concrete

The main advantage of LWA is lightness, however as low density is usually accompanied by low compressive strength, the ratio S/ρ_A (**Table 4**) is a useful parameter that represents the balance between both properties, working as a good indicator of the suitability of LWAs for concrete. The commercial LWA "Leca Strutturale" used in structural concrete manufacture has a ratio S/ρ_A=3.46, being its average individual grain S value of 4.5 MPa [48]. In Table 4, the highlighted LWAs are suitable for producing lightweight structural concrete. Despite having lower mechanical strengths, the application in structural concrete of the expanded LWAs should not be discarded until performing additional investigations with concrete specimens. In any case, they could be used for other purposes, such as non-structural members, precast lightweight structures, insulation lightweight concretes, or geotechnical applications [49].

4.4. Conclusion

In this research, different zones of Pakistan were selected to manufacture the artificial lightweight expanded clay aggregate. These clays were investigated according to their ability to form granules, their potential to burst during heating, energy cost, and their mechanical properties, with particular attention to the density and the compressive strength. A variety of lightweight aggregates were produced, and the following conclusion has been drawn:

- As the pellet size increases from the maximum point bloating index and loss on ignition decreases due to the non-uniform distribution of temperature inside the core of the pellet.
- By increasing the percentage of kerosene oil, bloating of aggregates increases after exceeding the optimum dose; there was no significant increment in pellets' bloating and bursting problems of pellets occurred. The optimum dose of fly ash was 15%, and after exceeding this percentage bursting problems were faced, and the strength of expanded clay aggregates was also decreased.
- The clays which have higher ratios of $SiO_2/\sum$ Flux require higher working temperatures. The $SiO_2/\sum$ Flux ratio of Sibbi clay is 4.45 with the required bloating temperature of 1250^{o}C.
- Although the Sibbi clay aggregate strength is good but due to the higher density of pellets and not developing the typical structure (highly porous core) of lightweight aggregates not suitable for producing expanded clay aggregate according to protocols followed in this research.

- The effective time period and temperature in the furnace changed according to clay type. Thus, tests were conducted to find each clay's effective time period and temperature. The temperature rate is kept at 20ºC/min for all clays, and bloating temperatures of clays are DIK-1150 ºC, Nandipur-1200 ºC, Multan-1200 ºC, Mirpur-1200 ºC, and Sibbi-1250 ºC.
- The four clays—Nandipur, Multan, DIK, and Mirpur—have demonstrated the best aptitudes. It is remarkable that the Nandipur clay, which has the lowest energetic cost of the clay under investigation, produced the lightest aggregate (bulk density of 0.39 g/cm3 and BI of 26.3%) sintered at 1200ºC. Another advantage is that these LWAs' mechanical strength has been shown to be more than that of a commercial LWA used in structural concrete.

The results of this study reveal that certain clays with greater aptitudes especially the Nandipur clay produce a new market line within the LWA sector, whose contribution is of enormous significance in industries like building, agriculture, or civil and environmental engineering.

References

[1] "Aggregates Market Growth | Industry Report, 2020-2027." https://www.grandviewresearch.com/industry-analysis/aggregates-market# (accessed Jan. 14, 2023).

[2] I. Ocak, "Environmental problems caused by Istanbul subway excavation and suggestions for remediation," Environmental Geology, vol. 58, no. 7, pp. 1557–1566, Oct. 2009, doi: 10.1007/s00254-008-1662-9.

[3] M. J. González and J. García Navarro, "Assessment of the decrease of CO_2 emissions in the construction field through the selection of materials: Practical case study of three houses of low environmental impact," Build Environ, vol. 41, no. 7, pp. 902–909, Jul. 2006, doi: 10.1016/j.buildenv.2005.04.006.

[4] A. Tawfik, H. Awaad, T. M. El-Sokkary, and F. Abd El-Raoof, "Effect of SiC additions on bloating in clay from Toshka, Egypt," InterCeram: International Ceramic Review, vol. 63, no. 4, pp. 198–201, 2014, doi: 10.1007/bf03401058.

[5] A. Ozguven and L. Gunduz, "Examination of effective parameters for the production of expanded clay aggregate," Cem Concr Compos, vol. 34, no. 6, pp. 781–787, Jul. 2012, doi: 10.1016/j.cemconcomp.2012.02.007.

[6] A. V. Rodrigues and S. R. Braganç, "An evaluation of the increased expansion of clayaggregates fired at 1300°C to maximize lightnessfor non-structural concrete," Boletin de la Sociedad Espanola de Ceramica y Vidrio, 2021, doi: 10.1016/j.bsecv.2021.11.003.

[7] H. J. Chen, S. Y. Wang, and C. W. Tang, "Reuse of incineration fly ashes and reaction ashes for manufacturing lightweight aggregate," Constr Build Mater, vol. 24, no. 1, pp. 46–55, Jan. 2010, doi: 10.1016/j.conbuildmat.2009.08.008.

[8] H. Ahmad, M. Hilton, N.M. Noor, Physical properties of local palm oil clinker and fly ash. Proceedings of EnCon. 1st Engineering Conference on Energy and Environment, 27-28 December 2007, Kuching, Sarawak, Malaysia, 2007.

[9] M. Ziada, S. Erdem, Y. Tammam, S. Kara, and R. A. G. Lezcano, "The effect of basalt fiber on mechanical, microstructural, and high-temperature properties of fly ash-based and basalt powder waste-filled sustainable geopolymer mortar," Sustainability (Switzerland), vol. 13, no. 22, Nov. 2021, doi: 10.3390/su132212610.

[10] J. M. Moreno-Maroto, B. González-Corrochano, J. Alonso-Azcárate, and C. Martínez García, “A study on the valorization of a metallic ore mining tailing and its combination with polymeric wastes for lightweight aggregates production,” J Clean Prod, vol. 212, pp. 997–1007, Mar. 2019, doi: 10.1016/j.jclepro.2018.12.057.

[11] A. V. Rodrigues and S. R. Braganç, “An evaluation of the increased expansion of clay aggregates fired at 1300 °C to maximize lightness for non-structural concrete,” Boletín de la Sociedad Española de Cerámica y Vidrio, Nov. 2021, doi: 10.1016/J.BSECV.2021.11.003.

[12] B. Ayati, V. Ferrándiz-Mas, D. Newport, and C. Cheeseman, “Use of clay in the manufacture of lightweight aggregate,” Construction and Building Materials, vol. 162. Elsevier Ltd, pp. 124–131, Feb. 20, 2018. doi: 10.1016/j.conbuildmat.2017.12.018.

[13] N. Kanari, F. Diot, C. Gauthier, and J. Yvon, “Use of residual materials for synthesis of lightweight granulates by thermal treatment process,” Appl Clay Sci, vol. 123, pp. 259–271, Apr. 2016, doi: 10.1016/j.clay.2015.12.027.

[14] T. I. Anan and A. G. Abd El-Wahed, “The Maastrichtian-Danian Dakhla Formation, Eastern Desert, Egypt: Utilization in manufacturing lightweight aggregates,” Appl Clay Sci, vol. 150, pp. 10–15, Dec. 2017, doi: 10.1016/j.clay.2017.08.027.

[15] M. Loutou and M. Hajjaji, “Clayey wastes-based lightweight aggregates: Heating transformations and physical/mechanical properties,” Appl Clay Sci, vol. 150, pp. 56–62, Dec. 2017, doi: 10.1016/j.clay.2017.09.011.

[16] A. International and files indexed by mero, “Standard Test Methods for Liquid Limit, Plastic Limit, and Plasticity Index of Soils 1.”

[17] “Standard Test Method for Shrinkage Factors of Soils by the Mercury Method 1.” [Online]. Available: www.astm.org,

[18] C. M. Riley, “Relation of Chemical Properties to the Bloating of Clays.”

[19] K. G. Lee and K. G. Lee, “Bloating Mechanism for Artificial Light Weight Aggregate of Surface Modification with Coal ash,” Journal of the Korean Ceramic Society, vol. 52, no. 2, p. 159, Mar. 2015, doi: 10.4191/KCERS.2015.52.2.159.

[20] M. Bernhardt, H. Justnes, H. Tellesbø, and K. Wiik, “The effect of additives on the properties of lightweight aggregates produced from clay,” Cem Concr Compos, vol. 53, pp. 233–238, Oct. 2014, doi: 10.1016/J.CEMCONCOMP.2014.07.005.

[21] Y. M. Wie and K. G. Lee, “Optimum bloating-activation zone of artificial lightweight aggregate by dynamic parameters,” Materials, vol. 12, no. 2, Jan. 2019, doi: 10.3390/ma12020267.

[22] J. M. Moreno-Maroto and J. Alonso-Azcárate, “Plastic limit and other consistency parameters by a bending method and interpretation of plasticity classification in soils,” Geotechnical Testing Journal, vol. 40, no. 3, pp. 467–482, May 2017, doi: 10.1520/GTJ20160059.

[23] “BOI | Board Of Investment.” https://invest.gov.pk/?language_id=en (accessed Sep. 28, 2022).

[24] S. K. Leghari, M. A. Zaidi, M. F. Siddiqui, A. M. Sarangzai, S. U. R. Sheikh, and Arsalan, “Dust exposure risk from stone crushing to workers and locally grown plant species in Quetta, Pakistan,” Environ Monit Assess, vol. 191, no. 12, Dec. 2019, doi: 10.1007/s10661-019-7825-1.

[25] “Pakistan: A summary report on Muzaffarabad earthquake - Pakistan | ReliefWeb.” https://reliefweb.int/report/pakistan/pakistan-summary-report-muzaffarabad-earthquake (accessed Dec. 05, 2022).

[26] A. Mian, M. Yasin, and J. Mirza, “PAKISTAN’S SOIL RESOURCES.”

[27] M. H. Khalid, B. Alshameri, and U. Abid, “Application of Kriging for development of SPT N value contour maps and USCS-based soil type qualitative contour maps for Islamabad, Pakistan,” Environ Earth Sci, vol. 80, no. 11, Jun. 2021, doi: 10.1007/s12665-021-09720-5.

[28] T. A. Tawfik, D. M. AlSaffar, B. A. Tayeh, K. A. Metwally, and I. M. ElKattan, “Role of expanded clay aggregate, metakaolin and silica fume on the of modified lightweight concrete properties,” Geosystem Engineering, vol. 24, no. 3, pp. 145–156, 2021, doi: 10.1080/12269328.2021.1887002.

[29] “(1) (PDF) A literature review on alkali silica reactivity of concrete in Pakistan.” https://www.researchgate.net/publication/299437103_A_literature_review_on_alkali_silica_reactivity_of_concrete_in_Pakistan (accessed Dec. 10, 2022).

[30] R. Vijayalakshmi and S. Ramanagopal, “Structural concrete using expanded clay aggregate: a review,” Indian J Sci Technol, vol. 11, no. 16, pp. 1–12, Apr. 2018, doi: 10.17485/ijst/2018/v11i16/121888.

[31] M. C. S. Nepomuceno and P. D. Silva, “Experimental evaluation of cement mortars with phase change material incorporated via lightweight expanded clay aggregate,” Constr Build Mater, vol. 63, pp. 89–96, Jul. 2014, doi: 10.1016/j.conbuildmat.2014.04.027.

[32] K. H. Lee, J. H. Lee, Y. M. Wie, and K. G. Lee, “Bloating Mechanism of Lightweight Aggregates due to Ramping Rate,” Advances in Materials Science and Engineering, vol. 2019, 2019, doi: 10.1155/2019/2647391.

[33] K. G. Lee, “Bloating mechanism of lightweight aggregate with the size,” Journal of the Korean Ceramic Society, vol. 53, no. 2, pp. 241–245, Mar. 2016, doi: 10.4191/kcers.2016.53.2.241.

[34] J. M. Moreno-Maroto, C. J. Cobo-Ceacero, M. Uceda-Rodríguez, T. Cotes-Palomino, C. Martínez García, and J. Alonso-Azcárate, “Unraveling the expansion mechanism in lightweight aggregates: Demonstrating that bloating barely requires gas,” Constr Build Mater, vol. 247, Jun. 2020, doi: 10.1016/j.conbuildmat.2020.118583.

[35] “Sintering of Ceramics - Mohamed N. Rahaman” https://www.routledge.com/Sintering-of-Ceramics/Rahaman/p/book/9780849372865, ISBN: 9780849372865

[36] J. M. Moreno-Maroto, B. González-Corrochano, J. Alonso-Azcárate, L. Rodríguez, and A. Acosta, “Manufacturing of lightweight aggregates with carbon fiber and mineral wastes,” Cem Concr Compos, vol. 83, pp. 335–348, Oct. 2017, doi: 10.1016/j.cemconcomp.2017.08.001.

[37] T. Y. Lo, H. Cui, S. A. Memon, and T. Noguchi, “Manufacturing of sintered lightweight aggregate using high-carbon fly ash and its effect on the mechanical properties and microstructure of concrete,” J Clean Prod, vol. 112, pp. 753–762, Jan. 2016, doi: 10.1016/j.jclepro.2015.07.001.

[38] B. González-Corrochano, J. Alonso-Azcárate, and M. Rodas, “Effect of prefiring and firing dwell times on the properties of artificial lightweight aggregates,” Constr Build Mater, vol. 53, pp. 91–101, Feb. 2014, doi: 10.1016/j.conbuildmat.2013.11.099.

[39] J. M. Moreno-Maroto, M. Uceda-Rodríguez, C. J. Cobo-Ceacero, T. Cotes-Palomino, C. Martínez-García, and J. Alonso-Azcárate, “Studying the feasibility of a selection of Southern European ceramic clays for the production of lightweight aggregates,” Constr Build Mater, vol. 237, Mar. 2020, doi: 10.1016/j.conbuildmat.2019.117583.

[40] S. Yashima 277 Velocity and S. San0, “Relationships Between Particle Size and Fracture Energy or Impact Required to Fracture as Estimated from Single Particle Crushing,” 1987.

[41] Y. Li et al., “Measurement and statistics of single pellet mechanical strength of differently shaped catalysts,” 2000. [Online]. Available: www.elsevier.comrlocaterpowtec

[42] R. de’ Gennaro, P. Cappelletti, G. Cerri, M. de’ Gennaro, M. Dondi, and A. Langella, “Zeolitic tuffs as raw materials for lightweight aggregates,” Appl Clay Sci, vol. 25, no. 1–2, pp. 71–81, 2004, doi: 10.1016/j.clay.2003.08.005.

[43] E. Murad and U. Wagner, “The Thermal Behaviour Of An Fe-Rich Illite,” 1996.

[44] M. 1944- Földvári, Handbook of thermogravimetric system of minerals and its use in geological practice. Geological Institute of Hungary, 2011.

[45] M. S. Moayeri, H. R. Ashrafi, and P. Beiranvand, “Investigating the physical characteristics of non-structural lightweight aggregate blocks of built with region materials,” Buildings, vol. 7, no. 1, 2017, doi: 10.3390/buildings7010002.

[46] EN-13055-1, 2002. Lightweight aggregates. Part 1: Lightweight aggregates for concrete, mortar and grout. European Committee for Standardization.

[47] EN-1097-6, 2013. Tests for mechanical and physical properties of aggregates. Part 6: Determination of particle density and water absorption. European Committee for Standardization.

[48] R. de Gennaro et al., “Campanian Ignimbrite as raw material for lightweight aggregates,” Appl Clay Sci, vol. 37, no. 1–2, pp. 115–126, Jun. 2007, doi: 10.1016/j.clay.2006.11.004.

[49] B. González-Corrochano, J. Alonso-Azcárate, and M. Rodas, “Production of lightweight aggregates from mining and industrial wastes,” J Environ Manage, vol. 90, no. 8, pp. 2801–2812, Jun. 2009, doi: 10.1016/j.jenvman.2009.03.009.

Chapter 5

MODULE-2

Machine learning based predictive modeling of sustainable lightweight aggregate concrete

Abstract:

Nowadays, lightweight aggregate concrete is becoming more popular due to its versatile properties. It mainly helps to reduce the dead loads of the structure, which ultimately reduces design load requirements. The main challenge associated with lightweight aggregate concrete is finding an optimized mix per requirements. However, the conventional material design of this composite is quite costly, time-consuming, and iterative. This research proposes a simplified methodology for mix designing of structural and non-structural lightweight aggregate concrete by incorporating machine learning. For this purpose, five distinct machine learning algorithms; Support vector machine (SVM), Artificial neural network (ANN), Decision tree (DT), Gaussian process of regression (GPR), and Extreme gradient boosting tree (XGBoost) algorithms were investigated. For the training, testing, and validation process, a total of 420 data points were collected from 43 published journal articles. The performance of models was evaluated based on statistical performance indicators. Overall, 11 input parameters, including ingredients of the concrete mix and aggregate properties were entertained; the only output parameter was the compressive strength of lightweight concrete. The results revealed that the GPR model outperformed the remaining four machine learning models by attaining R^2 0.99, RMSE 1.34, MSE 1.79, and MAE 0.69. In a nutshell, these simplified modern techniques can be employed to make the design of lightweight aggregate concrete easy without extensive experimentation.

5.1. Introduction:

Concrete is considered to be the second most consumed material after water globally. Its remarkable binding property helps to support large structures which increases its demand daily. Due to its numerous benefits, the consumption of concrete tolls up to a giant figure of 30 billion tons per annum. [1]. In concrete structures, the majority of the stresses resulting from the action of heavy dead loads. These heavy dead loads can be reduced by using lightweight aggregate concrete. The weight of aggregate generally used in concrete is almost 70% of the composite, indicating that

most of the weight in concrete is occupied by the aggregate [2]. Using natural or artificial lightweight aggregate instead of normal aggregate could reduce the weight of the concrete significantly. Lightweight aggregate is broadly divided into two categories a) natural lightweight aggregate includes vermiculite, perlite, pumice, diatomite, scoria etc. b) Artificial lightweight aggregate includes expanded clay aggregate, expanded perlite, plastic aggregate, and expanded polystyrene beads, etc. [3]. The use of LWAC is increasing especially in high-rise buildings and long-span bridges due to its numerous benefits. These benefits include lower gravity load, better heat insulation and sound insulation, reduced risk of earthquake damage, improved fire resistance, lower shrinkage, and creep resistance as compared to conventional concrete [4]–[10]. LWAC is also a sustainable alternative for making energy-efficient buildings through heat insulation properties and cost-effective structures. The lower dead loads eventually lowers the structural members' design actions that help reduce the cross-section and reinforcement requirements [11]. Due to the lower self-weight, the cross-section of the structural members also decreases leading to lesser use of the cement which is primary contributor of the greenhouse gases as well as aggregate [12]. Furthermore, waste of the different sectors is also utilized as lightweight aggregate such as, crumb rubber, electric arch furnace slag, fly ash, etc, [12]–[15]. Artificial lightweight aggregate is also manufactured using local clays and fly ash, which is replacing the natural aggregate in order to reduce the usage of natural reserves [12], [16], [17].

Shaiksha et al. [18] reported that using artificial lightweight aggregate instead of natural aggregate could significantly reduce the cost by 18% due to a 22% reduction in the unit weight of the concrete. Lydon et al. [19] confirmed that the compressive strength of the LWAC is directly dependent on the density of the LWA used [4]. Furthermore, Huang et al. [20] confirmed that the mechanical properties of the LWAC are also a function of the rheological properties and water/binder ratio, as LWA has a high absorption capacity due to their porous microstructure. The main challenge of LWAC is to select the appropriate water/binder ratio owing to the high absorption capacity of the LWA [15]. This ultimately leads to rapid slump loss and decreases the setting time of concrete.

The mix design process for lightweight aggregate concrete is a bit complicated due to the inclusion of different properties of the lightweight aggregate. The main problem associated with the proper mix design of lightweight aggregate concrete is the variation in water absorbing capacity, and the density of the lightweight aggregate. To avoid the extensive mix design process, researchers have

developed different types of machine learning (ML) models to predict the strength parameters of the concrete [21]–[24]. The use of Artificial Intelligence (AI) in concrete technology is not new; firstly, it was started simply to predict the compressive strength of the concrete and later also used to predict other properties of concrete due to its promising results [25]. Over the years, different approaches to machine learning have been made to predict the different parameters of a material or concrete. These include Support vector machine (SVM), Random forest (RF), Decision tree (DT), Gene expression programming (GEP), and Artificial neural network (ANN), [26]–[30]. Aslam et al. [44] predict the compressive strength of high-strength concrete using the GEP algorithm [31]. Using the ANN algorithm, Siddique et al. [13] predicted the compressive strength of self-compacting concrete containing bottom ash [32]. Chithra et al. adopted an ANN model technique to predict the compressive strength of concrete containing nano-silica and copper slag [33]. Similarly, ML-based predictive models have also been developed for special concrete, such as fiber-reinforced concrete [72].

Young et al. [23] adopted the ANN modeling technique to predict the compressive strength of the lightweight aggregate concrete; however, this model lacked several important input parameters associated with the properties of aggregate, including water absorption, the density of the LWA as well as the accuracy of the model was also compromised with R^2 of 0.71. Tenza-Abril et al. [24] also developed an ANN model using ultrasonic pulse velocity as input to predict the compressive strength of the segregated lightweight aggregate concrete. The model developed by Tenza-Abril was good in terms of accuracy with an R^2 of 0.82. These aforementioned purposed models for LWAC were limited in terms of input parameters, along with compromised accuracies [24].

Therefore, there is a serious need for a comprehensive model involving all the important input parameters with high accuracy to predict the compressive strength of the lightweight aggregate concrete incorporating the properties of aggregate. This paper proposes a comprehensive approach to predict the compressive strength of structural and non-structural lightweight aggregate concrete. It is the first time that lightweight aggregate characteristics such as water absorption capacity, and density of the lightweight aggregate have been included in the dataset to predict the compressive strength of lightweight aggregate concrete based on input data that has not yet been utilized by the network. Also, the purposed machine learning model has a good accuracy as compared to already existing lightweight aggregate concrete compressive strength predictive models. Initially, a comprehensive dataset comprising 420 data points was extracted from the published journal

articles [1], [34]–[74]. To make the dataset coherent, a detailed statistical analysis was performed for data cleaning to remove the outliers from the dataset. For the training of the models, a total of five ML-based algorithms were considered for comparative analysis. To avoid overfitting and underfitting the trained model, the dataset was divided into three separate parts, out of which one was used for training, the second for testing, and the third for validation. Finally, the accuracies of the models were evaluated based on statistical error indicators, and then the best model was used to predict the compressive strength.

5.2. Data collection and analysis:

5.2.1. Data collection

This study utilizes 420 data points for the prediction modeling of lightweight aggregate concrete, which were collected from published literature and are shown in **Table. 5**. A dataset with 12 instances was used, from which 11 are input parameters and one is output. In the dataset, the input parameters are cement, sand, water-to-cement ratio (w/c), lightweight aggregate (LWA), normal aggregate (Normal Agg.), the density of lightweight aggregate, water absorption of lightweight aggregate, superplasticizer, curing time, fly ash (FA) and lightweight aggregate type. The output variable is compressive strength. The box plot of input and output variables is shown in **Fig. 14**. The name, unit, minimum and maximum values, mean, mode, and standard derivation (SD) are listed in **Table 5**. The statistical distribution of the parameters used in the dataset is shown in **Fig. 13**.

5.2.2. Pre-processing of dataset

The preprocessing data sample points initiate the development of the ML model. A correlation matrix was developed to determine the relationship between the dependent and independent variables which is shown in **Fig. 15**. The Pearson correlation matrix is a comprehensive graph that shows the relationship between the variables in terms of Pearson correlation coefficients [75]. In the correlation matrix, the correlation coefficient range lies between +1 and -1. The correlation coefficient values range between -1 and +1 for the non-diagonal entries and exactly 1 for the diagonal entries since the relation of one variable with itself will always be perfect [76]. It is evident from signs that the positive values show direct relation and negative show inverse relation between the variables[76]. The equation expressing the Pearson correlation coefficient is:

$$r = \frac{\sum (x_i - \bar{x})(y_i - \bar{y})}{\sqrt{\sum (x_i - \bar{x})^2 \sum (y_i - \bar{y})^2}} \quad (1)$$

5.2.3. Dataset normalization

The major challenge faced after data collection is processing the raw data to make it compatible with the ML models used. For instance, in our dataset, there was a considerable difference between the numerical values of cement, w/c, and normal aggregate used. This difference affected the accuracy of our model adversely. This issue was tackled using the data normalization technique. Data normalization means transforming data into the unit sphere or scaling down the actual values to numerical indexes between 0 and 1. It leads to data cleansing and convergence and significantly enhances the model's efficiency. It also improves data execution by reducing the data set's redundancy. The governing equation taken into consideration for data normalization is mentioned below, where the normalized value of a certain input variable is a function of the actual, minimum, and maximum values of that variable in the data set.

$$x_{norm} = \frac{x_i - x_{\min}}{x_{\max} - x_{\min}} \quad (2)$$

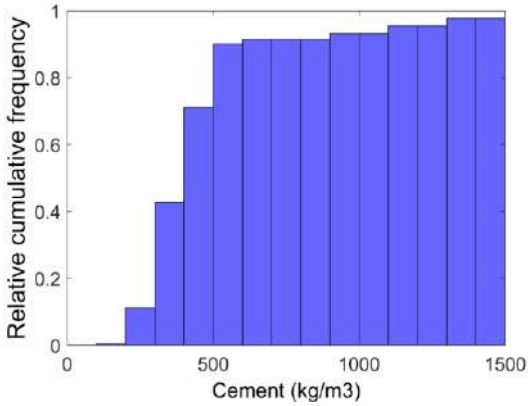

1. a

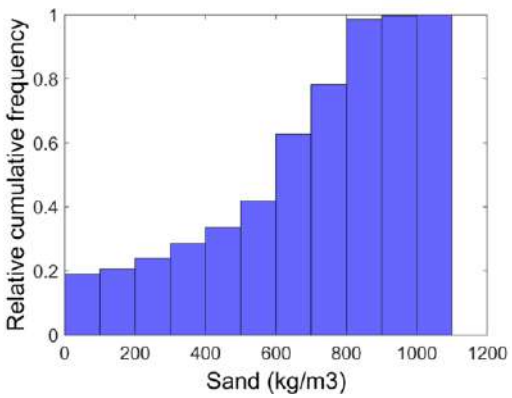

1. b

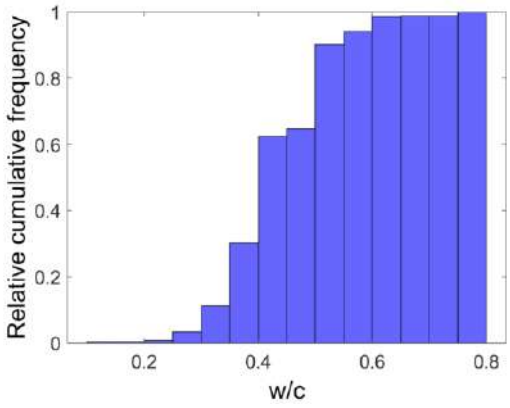

1. c

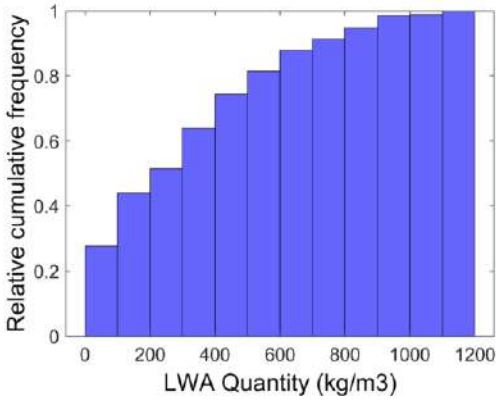

1. d

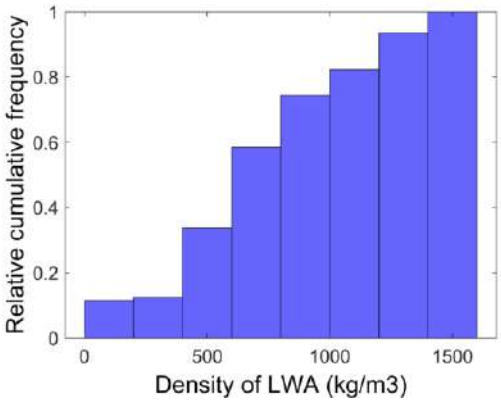

1. e

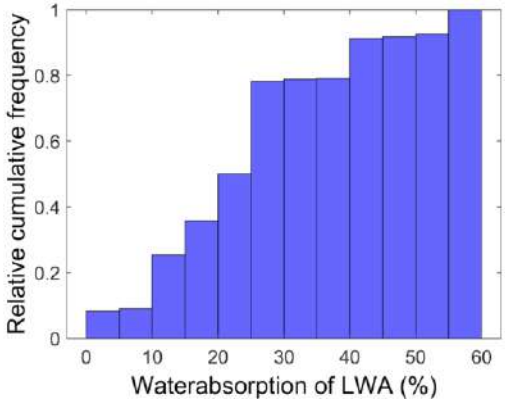

1. f

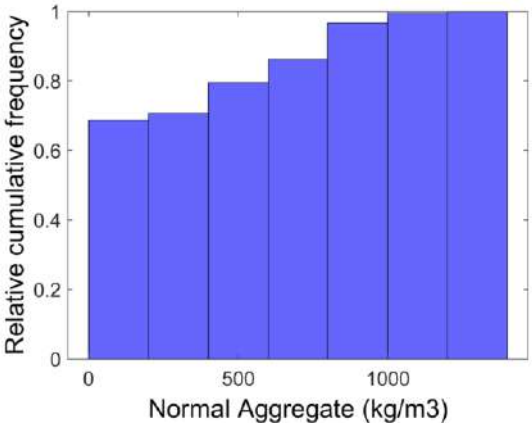

1. g

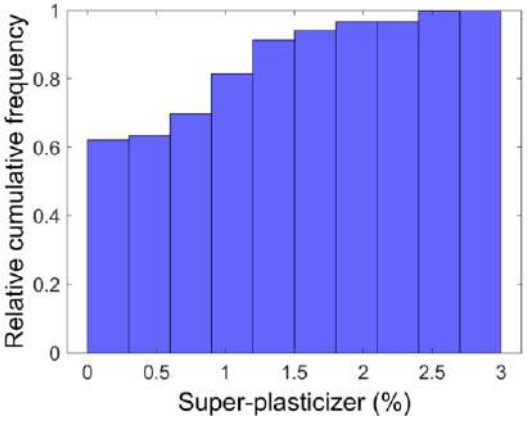

1. h

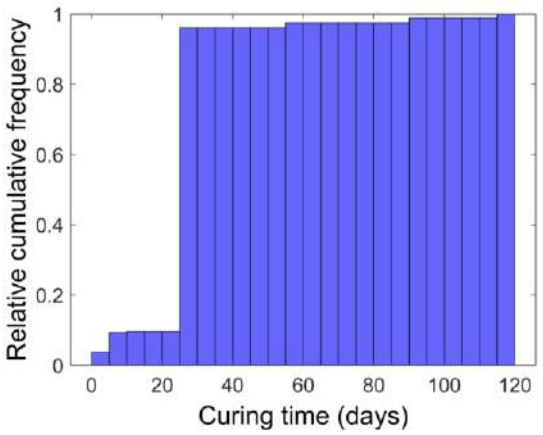

1. i

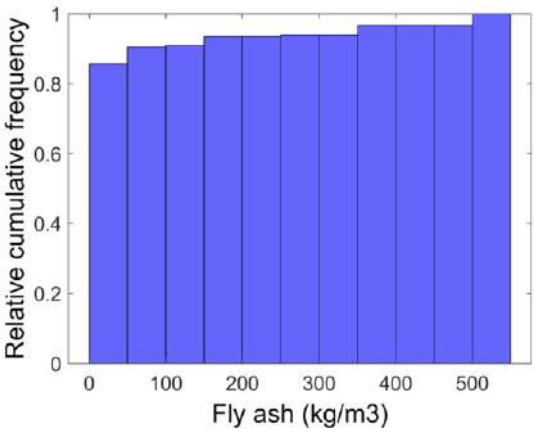

1. j

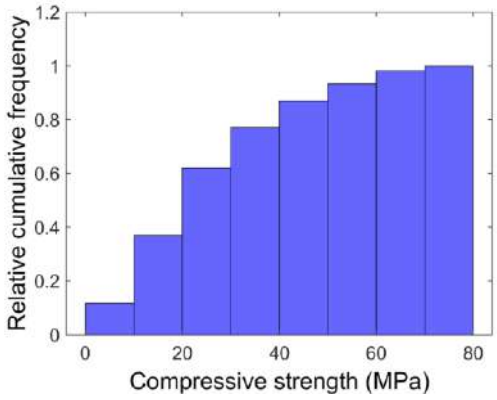

1. k

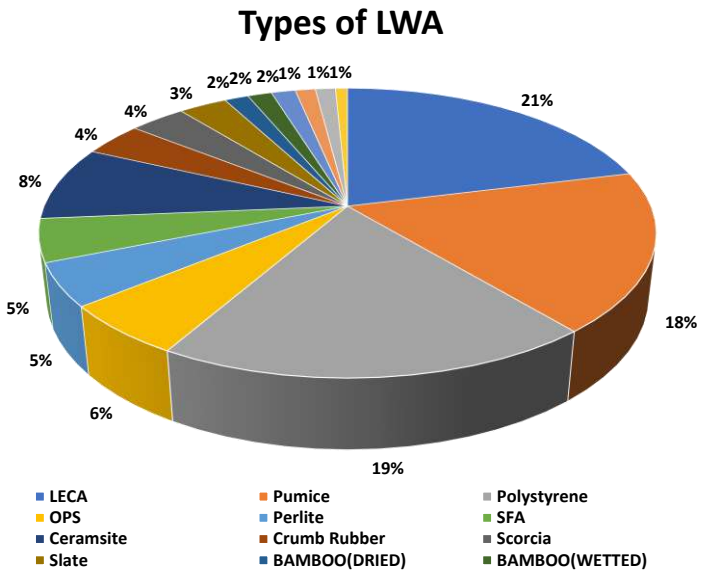

Fig. 13. Statistical distribution of the input/output variables.

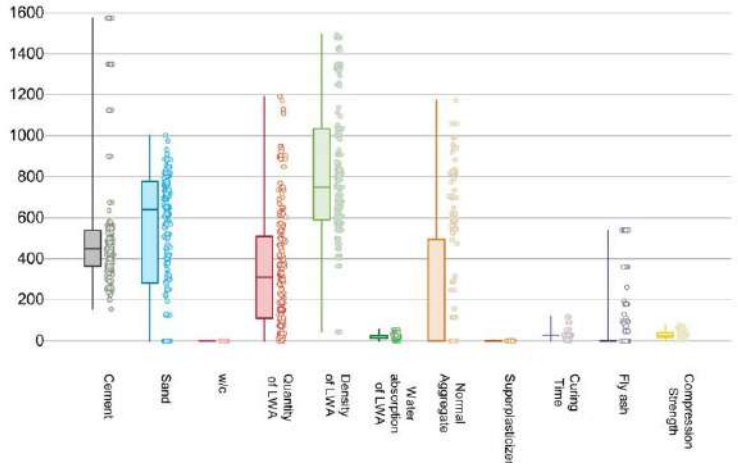

Fig. 14. Statistical distribution of the input/output variables.

Table 5

Summary of dataset for ML models training.

Parameters	Unit	Minimum	Maximum	Median	Mode	SD	Type
Cement	Kg/m^3	156	1500	467	480	378.42	Input
Sand	Kg/m^3	0	1193	664	0	330.15	Input
Water-to-cement ratio	1	0.15	0.80	0.45	0.5	0.08	Input
LWA Quantity	Kg/m^3	23.80	1191	308	37	297.28	Input
Density of LWA	Kg/m^3	415	1489	783	575	357.65	Input
Water absorption of LWA	%	0.92	58.30	25.20	40	13.83	Input
Normal aggregate	Kg/m^3	0	1326	0	0	353.98	Input
Super-plasticizer	%	0	3	0	0	0.70	Input
Curing Time	Days	1	120	28	28	14.27	Input
Fly ash	Kg/m^3	0	540	0	0	117.61	Input
Lightweight aggregate Types	-	-	-	-	-	-	Input
Compressive Strength	MPa	2.03	79	24.58	25	16.68	Output

Table 6

Summary of dataset for ML models testing.

Parameters	Unit	Minimum	Maximum	Median	Mode	SD	Type
Cement	Kg/m^3	139	1350	384	450	197.70	Input
Sand	Kg/m^3	0	1178	630	0	294.92	Input
Water-to-cement ratio	1	0.23	0.8	0.42	0.35	0.07	Input
LWA Quantity	Kg/m^3	0	950	155	0	270.29	Input
Density of LWA	Kg/m^3	406	1480	750	610	320.11	Input
Water absorption of LWA	%	0.92	56	20.5	20.5	13.54	Input
Normal aggregate	Kg/m^3	0	941.2	0	0	282.15	Input
Super-plasticizer	%	0	2.5	0.5	0	0.687	Input
Curing Time	Days	1	120	28	28	23.4	Input
Fly ash	Kg/m^3	0	540	0	0	111.38	Input

Lightweight aggregate Types	-	-	-	-	-	-	Input
Compressive Strength	MPa	4.28	65.14	27	25	15.54	Output

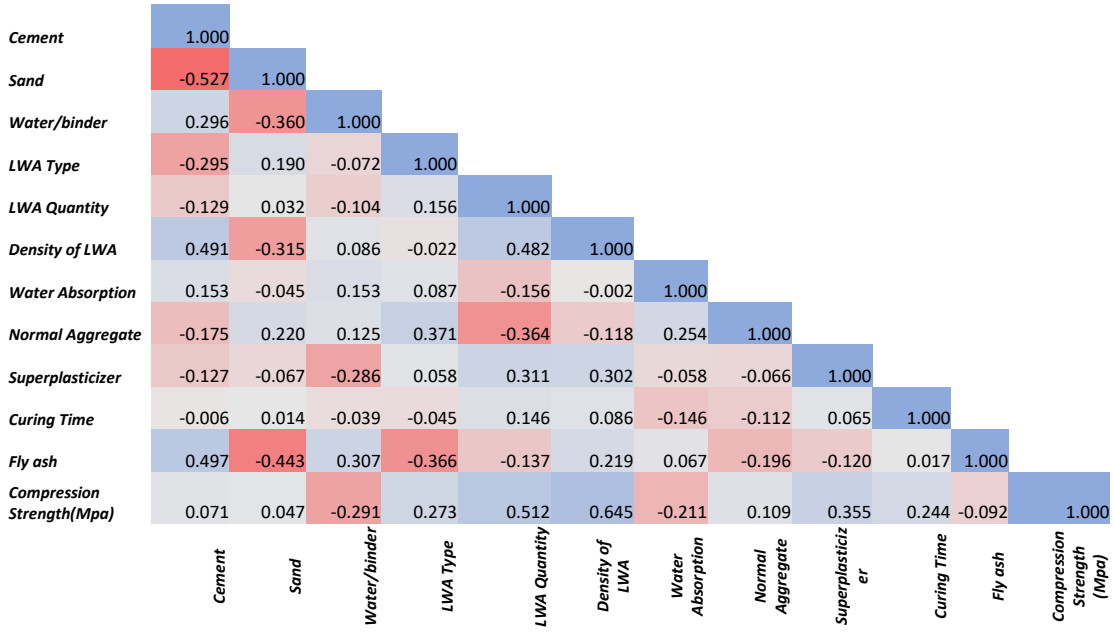

Fig. 15. Pearson correlation matrix.

5.3. Methodology

5.3.1. Overview of machine learning

Implementing machine learning (ML) in civil engineering is considered a renaissance in this field. ML models enhanced numerical computational power and higher accuracy. The ML is a branch of artificial intelligence (AI) and can be used for several objectives like classification, clustering, regression, etc. The basic working flowchart of machine learning is shown in **Fig. 16**. Predicting the compressive strength of lightweight concrete is just one application of the ML models. An ML follows certain algorithms that can learn from the input data themselves, and after hyperparameter tuning, it gives highly accurate results. An ML model that has been accurately trained and precisely calibrated has shown significant similarity with practical experimental data. The juggernaut behind this AI arena is that we allow the computer algorithms to learn from a given dataset rather than programing them conventionally. Hence, the algorithm comes up with a model

that can interpret all the data fed to it. **Table 7** summarizes some of the latest work conducted in the domain concrete with the integration of ML tools.

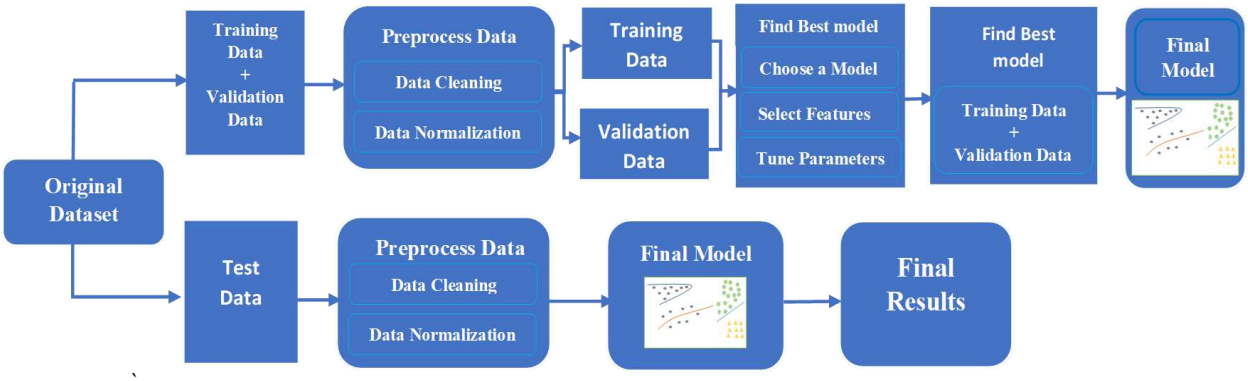

Fig. 16. Machine learning implementation process.

Table 7

Recent used of advanced machine learning modeling in research.

Sr. No.	Machine Learning Algorithms	Data sets	Input parameters	Output Parameters	Ref.
1.	GB_PSO & SVR	721	Water content, aggregate content, RCA content, NA content, sand content, cement content, RCA water absorption, NA water absorption.	Compressive Strength	[77]
2.	Gaussian process regression, Kernel transformations and regression, SVR	1681	Cement, fly ash and water content	Compressive Strength	[78]
3.	GPR, ANN SVR	406	Water, cement , slag, fine steel slag, coarse steel slag	Compressive Strength	[79]
4.	ELM, SVM and GMDH	2028	Curing ages of 1, 3, 7, 28 and 90 days.	Compressive strength and ultrasonic pulse velocities	[80]
5.	RF (Random Forest)	-	FA, RM, and GP	Compressive strength, Split tensile strength and flexural strength	[81]
6.	ANN & DNN	335	Fly ash, water glass solution, sodium hydroxide solution, coarse aggregate, fine aggregate, water, concentration of sodium hydroxide solution, curing time, and curing temperature.	Compressive strength	[82]
7.	SVM, ANN, adaboost, CNN	380	C-G: cement strength class, W/B: water-binder ratio; S-R: sand ratio, P/A: paste-aggregate ratio, RA/A: recycled coarse aggregate replacement proportion, F/B: fly ash replacement proportion, SF/B: silica fume replacement proportion, S/B: slag replacement	Compressive strength	[83]
8.	RF, adaboost, GB, SVR & XGB	220	W/C ratio and silica fume, Silica fume content and fiber volume fraction	Compressive strength and flexural strength	[84]

9.	ANN, GB, XGB, SVR, KNN LR	630	Cement, fines, coarse aggregate, superplasticizer and curing age	Compressive strength	[85]
10.	Least square support vector machine Coupled simulated annealing CSA LSSVM-CSA, GP	-	W/c ratio, coarse–fine aggregate (CA/FA) ratio, proportion of CA to FA	Compressive strength	[86]
11.	Multiple linear regression, Genetic algorithm-BPNN, Backpropagation neural network, Gaussian process regression, Radial basis function neural network.	2045	Water-cement ratio, water-binder ratio, aggregate-cement ratio, cement content (kg/m3), silica fume content (% cement mass), fly ash content (% cement mass), slag content (% cement mass), calcined clay content (% cement mass) (denoted as metakaolin), filler content (kg/m3), amount of superplasticizer (% cement mass), SAP content (% cement mass), SAP size (μm), SAP water uptake (g/g of SAP in cement slurry) and time since the beginning of shrinkage measurements (days)	Axial loading capacity	[87]
12.	Linear regression, K-nearest neighbors, Support vector regression, XGboost, Decision tree, Gaussian process regression, Gradient boosting, Artificial neural network, Random forest.	429	Wall features	The capacity of RC shear walls	[88]
13.	Data envelopment analysis	114	Super plasticizer, coarse aggregates, fine aggregates, water–binder ratio, fly ash replacement percentage, and the total binder content	Compressive strength, V funnel test, Slump test, L box test	[89]
14.	Support vector machine	15	AE parameters	Compressive strength	[90]
15.	Gene-expression programming	277	Binder content, fly ash, water–powder ratio, fine aggregate, coarse aggregate and superplasticizer	Axial capacity	[75]
16.	Adaptive neuro fuzzy inference system	7	Depth, thickness, yield strength of steel, the Compressive strength of concrete and the length of the CFST	Compressive strength	[91]
17.	Conventional-ANN	220	Mixtures incorporating 0%, 10 wt%, 20 wt%, 30 wt%, 50 wt%, 60 wt%, and wt 70% T-POFA as a replacement of ordinary Portland cement (OPC) at a constant water/binder (W/B) ratio of 0.35	Compressive strength	[92]
18.	Multivariate	21	W/c ratio, sand/cement ratio , curing days and dry density	Compressive strength	[93]
19.	Intelligent rule based enhanced multiclass support vector machine and fuzzy rules	114	Crumb rubber derived from end-of-life tires (grain size 0.5–3.5 mm) was replaced fine aggregate by 0%, 5%, 10%, 15%, 20%, 25%, and 30% of total aggregate volume. Silica fume was replaced cement by 0%, 5%, and 10% of the total cement mass	Compressive strength	[94]
20.	Multivariate adaptive regression spline	114	Cement (kg), fly ash (kg), water powder ratio (W/P) and super plasticizer (l/m3)	Compressive strength Slump test L-box test V funnel test	[95]
21.	Gene-expression programming	160	Fly ash as cement replacement	Post-fire behavior	[96]
22.	Gene expression programming (GEP), Random forest regression (RFR) and Support vector machine (SVM)	-	Temperature (T), recycled concrete aggregate (RCA) replacement level, and super plasticizer (SP) addition percentage	Compressive strength (f'c) of sugarcane bagasse ash (SCBA) concrete)	[97]
23.	Extreme learning machine (ELM)	324	SCBA dosage (SCBA%), the quantity of fine aggregate (FA) and coarse aggregate (CA), water-cement ratio (W/C) and cement content (CC).	Compressive strength of high-strength concrete (HSC).	[93]
24.	Gaussian process regression (GPR)	414	Water, cement, fine aggregate, coarse aggregate, and superplasticizer	Compressive strength of Miscanthus	[98]
25.	Support vector regressor (SVR), Random forest regressor (RFR), Extra trees regressor (ETR), and Gradient boosting regressor (GBR)	676	Curing time and pre-treatment condition	Compressive strength	[99]

26.	Gaussian process regression (GPR)	414	Mixture proportions and the chemical compositions	Compressive strength of Miscanthus lightweight concrete (MLWC)	[100]
27.	Multiple linear regression (MLR), Generalized linear modeling (GLM), Quadratic polynomial regression (QPR), and Support vector machine with linear kernel (SVML); non-linear models include Artificial neural network (ANN), Support vector machine with polynomial kernel (SVMP), Support vector machine with radial kernel (SVMR), Random forest (RF), and Extreme gradient boosting (xgboost)	12,107	Curing time and pre-treatment condition	Compressive strength of field concrete at 7 days	[99]
28.	Support vector machine (SVM)	1000	Water, cement, coarse aggregate, fine aggregate, fly ash, superplasticizing admixture, and water reducing admixture.	Compressive strength	[96]
29.	Support vector regression	115	Curing conditions	Compressive strength	[101]

5.3.1.1. Artificial neural networks

An Artificial neural network (ANN) is a data-driven ML-based approach inspired by the functioning of neural networks in the human brain. [102]. ANN has versatile applications from speech recognition to medical diagnosis and data sorting to clustering. The working principle of ANN is based on its ability to learn from the data provided and find a certain connection between the input and output parameters through hidden functions. Neurons are the building blocks of ANN and there is a weight and bias associated with every neuron. The data proceeds from the input layer towards the output layer through different intermediate hidden layers. All the corresponding layers are attached by discrete channels with distinct weights. In order to pass on the data through different layers, the input value of the preceding layer is multiplied by the weight of the channel attaching this neuron with the neuron of the succeeding layer. Then finally, the product of these two is added to bias, which is a numerical value assigned to the succeeding layer neurons. Our model comprises 11 input layers, 10 hidden layers, and one output layer. The number of input and output layers is upon users' discretion; however, the number of hidden layers is a variable that changes from data to data. The model is trained iteratively for the different number of hidden layers, and then the number of layers of the model with optimum accuracy are adopted.[103]. The basic architecture of the ANN model is shown in **Fig. 17**.

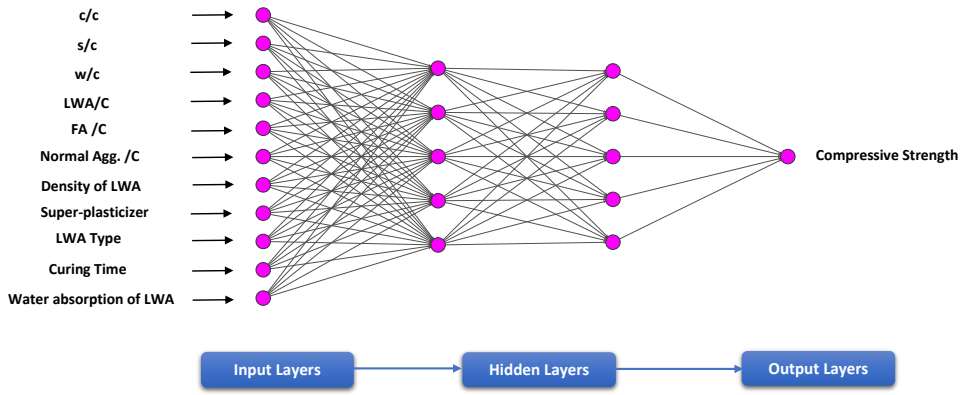

Fig. 17. Artificial neural network model.

5.3.1.2. Regression analysis

The regression analysis is a family of machine learning models which serves two primary purposes. Firstly, regression analysis is mainly used for the prediction in which their application has significant overlaps with the machine learning area. Secondly, regression analysis can identify the relationship between the dependent and independent variables [104]. According to the regression models, the independent variable 'x' predicts the dependent variable 'Y'. Regression is further classified into two main domains, linear and non-linear regression analysis. When the relationship between the dependent and independent variables is non-linear, non-linear regression analysis is performed, which is frequently the case in most of the real-world applications. Similarly, when the relationship between the dependent and independent variables is linear, linear regression analysis is performed.

$$Y = a + bx + cx^2 + dx^3 + ex^4 + \ldots\ldots \quad (3)$$

5.3.1.2.1 Support vector machine

Support vector machines (SVMs) are supervised learning models for classification and regression analysis that examine data and identify patterns. SVM differentiates cases with different class labels by developing hyperplanes in a multidimensional space. Multiple continuous and categorical variables can be handled by SVM, which allows both regression and classification tasks [105], [106].

5.3.1.2.2 Gaussian process regression

Gaussian process regression (GPR) is a Bayesian non-parametric technique that has been used widely in data-based modelling of a variety of systems, including those relevant to chemometrics. However, because it is challenging to formulate a covariance function for correlated multiple response variables that captures both the correlation between responses and the correlation between data points, most GPR implementations only simulate a single response variable [107], [108].

5.3.1.2.3 Extreme gradient boosting tree

A gradient boosting framework is used by the ensemble machine learning method XGBoost, which is decision-tree based. Artificial neural networks frequently outperform all other algorithms or frameworks in prediction issues involving unstructured data (pictures, text, etc.). However, decision tree-based algorithms are currently thought to be best-in-class for small- to medium-sized structured/tabular data [30], [106], [109].

5.3.1.2.4 Decision Tree

Decision Tree Analysis is a common, predictive modelling technique with applications bridging various areas. In general, decision trees are developed using an algorithmic method that defines how to divide a data set based on several criteria. It is among the most widespread and useful techniques for supervised learning. Decision Trees are a non-parametric supervised learning technique used for both classification and regression tasks. The aim is to learn straightforward decision rules derived from the data features to develop a model that predicts the value of a target variable [108], [110], [111].

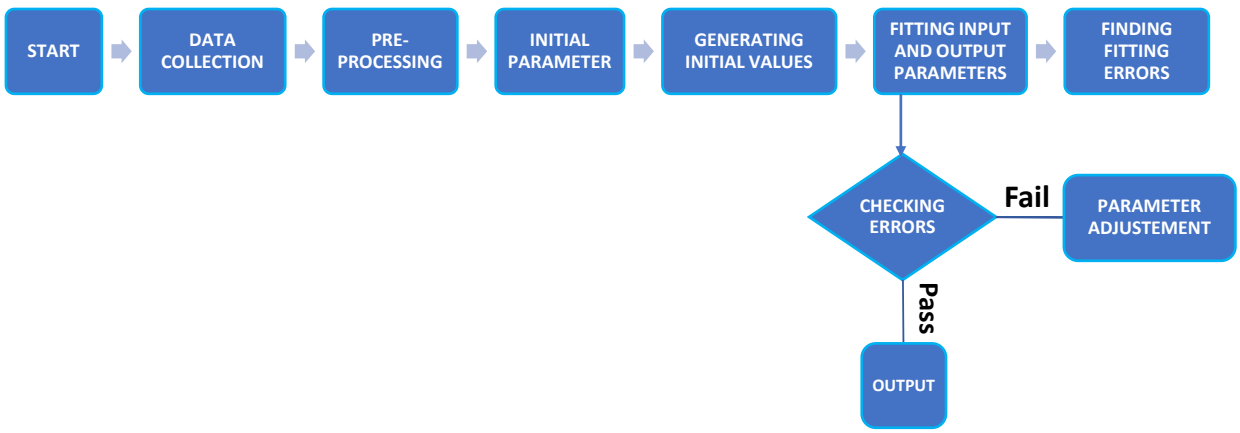

Support vector machine (SVM)

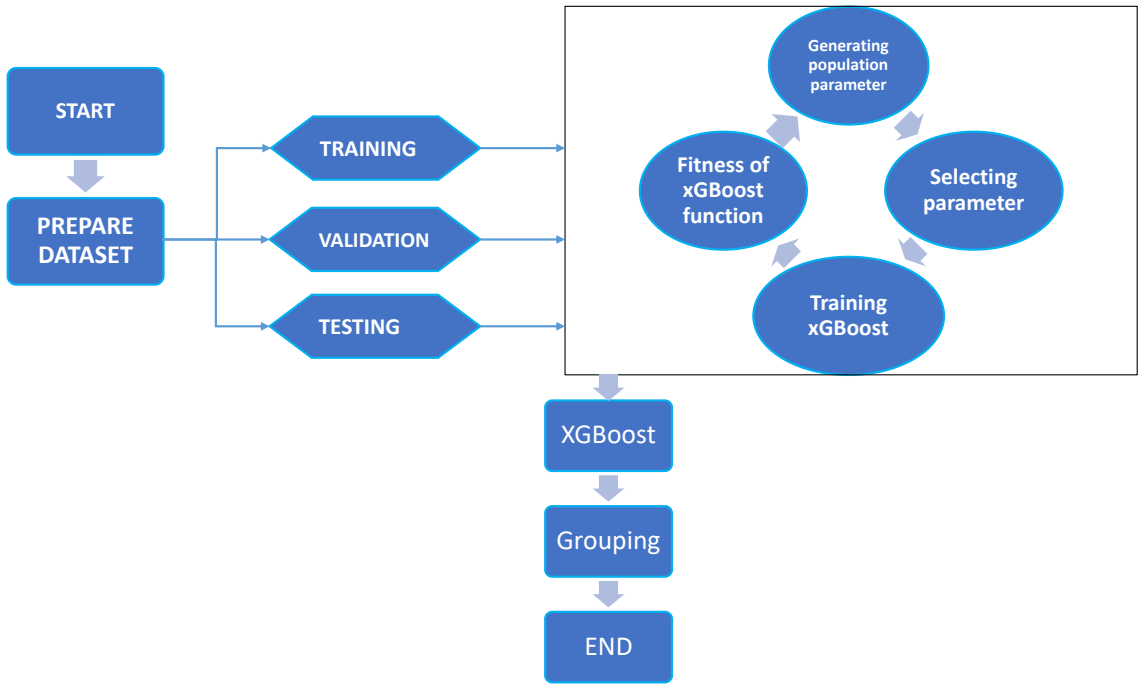

Extreme gradient boosting tree (XGBoost)

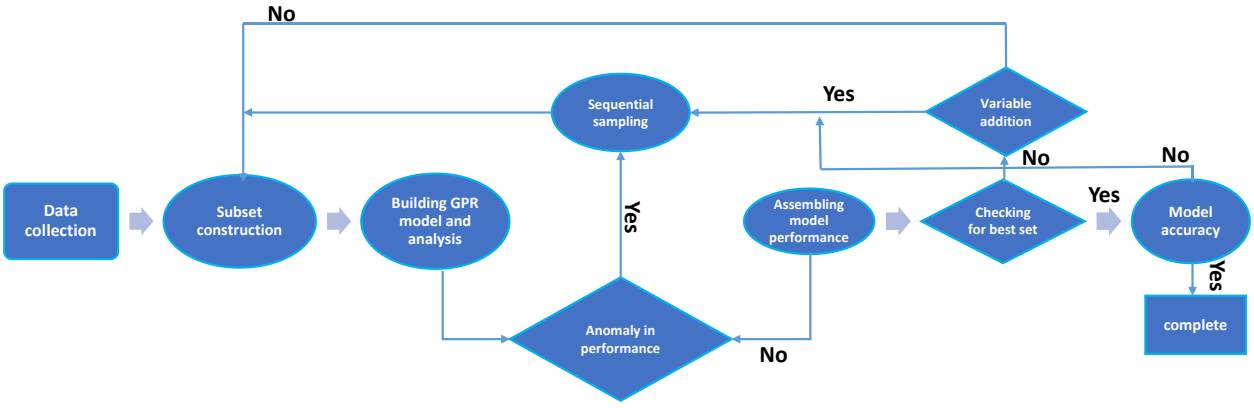

Gaussian process of regression (GPR)

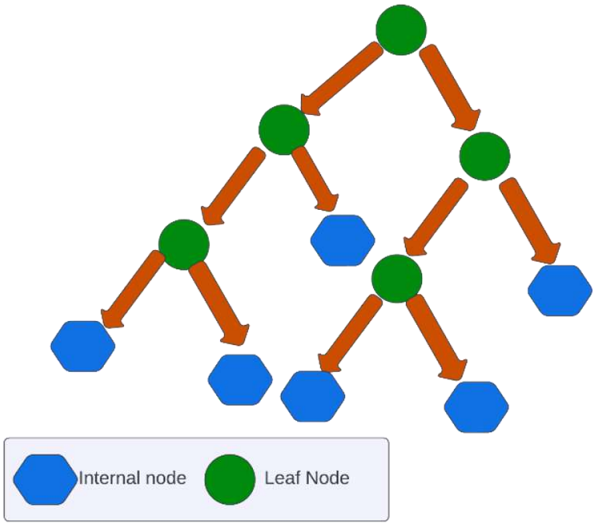

Fig. 18. Working flowcharts of Regression models.

5.4. Model development and construction

5.4.1. Anomalous data

The data were collected from the previously published literature, including hypothetical trials of the different samples. In the collected data, some points were affecting the accuracy of the trained models. These data points are outliers called anomalous data. Twenty-two such types of data points were removed, e.g., a sample that included the water/cement ratio of 1 was removed as the anomalous data considering its unrealistic nature. In the same way, 130MPa compressive strength of the lightweight aggregate concrete was reported without any additive and normal aggregate and was also included in outliers. Some data points did not even contain any lightweight aggregate, so those data points were also removed.

5.4.2. Hyperparameter tuning

Hyperparameter tuning is the setting of a learning algorithm before training any ML model. Hyperparameter tuning is an iterative process where selecting appropriate model parameters determine the model's accuracy. Model parameters vary from model to model as well as with dataset. The input variables and model parameters, such as number of hidden layers, learning rate, number of learners, leaf size, and percentage of the dataset for training, validation, testing, etc.,

were varied until the optimum model performance was achieved. Due to a large number of model parameters, only a few hyperparameters were tuned; the others were set to default. The hyperparameters of ML models that were optimized are shown in **Table 8.**

Table 8

Optimized hyperparameter for ML models.

Methods	Hyperparameters	Range	Optimum value
DT	Minimum Leaf size	1 - 50	4
SVM	Kernel Function Epsilon Kernel scale	 0.1 - 2 0.1 - 1.7	Cubic 1.6 1
XGBoost	Minimum Leaf size Number of learners Learning Rate	1-20 1-50 0.01-0.50	8 30 0.1
GPR	Kernel scale Sigma	1-80 1-15	52 12
ANN	Training algorithm Hidden Layer Size	Bayesian Regularization 1 – 40	10

5.4.3. Model performance indicators

To assess the performance of the ML models, four types of statistical performance indicators were used. The performance indicators used are root mean square error (RMSE), mean absolute error (MAE), mean square error (MSE), variance account factor (VAF), performance index (PI) and coefficient of determination R-squared (R^2). The coefficient of determination R^2 shows the variance in predicted values as compared to the actual values. The closer the value of R^2 is to 1, the higher is the accuracy of the model. On the other hand, RMSE and MSE indicate how much of the data points are converged on the regression line. MAE is also a similar measure of errors in paired observations. The formulation of the statistical performance indicators is given in **Table 8.** Where K_{pre} and K_{act} are the predicted and actual values, respectively; m refers to the total number of sample points, and $\bar{k}_{pre}$ refers to the mean of the predicted values.

Table 8.

Statistical performance indicators

$$RMSE = \sqrt{\frac{1}{m}\sum_{i=1}^{m}(k_{act} - k_{pre})^2} \qquad R^2 = 1 - \frac{\sum(k_{act} - k_{pre})^2}{\sum(k_{act} - \bar{k}_{pre})^2} \qquad MAE = \frac{\sum_{i=1}^{m}| k_{act} - k_{pre} |}{m}$$

$$MSE = \frac{\sum_{i=1}^{m}(k_{act} - k_{pre})^2}{m} \qquad VAF = (1 - \frac{\mathrm{var}(k_{act} - k_{pre})^2}{\mathrm{var}(k_{act})})x100$$

5.4.4. Training process

Rigorous and repeated model training is performed to achieve higher accuracy. The selection of appropriate parameters during the training process determines the model's accuracy. Therefore, the models were trained multiple times by changing input variables and parameters until the best model with the highest possible accuracy was obtained. **Fig. 19.** gives a basic overview of the training process for the machine learning models adopted in this research.

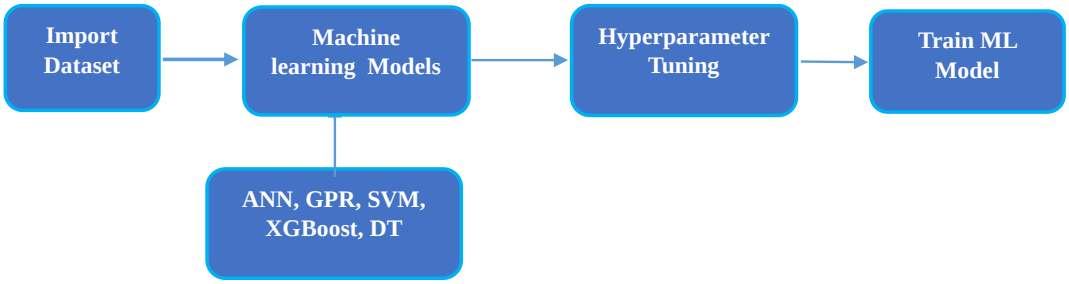

Fig. 19. The training process of ML Models.

5.5. Results and discussion

5.5.1. Predicted results and discussion

The five machine learning algorithms Support vector machine (SVM), Artificial neural network (ANN), Decision tree (DT), Gaussian process of regression (GPR), and Extreme gradient boosting tree (XGBoost) were trained and tested. The model's accuracy is measured in terms of R^2; the larger the value, the more accurate the model will be. While in the case of the RMSE, the lower the value, the greater accuracy of the model [17]. **Fig. 20.** compares the actual and predicted results of the output parameter. The trained model of GPR which outperforms all other models gives

RMSE of compressive strength for training data set 1.34, while the RMSE for testing data set is 7.79. While the model's accuracy for testing and training data set in terms of R^2 for compressive strength is 0.99 and 0.92 respectively.

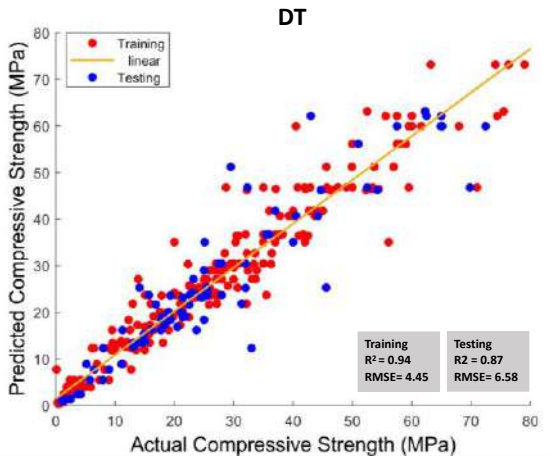

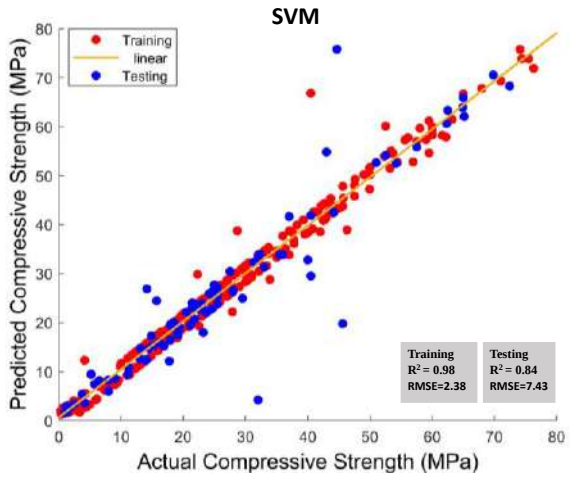

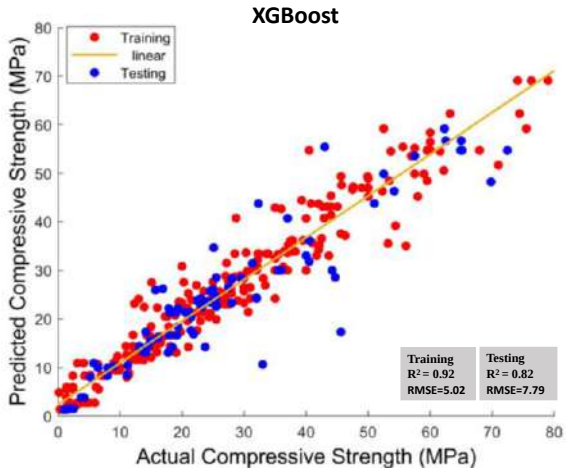

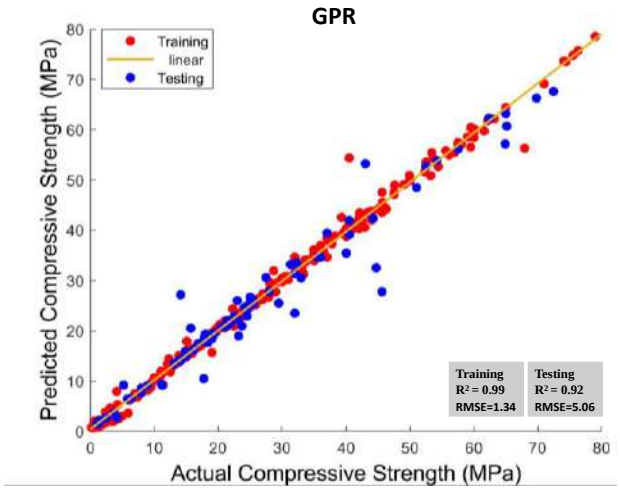

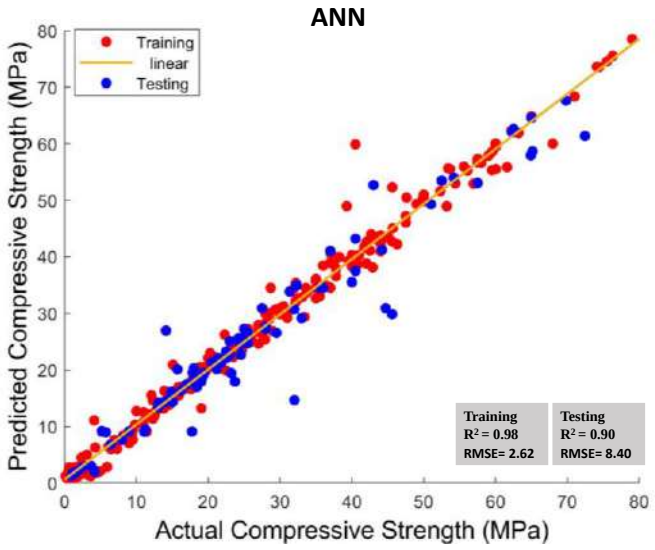

Fig. 20. Predicted vs Actual compressive strength of LWAC.

Table 9

Summary of trained models.

ML Models	Set	RMSE	R^2	MSE	MAE	VAF
DT	Training	4.45	0.94	19.78	2.68	93.81
	Testing	6.58	0.87	43.37	4.32	86.34
SVM	Training	2.38	0.98	5.64	1.58	98.29
	Testing	7.43	0.84	55.26	3.61	85.56
XGBoost	Training	5.02	0.92	25.22	3.39	92.91
	Testing	7.79	0.82	60.82	4.81	83.09
GPR	Training	1.34	0.99	1.79	0.69	99.40
	Testing	5.06	0.92	25.62	3.01	95.65
ANN	Training	2.62	0.98	6.89	1.71	98.59
	Testing	8.4	0.9	70.58	5.13	94.19

5.5.2. Rank analysis

To evaluate the overall performance of machine learning models, rank analysis is performed. Based on the results of the training and testing phases of the model, each model is rated based on the results of all statistical indices computed. The worst-performing model is ranked as having a model value of 1, while the best model is ranked as having a model value of 5. (as five models are used in this study). The total rank is then calculated in this method by adding all the individual

ratings. The model with the lowest rank is considered to be the best performing one, while the model with the highest rank is considered to be the worst performing one. The performance of the models is calculated by adding the models total rank of the training and testing set to find overall rank. As it can be seen in the **Table 10.** that the performance of the GPR model stand out of all the five models with overall rank=25. Following GPR, SVM stand as 2nd overall rank=27, DT as 3rd overall rank=29, XGBoost 4th overall rank=30, ANN 5th overall rank=39.

Table 10

Rank analysis of ML models.

ML Models	Set	RMSE	R^2	MSE	MAE	VAF	Total rank	Overall rank
DT	Training	4	2	4	4	2	16	29
	Testing	2	3	2	3	3	13	
SVM	Training	2	5	2	2	3	14	27
	Testing	3	2	4	2	2	13	
XGBoost	Training	5	1	5	5	1	17	30
	Testing	4	1	3	4	1	13	
GPR	Training	1	4	1	1	5	12	25
	Testing	1	5	1	1	5	13	
ANN	Training	3	3	3	3	4	16	39
	Testing	5	4	5	5	4	23	

5.5.3 Model performance analysis

Since it is evident from **Table. 9** that the GPR model was found to be the best fit for forecasting the compressive strength of lightweight aggregate concrete and a separate dataset was used to validate the predictive model. This data was not included during the model's training and testing process. The output (compressive strength) was monitored by varying the type of LWA, the density of LWA, and the water absorption of LWA, which is the prime input of the model. The results were highly encouraging, and the predicted compressive strength was almost the same as that was published in the literature. The summary of validation and the comparison of the predicted and actual data are shown in **Fig. 21.**

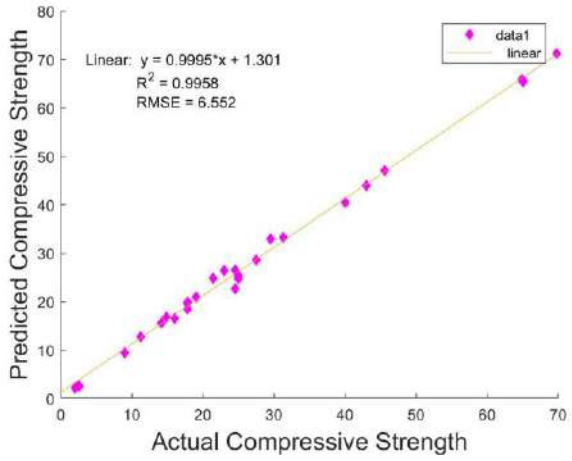

Fig. 21 Comparison of prediction using GPR model against the testing values.

5.6. Conclusions

This study used different machine learning tools to develop an optimized compressive strength predictive model of sustainable lightweight aggregate concrete including lightweight aggregate characteristics with 420 data points. Five ML models were trained with 11 input parameters and one compressive strength output.

- For the development of machine learning model's dataset was divided into three parts training, testing and validation.
- A detail statistical analysis was performed on the dataset to make it coherent before training the machine learning models.
- The statistical indicators were used to evaluate the performance of ML models, including root mean square error (RMSE), mean absolute error (MAE), mean square error (MSE) and coefficient of determination R-squared (R^2).
- To enhance the accuracy of the predictive models optimal hyperparameter tunning was done during the training process. After hyperparameter tuning, an optimized machine learning Gaussian process of regression model for compressive strength prediction of sustainable lightweight aggregate concrete was developed.

- The R^2 and RMSE of the GPR model were above 0.99 and 1.34, respectively, indicating that the GPR model exhibited better performance in predicting the compressive strength of lightweight aggregate concrete.
- It is therefore concluded that extensive, uneconomical, and time-consuming work of finding an optimum mix design can be replaced by using these ML algorithms with maximum accuracy to predict the compressive strength of LWAC.

Reference

[1] F. K. Alqahtani, "Sustainable green lightweight concrete containing plastic-based green lightweight aggregate," *Materials*, vol. 14, no. 12, 2021, doi: 10.3390/ma14123304.

[2] S. N. Vandanapu and M. Krishnamurthy, "Seismic Performance of Lightweight Concrete Structures," *Advances in Civil Engineering*, vol. 2018, 2018, doi: 10.1155/2018/2105784.

[3] A. Sadrmomtazi, J. Sobhani, and M. A. Mirgozar, "Modeling compressive strength of EPS lightweight concrete using regression, neural network and ANFIS," *Constr Build Mater*, vol. 42, pp. 205–216, 2013, doi: 10.1016/j.conbuildmat.2013.01.016.

[4] A. Karbassi, B. Mohebi, S. Rezaee, and P. Lestuzzi, "Damage prediction for regular reinforced concrete buildings using the decision tree algorithm," *Comput Struct*, vol. 130, pp. 46–56, 2014, doi: 10.1016/j.compstruc.2013.10.006.

[5] I. B. Topqu, "Lightweight concretes produced by volcanic slags," *Cem Concr Res*, vol. 27, no. 1, pp. 15–21, 1997.

[6] A. Bilodeau, V. K. R. Kodur, and G. C. Hoff, "Optimization of the type and amount of polypropylene fibres for preventing the spalling of lightweight concrete subjected to hydrocarbon fire," *Cem Concr Compos*, vol. 26, no. 2, pp. 163–174, 2004, doi: 10.1016/S0958-9465(03)00085-4.

[7] O. Kayali, M. N. Haque, and B. Zhu, "Some characteristics of high strength fiber reinforced lightweight aggregate concrete," *Cem Concr Compos*, vol. 25, no. 2, pp. 207–213, 2003, doi: 10.1016/S0958-9465(02)00016-1.

[8] K. S. Al-Jabri, A. W. Hago, A. S. Al-Nuaimi, and A. H. Al-Saidy, "Concrete blocks for thermal insulation in hot climate," *Cem Concr Res*, vol. 35, no. 8, pp. 1472–1479, 2005, doi: 10.1016/j.cemconres.2004.08.018.

[9] R. Şahin, R. Demirboğa, H. Uysal, and R. Gül, "The effects of different cement dosages, slumps and pumice aggregate ratios on the compressive strength and densities of concrete," *Cem Concr Res*, vol. 33, no. 8, pp. 1245–1249, 2003, doi: 10.1016/S0008-8846(03)00048-6.

[10] H. Al-Khaiat and M. N. Haque, "Effect of Initial Curing on Early Strength and Physical," *Cem Concr Res*, vol. 28, no. 6, pp. 859–866, 1998.

[11] H. Wei, T. Wu, and X. Yang, "Properties of lightweight aggregate concrete reinforced with carbon and/or polypropylene fibers," *Materials*, vol. 13, no. 3, 2020, doi: 10.3390/ma13030640.

[12] Y. B. Jung and K. H. Yang, "CO2 emission assessment of lightweight aggregate concrete using artificial lightweight and bottom ash particles," *J Mater Cycles Waste Manag*, vol. 24, no. 6, pp. 2172–2182, Nov. 2022, doi: 10.1007/s10163-022-01469-8.

[13] F. Faleschini, K. Brunelli, M. A. Zanini, M. Dabalà, and C. Pellegrino, "Electric Arc Furnace Slag as Coarse Recycled Aggregate for Concrete Production," *Journal of Sustainable Metallurgy*, vol. 2, no. 1, pp. 44–50, Mar. 2016, doi: 10.1007/S40831-015-0029-1/FIGURES/7.

[14] A. Kumar, Dr. S. Yadav, A. Kumar, and Dr. S. Yadav, "USE OF CRUMB RUBBER AS FINE AGGREGATE IN CONCRETE TO INCREASE THE STRENGTH OF CONCRETE BLOCK," *JETIR*, vol. 4, no. 11, pp. 150–155, 2017, Accessed: Dec. 15, 2022. [Online]. Available: https://www.jetir.org/view?paper=JETIR1711026

[15] "USING CRUMB RUBBER AS LIGHTWEIGHT AGGREGATE IN STRUCTURAL CONCRETE Lab Report Example | Topics and Well Written Essays - 8000 words." https://studentshare.org/engineering-and-construction/1879252-using-crumb-rubber-as-lightweight-aggregate-in-structural-concrete (accessed Dec. 15, 2022).

[16] Subandi, R. H. Cahyono, C. Kusuma, and M. N. Asnan, "Artificial aggregate lightweight structural," *Annales de Chimie: Science des Materiaux*, vol. 43, no. 4, pp. 213–216, 2019, doi: 10.18280/ACSM.430403.

[17] A. Sarabèr, R. Overhof, T. Green, and J. Pels, "Artificial lightweight aggregates as utilization for future ashes - A case study," *Waste Management*, vol. 32, no. 1, pp. 144–152, Jan. 2012, doi: 10.1016/j.wasman.2011.08.017.

[18] K. Shaiksha Vali and S. Bala Murugan, "Impact of manufactured fiber aggregate in the production of lightweight concrete," *Mater Today Proc*, no. xxxx, 2022, doi: 10.1016/j.matpr.2022.04.712.

[19] F. Zulkarnain and M. Ramli, "Durability Performance of Lightweight Aggregate," no. Icbedc, pp. 541–551, 2008.

[20] J. M. Chi, R. Huang, C. C. Yang, and J. J. Chang, "Effect of aggregate properties on the strength and stiffness of lightweight concrete," *Cem Concr Compos*, vol. 25, no. 2, pp. 197–205, 2003, doi: 10.1016/S0958-9465(02)00020-3.

[21] A. Ahmad *et al.*, "Prediction of geopolymer concrete compressive strength using novel machine learning algorithms," *Polymers (Basel)*, vol. 13, no. 19, Oct. 2021, doi: 10.3390/polym13193389.

[22] D. C. Feng *et al.*, "Machine learning-based compressive strength prediction for concrete: An adaptive boosting approach," *Constr Build Mater*, vol. 230, p. 117000, 2020, doi: 10.1016/j.conbuildmat.2019.117000.

[23] J. Y. Yoon, H. Kim, Y. J. Lee, and S. H. Sim, "Prediction model for mechanical properties of lightweight aggregate concrete using artificial neural network," *Materials*, vol. 12, no. 7, 2019, doi: 10.3390/ma12172678.

[24] A. J. Tenza-Abril, Y. Villacampa, A. M. Solak, and F. Baeza-Brotons, "Prediction and sensitivity analysis of compressive strength in segregated lightweight concrete based on artificial neural network using ultrasonic pulse velocity," *Constr Build Mater*, vol. 189, pp. 1173–1183, 2018, doi: 10.1016/j.conbuildmat.2018.09.096.

[25] M. Nikoo, F. Torabian Moghadam, and Ł. Sadowski, "Prediction of concrete compressive strength by evolutionary artificial neural networks," *Advances in Materials Science and Engineering*, vol. 2015, 2015, doi: 10.1155/2015/849126.

[26] R. Sarkhani Benemaran, M. Esmaeili-Falak, and A. Javadi, "Predicting resilient modulus of flexiblepavement foundation using extreme gradient boosting based optimised models," *International Journal of Pavement Engineering*, 2022, doi: 10.1080/10298436.2022.2095385.

[27] J. De-Prado-gil, O. Zaid, C. Palencia, and R. Martínez-García, "Prediction of Splitting Tensile Strength of Self-Compacting Recycled Aggregate Concrete Using Novel Deep Learning Methods," *Mathematics*, vol. 10, no. 13, Jul. 2022, doi: 10.3390/math10132245.

[28] J. De-Prado-gil, C. Palencia, P. Jagadesh, and R. Martínez-García, "A Comparison of Machine Learning Tools that Model the Splitting Tensile Strength of Self-Compacting Recycled Aggregate Concrete," *Materials*, vol. 15, no. 12, Jun. 2022, doi: 10.3390/ma15124164.

[29] A. Karbassi, B. Mohebi, S. Rezaee, and P. Lestuzzi, "Damage prediction for regular reinforced concrete buildings using the decision tree algorithm," *Comput Struct*, vol. 130, pp. 46–56, 2014, doi: 10.1016/j.compstruc.2013.10.006.

[30] J. De-Prado-gil, C. Palencia, P. Jagadesh, and R. Martínez-García, "A Comparison of Machine Learning Tools that Model the Splitting Tensile Strength of Self-Compacting Recycled Aggregate Concrete," *Materials*, vol. 15, no. 12, Jun. 2022, doi: 10.3390/ma15124164.

[31] F. Aslam *et al.*, "Applications of Gene Expression Programming for Estimating Compressive Strength of High-Strength Concrete," *Advances in Civil Engineering*, vol. 2020, 2020, doi: 10.1155/2020/8850535.

[32] R. Siddique, P. Aggarwal, and Y. Aggarwal, “Prediction of compressive strength of self-compacting concrete containing bottom ash using artificial neural networks,” *Advances in Engineering Software*, vol. 42, no. 10, pp. 780–786, 2011, doi: 10.1016/j.advengsoft.2011.05.016.

[33] S. Chithra, S. R. R. S. Kumar, K. Chinnaraju, and F. Alfin Ashmita, “A comparative study on the compressive strength prediction models for High Performance Concrete containing nano silica and copper slag using regression analysis and Artificial Neural Networks,” *Constr Build Mater*, vol. 114, pp. 528–535, 2016, doi: 10.1016/j.conbuildmat.2016.03.214.

[34] R. Vinoth and M. Vinod Kumar, “Strength and durability performance of Light Weight Self-Compacting Concrete (LWSCC) with Light Expanded Clay Aggregate (LECA),” *IOP Conf Ser Mater Sci Eng*, vol. 872, no. 1, 2020, doi: 10.1088/1757-899X/872/1/012104.

[35] S. Lanka and S. Lanka, “Lightweight Non-Load Bearing Blocks Using Expanded Polystyrene Beads”.

[36] M. Y. Vahabi, B. Tahmouresi, H. Mosavi, and S. Fakhretaha Aval, “Effect of pre-coating lightweight aggregates on the self-compacting concrete,” *Structural Concrete*, no. November 2020, pp. 1–12, 2021, doi: 10.1002/suco.202000744.

[37] Y. Askari Dolatabad, B. Abolpour, and M. A. J. Tazangi, “Investigating effects of Nano particles of silica on the properties of self-compacting concrete containing Perlite, Leca, and Scoria light weight aggregates,” *Arabian Journal of Geosciences*, vol. 14, no. 10, 2021, doi: 10.1007/s12517-021-07233-w.

[38] S. Dong, W. Yang, Y. Ge, S. Jiang, T. Sun, and J. Deng, “Mechanical Properties of Concrete Containing Ceramsite Sand,” *ICTE 2015 - Proceedings of the 5th International Conference on Transportation Engineering*, pp. 1259–1265, 2015, doi: 10.1061/9780784479384.158.

[39] M. S. Moayeri, H. R. Ashrafi, and P. Beiranvand, “Investigating the physical characteristics of non-structural lightweight aggregate blocks of built with region materials,” *Buildings*, vol. 7, no. 1, 2017, doi: 10.3390/buildings7010002.

[40] Q. Du, Q. Sun, J. Lv, and J. Yang, “Use of Preplaced Casting Method in Lightweight Aggregate Concrete,” *Advances in Materials Science and Engineering*, vol. 2017, no. Cc, 2017, doi: 10.1155/2017/7234761.

[41] H. A. Numan, M. H. Yaseen, and H. A. M. S. Al-Juboori, “Comparison Mechanical Properties of Two Types of Light Weight Aggregate Concrete,” *Civil Engineering Journal*, vol. 5, no. 5, pp. 1105–1118, 2019, doi: 10.28991/cej-2019-03091315.

[42] H.-J. Chen, C.-H. Huang, and C.-W. Tang, “Dynamic Properties of Lightweight Concrete Beams Made by Sedimentary Lightweight Aggregate,” *Journal of Materials in Civil Engineering*, vol. 22, no. 6, pp. 599–606, 2010, doi: 10.1061/(asce)mt.1943-5533.0000061.

[43] N. N. Hilal, “Hardened properties of self-compacting concrete with different crumb rubber size and content,” *International Journal of Sustainable Built Environment*, vol. 6, no. 1, pp. 191–206, 2017, doi: 10.1016/j.ijsbe.2017.03.001.

[44] S. A. Almawla, M. K. Mohammed, and A. I. Al-Hadithi, “Fresh and mechanical properties of self-compacting lightweight concrete containing ponza aggregates,” *Proceedings - International Conference on Developments in eSystems Engineering, DeSE*, vol. October-2019, pp. 100–104, 2019, doi: 10.1109/DeSE.2019.00028.

[45] L. Zhu, F. Dang, Y. Xue, W. Ding, and K. Jiao, “Experimental investigation of the thermal and mechanical properties of lightweight aggregate concrete mixed with microencapsulated phase change materials,” *Int J Energy Res*, vol. 45, no. 9, pp. 12864–12878, 2021, doi: 10.1002/er.6617.

[46] K. S. Elango, D. Vivek, S. Anandaraj, R. Saravanakumar, J. Sanfeer, and S. Saravanaganesh, “Experimental study on self compacting concrete using light weight aggregate,” *Mater Today Proc*, vol. 60, no. xxxx, pp. 1362–1366, 2022, doi: 10.1016/j.matpr.2021.10.240.

[47] R. Ahmmad, U. J. Alengaram, M. Z. Jumaat, N. H. R. Sulong, M. O. Yusuf, and M. A. Rehman, "Feasibility study on the use of high volume palm oil clinker waste in environmental friendly lightweight concrete," *Constr Build Mater*, vol. 135, pp. 94–103, 2017, doi: 10.1016/j.conbuildmat.2016.12.098.

[48] H. Zhang, L. Huang, L. Yu, and Z. Yang, "Macromechanical Properties and ITZ of Lightweight Aggregate Concrete from the Deck of Nanjing Yangtze River Bridge after 50 Years," *Journal of Materials in Civil Engineering*, vol. 32, no. 5, p. 05020005, 2020, doi: 10.1061/(asce)mt.1943-5533.0003126.

[49] A. Radlińska, M. Kaszyńska, A. Zieliński, and H. Ye, "Early-Age Cracking of Self-Consolidating Concrete with Lightweight and Normal Aggregates," *Journal of Materials in Civil Engineering*, vol. 30, no. 10, p. 04018242, 2018, doi: 10.1061/(asce)mt.1943-5533.0002407.

[50] S. M. F. Green, N. J. Brooke, L. G. McSaveney, and J. M. Ingham, "Mixture Design Development and Performance Verification of Structural Lightweight Pumice Aggregate Concrete," *Journal of Materials in Civil Engineering*, vol. 23, no. 8, pp. 1211–1219, 2011, doi: 10.1061/(asce)mt.1943-5533.0000280.

[51] K.-H. Yang, J.-H. Mun, J.-I. Sim, and J.-K. Song, "Effect of Water Content on the Properties of Lightweight Alkali-Activated Slag Concrete," *Journal of Materials in Civil Engineering*, vol. 23, no. 6, pp. 886–894, 2011, doi: 10.1061/(asce)mt.1943-5533.0000244.

[52] K. M. A. Hossain, S. Ahmed, and M. Lachemi, "Lightweight concrete incorporating pumice based blended cement and aggregate: Mechanical and durability characteristics," *Constr Build Mater*, vol. 25, no. 3, pp. 1186–1195, 2011, doi: 10.1016/j.conbuildmat.2010.09.036.

[53] O. Fatahi and S. Jafari, "Prediction of Lightweight Aggregate Concrete Compressive Strength," *Journal of Rehabilitation in Civil Engineering*, vol. 6, no. 2, pp. 45–57, 2018, doi: 10.22075/jrce.2017.11556.1192.

[54] A. Bicer, "The effect of fly ash and pine tree resin on thermo-mechanical properties of concretes with expanded clay aggregates," *Case Studies in Construction Materials*, vol. 15, no. May, p. e00624, 2021, doi: 10.1016/j.cscm.2021.e00624.

[55] A. M. Hameed and B. A. F. Ahmed, "Employment the plastic waste to produce the light weight concrete," *Energy Procedia*, vol. 157, no. January, pp. 30–38, 2019, doi: 10.1016/j.egypro.2018.11.160.

[56] P. Shafigh, M. Z. Jumaat, and H. Mahmud, "Mix design and mechanical properties of oil palm shell lightweight aggregate concrete: A review," *International Journal of Physical Sciences*, vol. 5, no. 14, pp. 2127–2134, 2010.

[57] H. K. Adai Al-Farttoosi, O. A. Abdulrazzaq, and H. K. Hussain, "Mechanical Properties of Light Weight Aggregate Concrete Using Pumice as a Coarse Aggregate," *IOP Conf Ser Mater Sci Eng*, vol. 1090, no. 1, p. 012106, 2021, doi: 10.1088/1757-899x/1090/1/012106.

[58] L. Domagała and E. Bryła, "The properties of lightweight aggregates pre-coated with cement pastes and their suitability for concrete," *Materials*, vol. 14, no. 21, 2021, doi: 10.3390/ma14216417.

[59] R. S. Szydłowski and B. Łabuzek, "Experimental evaluation of shrinkage, creep and prestress losses in lightweight aggregate concrete with sintered fly ash," *Materials*, vol. 14, no. 14, 2021, doi: 10.3390/ma14143895.

[60] S. S. Park, Y. long Hou, J. C. Lee, and S. W. Jeong, "Mechanical properties of concrete with bamboo chips," *Applied Sciences (Switzerland)*, vol. 9, no. 16, 2019, doi: 10.3390/app9163367.

[61] L. Domagała, "Durability of structural lightweight concrete with sintered fly ash aggregate," *Materials*, vol. 13, no. 20, pp. 1–20, 2020, doi: 10.3390/ma13204565.

[62] J. Lv *et al.*, "A new composite slab using crushed waste tires as fine aggregate in self-compacting lightweight aggregate concrete," *Materials*, vol. 13, no. 11, 2020, doi: 10.3390/ma13112551.

[63] H. Temperature, "Performance Degradation and Microscopic Analysis," 2020.

[64] L. Domagala, "Size effect in compressive strength tests of cored specimens of lightweight aggregate concrete," *Materials*, vol. 13, no. 5, 2020, doi: 10.3390/ma13051187.

[65] A. Petrella, R. Di Mundo, and M. Notarnicola, “Recycled expanded polystyrene as lightweight aggregate for environmentally sustainable cement conglomerates,” *Materials*, vol. 13, no. 4, 2020, doi: 10.3390/ma13040988.

[66] P. A and J. De Rose D, “Application of Light Expanded Clay Aggregate as Replacement of Coarse Aggregate in Concrete Pavement,” *International Journal of Engineering & Technology*, vol. 7, no. 4.2, p. 1, 2018, doi: 10.14419/ijet.v7i4.2.19974.

[67] G. Kim, G. Choe, M. Yoon, and T. Lee, “Mechanical properties of light weight concrete at elevated temperature,” *International Journal of Precision Engineering and Manufacturing*, vol. 16, no. 8, pp. 1867–1874, 2015, doi: 10.1007/s12541-015-0243-6.

[68] Y. Chen, Y. Deng, and Y. Liu, “Carrier and Delayed Release Properties of Lightweight Aggregates for Chemical Admixtures,” *Journal of Highway and Transportation Research and Development (English Edition)*, vol. 10, no. 3, pp. 67–73, 2016, doi: 10.1061/jhtrcq.0000520.

[69] M. S. Al-Lami and E. Abdul-Majeed Al-saadi, “The relationships between compressive strength and density of polystyrene lightweight concrete and their component ratios,” *Journal of Applied Engineering Science*, vol. 19, no. 1, pp. 175–185, 2021, doi: 10.5937/jaes0-27471.

[70] M. N. A. Ahmad Zawawi, K. Muthusamy, A. P.P. Abdul Majeed, R. Muazu Musa, and A. Mokhtar Albshir Budiea, “Mechanical properties of oil palm waste lightweight aggregate concrete with fly ash as fine aggregate replacement,” *Journal of Building Engineering*, vol. 27, no. August 2019, p. 100924, 2020, doi: 10.1016/j.jobe.2019.100924.

[71] H. Z. Cui, T. Y. Lo, S. A. Memon, and W. Xu, “Effect of lightweight aggregates on the mechanical properties and brittleness of lightweight aggregate concrete,” *Constr Build Mater*, vol. 35, pp. 149–158, 2012, doi: 10.1016/j.conbuildmat.2012.02.053.

[72] T. Parhizkar, M. Najimi, and A. R. Pourkhorshidi, “Application of pumice aggregate in structural lightweight concrete,” *Asian Journal of Civil Engineering*, vol. 13, no. 1, pp. 43–54, 2012.

[73] S. M. Samareh Hashemi, “Experimental study on mechanical properties of different lightweight aggregate concretes,” *Engineering Solid Mechanics*, vol. 2, no. 3, pp. 201–208, 2014, doi: 10.5267/j.esm.2014.4.003.

[74] R. Vijayalakshmi and S. Ramanagopal, “Structural concrete using expanded clay aggregate: a review,” *Indian J Sci Technol*, vol. 11, no. 16, pp. 1–12, 2018, doi: 10.17485/ijst/2018/v11i16/121888.

[75] I. Azim *et al.*, “Prediction model for compressive arch action capacity of RC frame structures under column removal scenario using gene expression programming,” *Structures*, vol. 25, no. March, pp. 212–228, 2020, doi: 10.1016/j.istruc.2020.02.028.

[76] A. H. Gandomi, A. Faramarzifar, P. G. Rezaee, A. Asghari, and S. Talatahari, “New design equations for elastic modulus of concrete using multi expression programming,” *Journal of Civil Engineering and Management*, vol. 21, no. 6, pp. 761–774, 2015, doi: 10.3846/13923730.2014.893910.

[77] V. Quan Tran, V. Quoc Dang, and L. Si Ho, “Evaluating compressive strength of concrete made with recycled concrete aggregates using machine learning approach,” *Constr Build Mater*, vol. 323, no. November 2021, p. 126578, 2022, doi: 10.1016/j.conbuildmat.2022.126578.

[78] M. A. DeRousseau, E. Laftchiev, J. R. Kasprzyk, B. Rajagopalan, and W. V. Srubar, “A comparison of machine learning methods for predicting the compressive strength of field-placed concrete,” *Constr Build Mater*, vol. 228, p. 116661, 2019, doi: 10.1016/j.conbuildmat.2019.08.042.

[79] R. E.-K. Penido, R. C. F. da Paixão, L. C. B. Costa, R. A. F. Peixoto, A. A. Cury, and J. C. Mendes, “Predicting the compressive strength of steelmaking slag concrete with machine learning – Considerations on developing a mix design tool,” *Constr Build Mater*, vol. 341, no. May, p. 127896, 2022, doi: 10.1016/j.conbuildmat.2022.127896.

[80] A. Çalışkan, S. Demirhan, and R. Tekin, “Comparison of different machine learning methods for estimating compressive strength of mortars,” *Constr Build Mater*, vol. 335, no. February, 2022, doi: 10.1016/j.conbuildmat.2022.127490.

[81] A. Ghosh and G. D. Ransinchung R.N., "Application of machine learning algorithm to assess the efficacy of varying industrial wastes and curing methods on strength development of geopolymer concrete," *Constr Build Mater*, vol. 341, no. May, p. 127828, 2022, doi: 10.1016/j.conbuildmat.2022.127828.

[82] K. T. Nguyen, Q. D. Nguyen, T. A. Le, J. Shin, and K. Lee, "Analyzing the compressive strength of green fly ash based geopolymer concrete using experiment and machine learning approaches," *Constr Build Mater*, vol. 247, p. 118581, 2020, doi: 10.1016/j.conbuildmat.2020.118581.

[83] Z. Zeng *et al.*, "Accurate prediction of concrete compressive strength based on explainable features using deep learning," *Constr Build Mater*, vol. 329, no. February, p. 127082, 2022, doi: 10.1016/j.conbuildmat.2022.127082.

[84] M. C. Kang, D. Y. Yoo, and R. Gupta, "Machine learning-based prediction for compressive and flexural strengths of steel fiber-reinforced concrete," *Constr Build Mater*, vol. 266, p. 121117, 2021, doi: 10.1016/j.conbuildmat.2020.121117.

[85] E. Asadi Shamsabadi, N. Roshan, S. A. Hadigheh, M. L. Nehdi, A. Khodabakhshian, and M. Ghalehnovi, "Machine learning-based compressive strength modelling of concrete incorporating waste marble powder," *Constr Build Mater*, vol. 324, no. February, p. 126592, 2022, doi: 10.1016/j.conbuildmat.2022.126592.

[86] B. A. Salami, T. Olayiwola, T. A. Oyehan, and I. A. Raji, "Data-driven model for ternary-blend concrete compressive strength prediction using machine learning approach," *Constr Build Mater*, vol. 301, no. May, p. 124152, 2021, doi: 10.1016/j.conbuildmat.2021.124152.

[87] B. Hilloulin and V. Q. Tran, "Using machine learning techniques for predicting autogenous shrinkage of concrete incorporating superabsorbent polymers and supplementary cementitious materials," *Journal of Building Engineering*, vol. 49, no. January, p. 104086, 2022, doi: 10.1016/j.jobe.2022.104086.

[88] H. Zhang, X. Cheng, Y. Li, and X. Du, "Prediction of failure modes, strength, and deformation capacity of RC shear walls through machine learning," *Journal of Building Engineering*, vol. 50, no. February, 2022, doi: 10.1016/j.jobe.2022.104145.

[89] M. Mirrashid and H. Naderpour, "Computational intelligence-based models for estimating the fundamental period of infilled reinforced concrete frames," *Journal of Building Engineering*, vol. 46, no. June 2021, p. 103456, 2022, doi: 10.1016/j.jobe.2021.103456.

[90] Z. Lv, A. Jiang, J. Jin, and X. Lv, "Multifractal Analysis and Compressive Strength Prediction for Concrete through Acoustic Emission Parameters," *Advances in Civil Engineering*, vol. 2021, 2021, doi: 10.1155/2021/6683878.

[91] T. Al-Mughanam, T. H. H. Aldhyani, B. Alsubari, and M. Al-Yaari, "Modeling of compressive strength of sustainable self-compacting concrete incorporating treated palm oil fuel ash using artificial neural network," *Sustainability (Switzerland)*, vol. 12, no. 22, pp. 1–13, 2020, doi: 10.3390/su12229322.

[92] D. Van Dao, H. B. Ly, H. L. T. Vu, T. T. Le, and B. T. Pham, "Investigation and optimization of the C-ANN structure in predicting the compressive strength of foamed concrete," *Materials*, vol. 13, no. 5, pp. 1–17, 2020, doi: 10.3390/ma13051072.

[93] R. Bušić, M. Benšić, I. Miličević, and K. Strukar, "Prediction models for the mechanical properties of self-compacting concrete with recycled rubber and silica fume," *Materials*, vol. 13, no. 8, 2020, doi: 10.3390/MA13081821.

[94] S. Selvaraj and S. Sivaraman, "Prediction model for optimized self-compacting concrete with fly ash using response surface method based on fuzzy classification," *Neural Comput Appl*, vol. 31, no. 5, pp. 1365–1373, 2019, doi: 10.1007/s00521-018-3575-1.

[95] A. Kaveh, T. Bakhshpoori, and S. M. Hamze-Ziabari, "M5' and mars based prediction models for properties of selfcompacting concrete containing fly ash," *Periodica Polytechnica Civil Engineering*, vol. 62, no. 2, pp. 281–294, 2018, doi: 10.3311/PPci.10799.

[96] S. Fakhrian, H. Behbahani, and S. Mashhadi, "Predicting post-fire behavior of green geopolymer mortar containing recycled concrete aggregate via gep approach," *Journal of Soft Computing in Civil Engineering*, vol. 4, no. 2, pp. 22–45, 2020, doi: 10.22115/SCCE.2020.220919.1182.

[97] M. I. Shah, M. F. Javed, F. Aslam, and H. Alabduljabbar, “Machine learning modeling integrating experimental analysis for predicting the properties of sugarcane bagasse ash concrete,” *Constr Build Mater*, vol. 314, no. PA, p. 125634, 2022, doi: 10.1016/j.conbuildmat.2021.125634.

[98] A. K. Al-Shamiri, J. H. Kim, T. F. Yuan, and Y. S. Yoon, “Modeling the compressive strength of high-strength concrete: An extreme learning approach,” *Constr Build Mater*, vol. 208, pp. 204–219, 2019, doi: 10.1016/j.conbuildmat.2019.02.165.

[99] P. Pereira Dias, L. Bhagya Jayasinghe, and D. Waldmann, “Machine learning in mix design of Miscanthus lightweight concrete,” *Constr Build Mater*, vol. 302, p. 124191, 2021, doi: 10.1016/j.conbuildmat.2021.124191.

[100] L. V. Zhang, A. Marani, and M. L. Nehdi, “Chemistry-informed machine learning prediction of compressive strength for alkali-activated materials,” *Constr Build Mater*, vol. 316, no. November 2021, p. 126103, 2022, doi: 10.1016/j.conbuildmat.2021.126103.

[101] I. Nunez, A. Marani, M. Flah, and M. L. Nehdi, “Estimating compressive strength of modern concrete mixtures using computational intelligence: A systematic review,” *Constr Build Mater*, vol. 310, no. June, p. 125279, 2021, doi: 10.1016/j.conbuildmat.2021.125279.

[102] F. Khademi, S. M. Jamal, N. Deshpande, and S. Londhe, “Predicting strength of recycled aggregate concrete using Artificial Neural Network, Adaptive Neuro-Fuzzy Inference System and Multiple Linear Regression,” *International Journal of Sustainable Built Environment*, vol. 5, no. 2, pp. 355–369, 2016, doi: 10.1016/j.ijsbe.2016.09.003.

[103] A. Hajnayeb, A. Ghasemloonia, S. E. Khadem, and M. H. Moradi, “Application and comparison of an ANN-based feature selection method and the genetic algorithm in gearbox fault diagnosis,” *Expert Syst Appl*, vol. 38, no. 8, pp. 10205–10209, 2011, doi: 10.1016/j.eswa.2011.02.065.

[104] D. Maulud and A. M. Abdulazeez, “A Review on Linear Regression Comprehensive in Machine Learning,” *Journal of Applied Science and Technology Trends*, vol. 1, no. 4, pp. 140–147, 2020, doi: 10.38094/jastt1457.

[105] “Machine Learning Techniques.” https://bookdown.org/jhvdz1/ml2/ (accessed Dec. 15, 2022).

[106] M. Mohtasham Moein *et al.*, “Predictive models for concrete properties using machine learning and deep learning approaches: A review,” *Journal of Building Engineering*, vol. 63. Elsevier Ltd, Jan. 01, 2023. doi: 10.1016/j.jobe.2022.105444.

[107] T. Chen and J. Ren, “Bagging for Gaussian process regression,” *Neurocomputing*, vol. 72, no. 7–9, pp. 1605–1610, Mar. 2009, doi: 10.1016/j.neucom.2008.09.002.

[108] Y. Xu, Y. Zhou, P. Sekula, and L. Ding, “Machine learning in construction: From shallow to deep learning,” *Developments in the Built Environment*, vol. 6, May 2021, doi: 10.1016/j.dibe.2021.100045.

[109] W. Dong, Y. Huang, B. Lehane, and G. Ma, “XGBoost algorithm-based prediction of concrete electrical resistivity for structural health monitoring,” *Autom Constr*, vol. 114, Jun. 2020, doi: 10.1016/j.autcon.2020.103155.

[110] “Decision Tree Algorithm.” https://towardsmachinelearning.org/decision-tree-algorithm/ (accessed Dec. 15, 2022).

[111] “Decision Tree - Learn Everything About Decision Trees.” https://www.smartdraw.com/decision-tree/ (accessed Dec. 15, 2022).

Chapter 6

MODULE-3

Development of Non-Structural Sustainable Lightweight Concrete Panels Incorporating Artificial lightweight Expanded Clay Aggregate

6.1 Introduction:

Concrete is a composite material made up of cement, water, and various aggregates such as sand, gravel, or crushed stone. It is one of the most commonly used construction materials due to its durability, strength, and versatility. The cement acts as a binder, holding the aggregates together, while the water allows the mixture to be poured and shaped. Once it sets and hardens, concrete forms a solid and long-lasting structure that can withstand a variety of environmental conditions. It is used in a wide range of construction projects, from roads and bridges to buildings and homes. The properties of concrete can be modified by adjusting the ratio of the ingredients, as well as incorporating additives such as fly ash, slag, or chemical admixtures.

Lightweight concrete is a type of concrete that has a lower density and a higher strength-to-weight ratio compared to traditional concrete. It is made by replacing some or all of the traditional aggregates, such as sand and gravel, with lightweight aggregates. There are two main types of lightweight concrete: precast and in-situ. Precast lightweight concrete is made in a factory and then transported to the construction site, while in-situ lightweight concrete is mixed on-site.

There are two types of lightweight aggregates used in lightweight concrete: artificial and natural as shown in **Fig. 22**. Artificial aggregates are made by processing materials such as expanded clay, shale, or slag, while natural aggregates are obtained from materials such as pumice, volcanic ash, or perlite. These lightweight aggregates are used to reduce the weight of the concrete while maintaining its structural integrity. Additionally, lightweight concrete can be modified to achieve specific properties by using different types of lightweight aggregates, adjusting the mix design, and incorporating chemical admixtures. Overall, lightweight concrete offers many benefits, including reduced dead loads, improved insulation, and easier transportation and placement.

Fig. 22. Types of natural and artificial lightweight aggregates.

The percentage of mix ingredients in concrete can vary depending on the specific application and desired properties. However, a typical mix might contain 10-15% cement, 20-25% water, 60-75% aggregates (such as sand and gravel), and small amounts of admixtures (such as accelerators, retarders, or plasticizers).

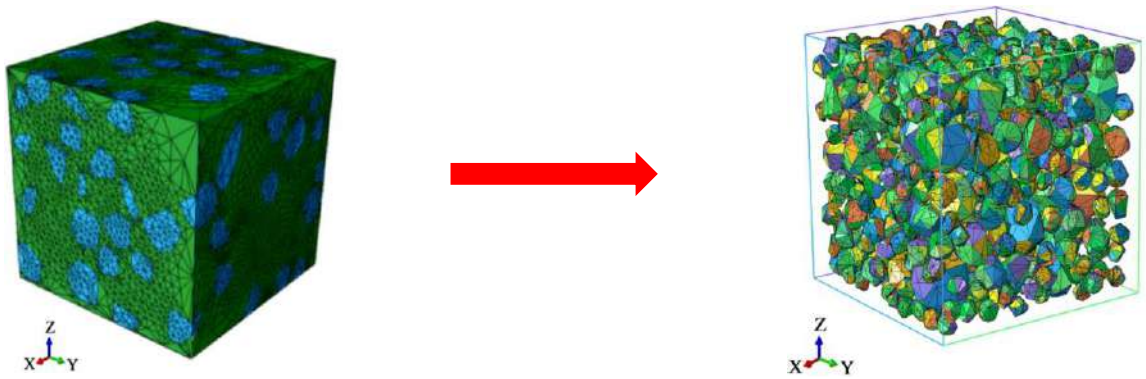

Fig. 23. Generally concrete matrix consists of 50 to 60 %of aggregate.

After careful consideration of the aggregate percentage in the concrete matrix, we have decided to replace the natural aggregate with lightweight expanded clay aggregate. This decision was made in order to achieve a more optimal distribution of the matrix, while also reducing the weight of the final product. By incorporating lightweight expanded clay aggregate, we can improve the thermal and sound insulation properties of the concrete, while also reducing its overall density. This substitution will also result in a more sustainable and eco-friendly construction project, as expanded clay aggregate is made from natural materials and requires less energy to produce than traditional natural aggregates.

6.2 Methodology

6.2.1 Mix ingredients of lightweight concrete

The mix ingredients of lightweight concrete typically include ALECA, cement, fly ash, and water as shown in **Fig. 24.** ALECA, or "Artificial Lightweight Expanded Clay Aggregate," is a lightweight and highly porous material that serves as the primary aggregate in lightweight concrete. It is made from clay that has been fired at high temperatures to create a lightweight, porous structure. Cement serves as the binding agent that holds the aggregate together, while fly ash is often added as a supplementary material to improve the strength and workability of the mixture. Water is added to achieve the desired consistency and to help the mixture bond together during the curing process. The resulting lightweight concrete has a lower density than traditional concrete, making it ideal for applications where weight is a concern, such as in building construction, bridge decks, and precast concrete products. The use of ALECA in the mixture also enhances thermal and acoustic insulation properties of the concrete, making it a highly desirable material for sustainable construction projects.

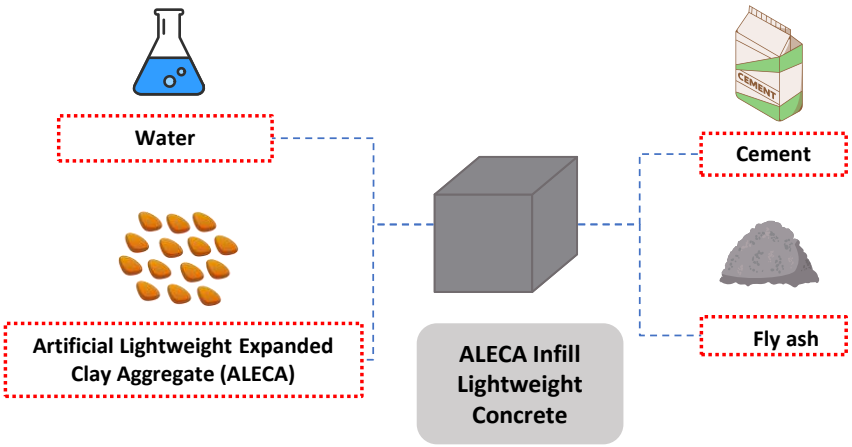

Fig. 24 Mix ingredients of lightweight concrete panels.

6.2.2 Artificial lightweight expanded clay aggregate (ALECA)

After preparing 120 mixes of artificial expanded clay aggregate, a thorough analysis was conducted to select the lightest mix that would be suitable for the preparation of non-structural lightweight concrete panels as shown in **Table 11**. The selection process involved carefully examining the properties of each mix, such as its density, compressive strength, and workability. The chosen mix was carefully formulated to achieve the desired properties of lightweight concrete,

including low density and high insulation properties. The mix was then used to prepare a series of test panels, which were subjected to a battery of rigorous tests to ensure they met all necessary quality and safety standards.

Table 11

Final properties of ALECA for development of lightweight concrete panels.

Physical property of Artificial Lightweight Expanded Clay Aggregate (ALECA)	
loose bulk density (g/m^3)	0.39
Practical density (g/m^3)	0.43
Compressive strength of Single Aggregate (MPa)	2.5
Water absorption (%)	10.50
Loss on ignition (%)	24.32
Bloating index (%)	33.33

6.2.3 Concrete mix design

To achieve the desired properties of lightweight concrete, three mixes were designed, each with varying proportions of cement, fly ash, and pre-placed ALECA (artificial lightweight expanded clay aggregate) as shown in **Fig**. **25.** The first mix comprised of 70% cement, 30% fly ash, and pre-placed ALECA in the mold, with a water-cement ratio (w/c) of 0.45-0.55. The second mix consisted of 50% cement, 50% fly ash, and pre-placed ALECA in the mold, with the same w/c ratio as the first mix. The third mix comprised of 30% cement, 70% fly ash, and pre-placed ALECA in the mold, with the same w/c ratio as the previous two mixes. Each mix was designed to produce lightweight concrete with low density and high insulation properties, making them ideal for non-structural applications such as panels. The variations in the proportions of cement, fly ash, and pre-placed ALECA in each mix allowed for the desired properties to be achieved while also ensuring that the mix was easy to work with and could be easily molded into the desired shape. Overall, the careful design and selection of these mixes were essential to achieving the desired properties of lightweight concrete and ensuring that the finished product met all necessary quality and safety standards.

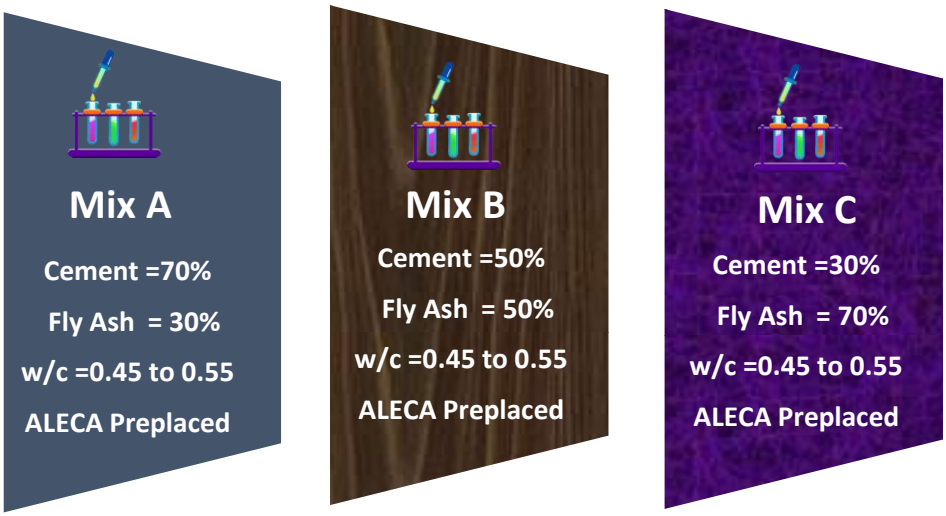

Fig. 25 Mix design for lightweight concrete panels.

6.2.4 Two stage casting process

The two-stage casting process for lightweight concrete is a highly effective technique for achieving superior performance and sustainability while reducing the overall weight of a structure. This approach involves carefully placing the lightweight aggregate in the mold, followed by the pouring of the first layer of mortar mix as shown in **Fig**. **26.** The first layer is typically denser and helps to create a strong foundation for the structure. After the first layer partially cures, the second layer of mortar mix is poured on top, which usually contains a higher proportion of lightweight aggregates such as perlite or vermiculite. The lightweight aggregates reduce the overall weight of the finished product while the second layer of mortar provides additional strength and stability. This two-stage casting process enables greater control over the final appearance and properties of the finished product, making it ideal for use in decorative panels, cladding, and other non-structural applications. Overall, this method is a popular choice for architects and builders looking to achieve lightweight, high-performance concrete solutions that meet their needs for both form and function.

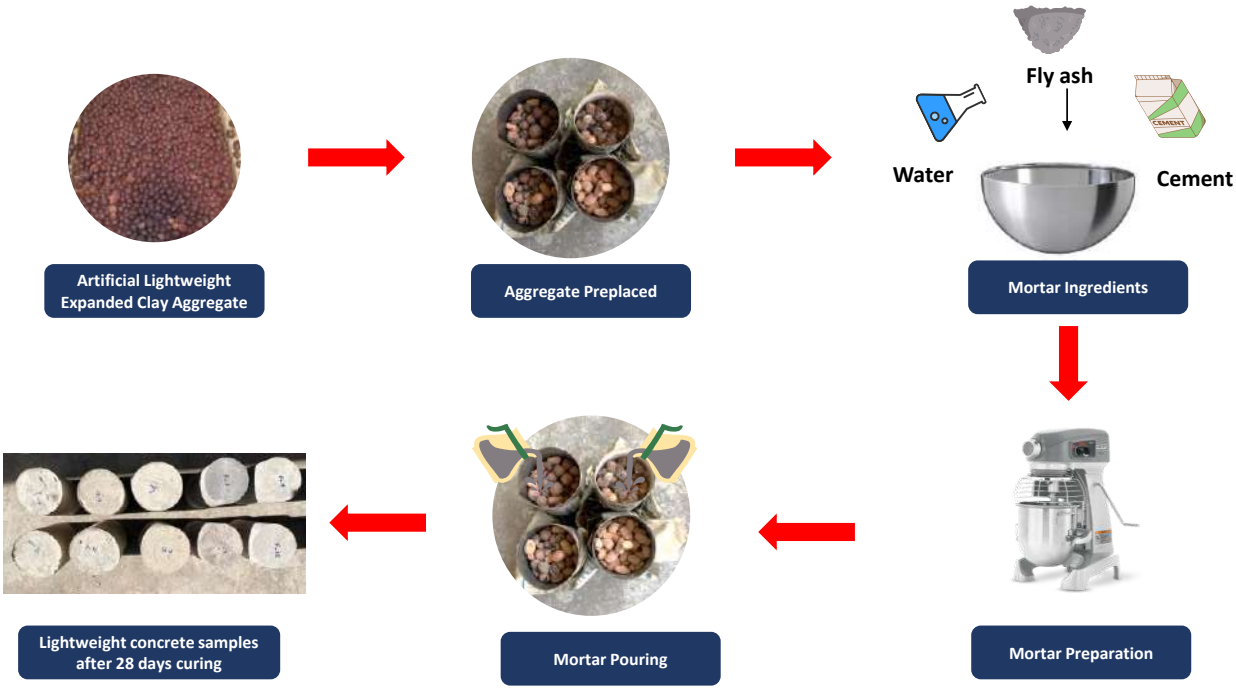

Fig. 26 Two stage casting process of lightweight concrete.

6.2.5 Testing phase

In the testing phase of non-structural lightweight concrete, various tests were conducted to assess the performance and quality of the product. The compression test, which was carried out in accordance with ASTM C39/C39M, evaluated the concrete's ability to withstand compressive loads. Split tensile testing, conducted in accordance with ASTM C496/C496M, measured the tensile strength of the concrete. Thermal conductivity was tested using ASTM C177, which involved measuring the rate at which heat transferred through the concrete. Density measurements were taken using ASTM C642, which involved weighing the concrete and calculating its volume to determine its density. Ultrasonic pulse velocity tests, conducted in accordance with ASTM C597, were used to assess the concrete's resistance to damage and cracking. Fire performance measurements were taken using ASTM E119, which evaluated the concrete's ability to withstand high temperatures and flames. Water absorption measurements were carried out using ASTM C642, to assess the concrete's ability to resist water penetration. These tests were critical in ensuring that the lightweight concrete was suitable for non-structural purposes such as blocks, panels, and other similar applications. **Fig. 27.** shows some pictures of tests which we have conducted to access the performance of lightweight concrete for non-structural purposes.

Fig. 27. Experimental program for performance assessment of ALECA infill lightweight concrete.

6.3 Results and discussion

6.3.1 Experimental results and comparison

The testing phase for the ALECA infill lightweight concrete panels produced encouraging results. The compressive strength of the panels was found to be higher than the other existing lightweight concrete like EPS panels, Foam concrete etc. used in Pakistan, according to the results in **Table 12**. In addition, the split tensile strength of the panels was also found to be superior to other lightweight concrete options in the region. Moreover, the thermal conductivity of the ALECA infill concrete panels was low, indicating its excellent insulation properties. The density measurement results were consistent with the desired lightweight concrete range. The ultrasonic pulse velocity test indicated a high resistance to cracking and other forms of damage, making the ALECA infill concrete ideal for non-structural purposes like blocks, panels, etc. The fire performance test results also demonstrated that the concrete could withstand high temperatures and flames for a sufficient duration. Finally, the water absorption measurement showed that the ALECA infill concrete had a low level of water penetration, which is desirable in most construction projects. Furthermore, the

low price of the ALECA infill concrete, as compared to other lightweight concrete options, makes it a cost-effective solution for the construction industry in Pakistan.

Table 12

Comparison of ALECA infill concrete properties with other lightweight concrete.

Properties	Units	ALECA Infill Panels	EPS Panels	AAC Blocks	Bricks
Concrete Density	Kg/m3	870-1150	850 - 1000	400 - 700	1800 - 2000
Compression Strength	MPa	8 - 14	2.5 - 3.83	1.5 - 3.2	6 - 14
Flexural Strength	MPa	0.35 - 0.84	0.67	0.3 - 0.42	-
Water Absorption	%	8 - 10.5	10-13	12 - 14	12 - 15
Combustion Performance	Grade	A	A	A	A
Fire Rated Partition	Hours	>4	4	3-4	>4
Thermal Conductivity	W/m.k	0.19	0.25	0.20	0.6 - 1.2
Acoustic Performance	dB	39-42	37 - 41	38 - 45	33 - 37

Conclusion

In conclusion, the work presented here has successfully developed a sustainable and cost-effective lightweight concrete using artificial lightweight expanded clay aggregate. This new approach for casting lightweight concrete, where the aggregate is first placed and then mortar is poured, has also proven to be time-saving. Additionally, the replacement of a significant amount of cement with fly ash (70% fly ash and 30% cement) in the concrete mix is a significant step towards green construction. These findings suggest that this lightweight concrete can be a viable alternative to conventional bricks in non-structural applications, such as panels, hollow blocks , etc. The results of the tests conducted also indicate that this ALECA infill concrete performs better than other existing lightweight concrete used in Pakistan, which makes it a promising material for use in the country's construction industry. Overall, this work demonstrates the potential of lightweight concrete as a sustainable and cost-effective construction material.

Chapter 7

MODULE - 4

Development Cost Comparison and Performance Assessment of High-rise Buildings with different Types of Infill Panels

7.1 Cost Comparison

This section discusses the cost comparison of a case study building, Sky Garden, originally designed for Lahore, Pakistan, in five major cities across the country. The 23-story building was redesigned with two different infill panels in each of the five cities: Lahore, Peshawar, Quetta, Karachi, and Islamabad. The redesign process followed the structural design codes ACI-318 and ASCE 7-16, as well as the detailing guidelines outlined in the ACI detailing manual. The cost estimation for the construction of the four buildings, each with a different infill panel, was based on the latest market rate systems for each respective city. The results of the cost comparison show that economic building design can be achieved by using ALECA infill panels compared to other brick infill option. **Fig. 28** shows that by using ALECA infill panels we can save money up to 16.2% as compared to a building with bricks as infill.

Description of Selected Building

- Building: Sky Garden (Lahore)
- 23 story residential building
- 37m by 67.5m covered area
- Dual Structural System
- MAT foundation

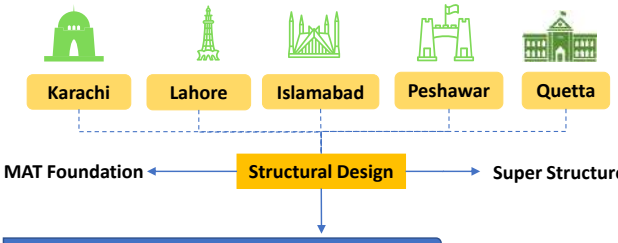

Table. Summary of cost as per market rate-2023

Material	Price
Concrete	276–290
Steel	985–1059
Bricks as infill	6-6.3
Total Price (avg)	PKR 1311.2 million
Concrete	251-257
Steel	758-916
ALECA Infill Panels	7-7.2
Total Price (avg)	PKR 1098.1 million

16.2%

Reduction in overall material cost of structure

Fig. 28. Etabs building model for cost comparison.

7.2 Non-Linear Performance Assessment

In this section, we will compare the performance of two designed buildings (sky garden) in Islamabad using non-linear static pushover analysis in Perform 3D. The first building has masonry infills, while the second has ALECA infills. We will use non-linear fiber modeling for columns and shear walls, and plastic hinge modeling for beams. The CP (collapse prevention) limit state will be used to check failure criteria for infill panels, shear walls, beams, and columns. Given the highly irregular and non-linear behavior of infill panels, it is crucial to model them accurately to capture their true performance contribution during dynamic loadings. However, there is currently a gap in research and industry as practical approaches to model infill panels are limited and often lack the ability to incorporate variations present in the field. To address this, we have developed a novel macro modeling approach for modeling infill panels that incorporates all possible variabilities, including frame geometry and material properties, infill frame and material properties, and interface stiffness. We have validated and compared this approach with available experimental data in the literature, along with other practical approaches.

The current practices of structural analysis and design of buildings involve taking into consideration the effect of structural members only (beams, columns, slabs, shear walls, etc.) without considering the effect of non-structural components. However, several studies have shown that the non-structural infill walls have a considerable influence on the overall response of the structure. This issue has been successfully addressed by many researchers by modeling the infill walls as diagonal struts. However, most of the proposed relationships are empirical and are very limited to specific types of infill panels. Therefore, this research proposes a novel approach to accurately model the effect of infill panels. In this study, the effect of the flexible and rigid joints was also accounted in developing the generalized relationship for equivalent diagonal strut width. For this purpose, the classical initial stiffness formula was used to evaluate the width of the diagonal strut. Furthermore, the finite element model of the wall is developed using a thin shell element bounded by structural frame elements, while the interface of the shell being modeled as a gap element of adjustable (variable) stiffness. On the other hand, the strut model constitutes of equivalent compression only strut in replacement of shell element. Furthermore, a stiffness reduction factor was also introduced to account for the openings in the infill panels. A detailed parametric study and global validation has been performed and the effect of variation in joint

stiffness, infill stiffness, frame stiffness, geometric properties of frames and infill and multiple stories to evaluate the performance of the proposed strut modelling approach under lateral monotonic and cyclic loads. Finally, the performance of the proposed model and several other frequently used diagonal strut approaches are compared with experimental results. The results indicate that despite being comprehensive in terms of its functionality the proposed equation can accurately model the behavior of any infill panel.

1. Introduction:

The Infilled Frame structural system has a long and rich history, dating back to ancient times where masonry infill walls were utilized for construction applications. Despite their vast applications and importance, they are not included in analytical models for structural analyses, as they are considered non-structural elements. However, the several studies have proven that the infilled panels show a reasonable contribution toward the lateral stiffness, strength, and overall behavior of the structure [1]. Furthermore, as it offers most of its rigidity in the lateral direction, hence its contribution becomes significant in case of extreme lateral loadings arising due to seismic and wind excitations. The infills manifest an ambiguous behavior when exposed to seismic loadings. In the case of seismic excitation initially, the infills interact with frames and increase the overall strength, stiffness, and lateral resistance of the structure. Later, when the stresses exceed a particular value (when structure enters the nonlinear range), irregular distribution of stresses and weak out-of-plane behavior instigates failure in the structure due to which infill panels fail first due to their high in-plane rigidity [1]. Due to its uncertain and complex nonlinear behavior there was a need to model the nonlinear response of infill panels to evaluate the accurate response of the building structures. For this several numerical and experimental attempts have been made to simulate their contribution to accurately model the response of the entire structure [1-5]. Briefly, the contemporary techniques for the analysis of Infilled Frame structures can be summed up under two main approaches.

The first approach, which is highly reliable but is computationally pervasive, is the micro modeling approach. The micro modeling technique is a detailed process in which the localized behavior, stress concentrations of the infill, along with its complete three-dimensional response can be investigated using the finite element method (FEM) [2]. This method discretizes the continuum into small, connected elements and perform analysis on specific points called nodes. The elements used for modeling infill panels are shells and membranes [3]. Moreover, the inelastic properties of

both masonry units and mortar along with basic mechanical parameters such as elastic modulus, and Poisson's ratio are required for the detailed analyses. In short, the micro-modeling approach deals with all the components of masonry individually and considers the effect of all the prospective failure modes.

The second method, the macro modeling method is more practical from a modeling perspective and is based on the physical behavior of infill panels. The collective mechanical and physical properties of mortar joints and units are recognized to obtain more simplified solutions [4]. In this approach, one-dimensional struts along with springs in different orientations are used to portray the behavior of infills in frames [3]. The idea behind using struts lies in the failure mechanism of most of the infills which is based on diagonal compression, that can be represented by pin connected compression only struts. In the case of low lateral loading, the walls behave as shear walls initially and contribute positively towards the overall stiffness of the structure. But after a certain limit, when the out-of-plane stresses and displacements increase, the stresses in infill panels concentrate along one of the diagonals, known as participating diagonal. This usually causes excessive cracks along the participating diagonal, and gaps are formed between infill and frames on the non-participating diagonal [4]. Therefore, this behavior of the participating diagonal along which stresses concentrate is represented with an equivalent compression-only strut. Now, most of the commercially available FEM softwares do not have the computational capacity to analyze the non-linear behavior of the infill shells easily. Whereas the non-linear model of these can be easily represented using the strut approach which requires relatively lower computational power. Strut approach of infill panels is also recommended in American and Canadian design standards [5],[6]. This strut approach was initially proposed by Polyakov [7] to model the infill walls as a strut for the effective transfer of stress. Later Holmes [8] made a further contribution to this by suggesting a rule of thumb for the calculation of the effective width of the compression strut which was 1/3 of the diagonal length. Furthermore, Smith and Carter [9], [10] contributed with their two pin-end connected struts in which the strut is a function of the type of material and thickness of the wall. Later, Mainstone and Weeks [11] recommended an empirical method to evaluate the strut width for infill walls subjected to monotonic lateral loads. This equation was later adopted by FEMA 274, FEMA 306, FEMA 356, and is widely used nowadays. The equation takes the initial stiffness, ultimate strength, stiffening, and strengthening effect of the infill into consideration. Further, in terms of the interaction of the infill with the bounding frame, several studies [12], [13]

suggested that a single diagonal strut is not enough to capture the shear force and bending moment transferred from frame members to infill. Cavalieri and Di Trapani [14] suggested an equation that considered the effect of the interaction of the frame with the infill wall using the strut approach. Later several studies were also conducted to accurately capture the effect of infill panels by modeling them as multiple struts [15]. Crisafulli [16] further investigated the effects of multiple compression strut models on the entire structural response of the infill walls in RC frames.

Currently, various single and multiple strut models are being developed [17] but still, the designers are reluctant to accept these techniques. A model that contains several diagonal struts and springs at various locations may very well be extraordinarily precise, yet it is unlikely to attract professional engineers owing to the amount of effort involved in its modeling. Even some of the user-friendly strut models are not welcomed by the industry since they are empirical in nature and most of them lack a well-established classical background and conceptual underpinning [18]. Therefore, there is a dire need for a generalized and comprehensive model which incorporates all the prospective variations in the material as well as the stiffness of the infill wall, bounding frames, and joints.

This research proposes a novel macro modelling approach for simulating the in-plane behavior of Reinforced Concrete frames infilled with wall panels having several types of joint flexibility. An approach was developed that considers the effect of strut compression failure, frame-wall interaction failure and openings in the wall simultaneously. This approach utilizes two compression-only struts along the diagonal with the gap elements at each corner. The performance of this model to predict the stiffness, strength, local, and global response of infilled frames has been validated against a wide range of material and geometric parameters of infill, joints as well as frame elements (beams and columns), and under lateral monotonic as well as cyclic loadings. The overall structural response of the model after modeling the infills as shells and struts is also compared for the validation of the proposed approach. All the possible parameters such as time period, frequency, base shear, overturning moment, story drifts, and displacements are compared to calculate the performance of the model. Lastly, experimental validation of the proposed strut model was also performed by comparing its results with experimentation performed by Mehrabi [19]. Finally, to acquire a better insight into the model's performance, other frequently used models were also evaluated against the same set of experimental data. The results showed that the proposed

model was able to successfully predict the response of the frame as per the experimental results and results were comparatively better as compared to other models.

2. Development of strut formula:

2.1.Theory:

The initial aim is to calculate the width of the diagonal strut (as the other two dimensions are already known from the geometry of frame). The width of diagonal strut is evaluated based on the classical initial stiffness formula. An approach for the identification of the equivalent strut providing similar lateral stiffness as of the frames structure infilled with different types of wall panel. The width of the equivalent strut can be found by extending the study of a single-story single bay frame. The idea is to impose the condition that initial stiffness of actual structure is equal to initial stiffness of same frame with pin connected equivalent strut system as shown in **Fig. 29**.

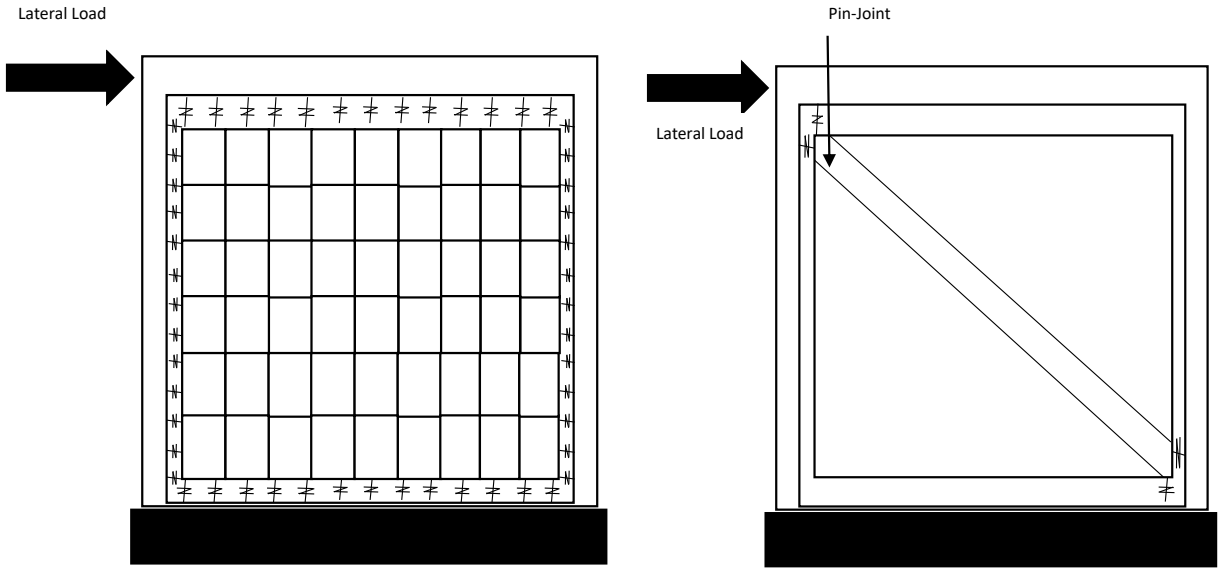

(a) (b)

Fig. 29. The representation of the infill panels (a) micro-modeling (b) macro-modeling (using strut).

2.2.Derivation:

The first step is to find the stiffness using the classical initial stiffness formula as represented in equation 1. The idea is to equate the stiffness of braced and shelled frames as shown in **Fig. 29**.

$$D_i = \left(\frac{6\alpha+\beta}{6\alpha+4\beta}\right) x \frac{24EI_c}{Lc^3} + \frac{K_d \cos^2\theta}{1+\frac{K_d \sin^2\theta}{k_c}+\frac{1.K_d \cos^2\theta}{4k_b}} = D_D + D_F \quad (1)$$

$$k_d = \frac{E_d t_w}{d} \quad 2(a)$$

$$k_c = \frac{E_f A_c}{h'} \quad 2(b)$$

$$k_b = \frac{E_f A_b}{l'} \quad 2(c)$$

$$\beta = \frac{L_b}{L_c} \quad 2(d)$$

$$\alpha = \frac{I_b}{I_c} \quad 2(e)$$

$$D_D = D_i - D_F \quad (3)$$

$$k_d = \frac{D(4k_b k_c)}{4k_c k_b(\cos\theta)^2 - D_D(4k_b(\sin\theta)^2 + k_c(\cos\theta)^2)} \quad (4)$$

Where k_d, k_c, k_b are elastic axial stiffnesses of equivalent strut, column and of the beam respectively while D_D, D_i and D_F are lateral stiffnesses provided by pin-connected strut, infill frame and of bare frame.

I_b, I_c are moment of inertia of beam and column.

E_d, E_f: are material stiffnesses of infill and frame.

h, h' and l, l' are the dimensions of frame as shown in **Fig. 30**.

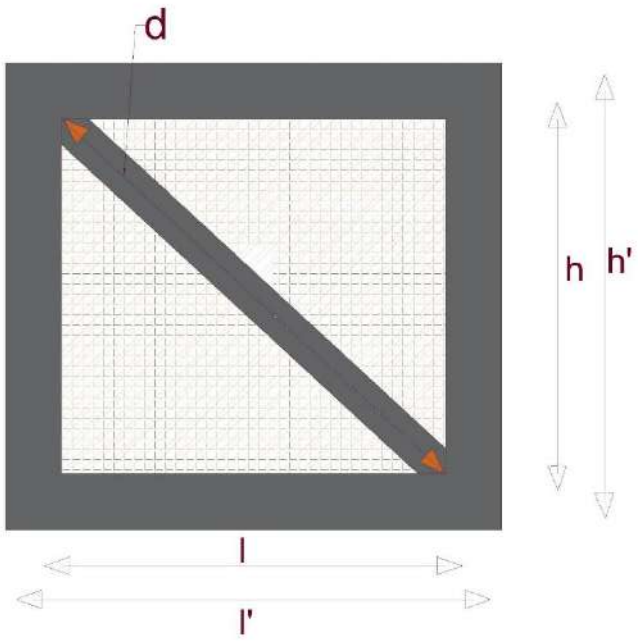

Fig. 30. The schematic diagram showing the representation of different variables.

Initially, the stiffness of the entire bay (D_i) is calculated utilizing the classical approach through the use of Finite Element Method (FEM). This serves to evaluate the stiffness of the frame by utilizing the classical formula shown in equation (3) by subtracting the stiffness of the infilled frame from that of the bare frame, resulting in the lateral stiffness of the strut. Subsequently, equation (4) is employed to determine the required axial stiffness of the strut. Finally, the width of the strut is determined through utilization of the general axial stiffness formula for a strut as outlined in equation (2a).

3. Methodology:

This study presents a Novel and practical approach for modeling infill panels. The methodology involves the integration of micro, macro modeling and classical initial stiffness formulae for developing a useful modeling approach for infill panels. As it can be seen in **Fig. 31**, the finite element model used to develop the diagonal strut formula is composed of three sections:

- Fixed base to illustrate the infill frame's base fixity.
- Beam and column frame to portray the frame element that is filled with shell elements of a wall panel.

- The interface between the frame and the wall panel is modeled as GAP elements. As gap element has better ability to transmit forces directly from the external frame components to the infill wall. [20]–[23]

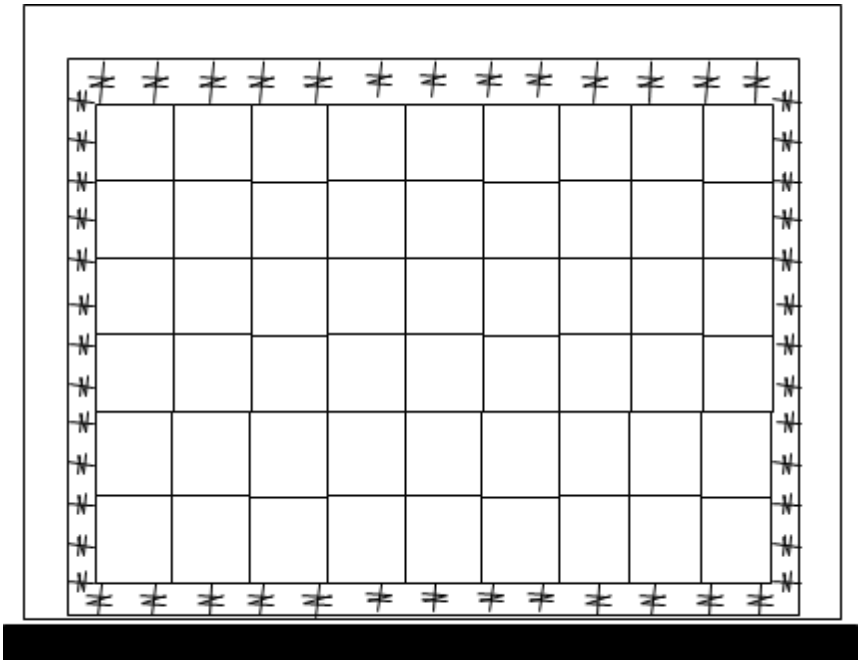

Fig. 31. The FEM of frame employing gap elements.

This study also aims to investigate the effect of variable stiffness of gap elements, frame elements, infill material and geometry on the overall stiffness of an infill frame. A single story, single bay micro model of an infill frame as shown in **Fig. 31.** was developed using finite element software. The lateral stiffness of the infill frame (Di) was determined through the application of static lateral loading conditions. Subsequently, the numerically calculated initial stiffness of the bare frame (D_F) was subtracted from D_i to determine the lateral stiffness provided by the equivalent strut.

The determined lateral stiffness was then utilized in equation (4) to calculate the required axial stiffness of the strut. This axial stiffness was then incorporated in equation (2a) to determine the width (w) of the strut. By varying the stiffness of the gap element, frame elements, infill material, and geometry, the effect on the overall stiffness of the infill frame can be determined.

3.1.Stiffness reduction factors for opening ratios:

The infill panels are not always fully enclosed and often include openings for architectural accessories such as doors and windows. These openings can significantly reduce the stiffness provided by the infill panels and must be considered during the structural analysis. In this study, stiffness reduction factors were introduced as a function of opening ratios in the infill panels to account for the effect of these openings on the overall stiffness of the infill panels. The proposed methodology aims to provide a more accurate representation of the infill panel's behavior and contribute to the understanding of the effect of openings on the overall stiffness of the structure.

The width of the strut for infill walls with openings was found using a trial-and-error approach. The width for which the forces versus displacements curves, in plane stress, and global responses are similar to those of infill panel (micro model) with openings, was considered the width of the strut. Data for strut width is extracted with openings percentages of 0 %, 8 %, 13 %, 24 %, 30 %, 43 %, and 48%. This data set is used to find the stiffness/strength reduction factor, a coefficient multiplied by initial width of the strut at variable opening percentages so that the strut width for the walls with openings are found. The best-fit equation for the above data set was found using nonlinear regression analysis is shown in **Fig. 32**.

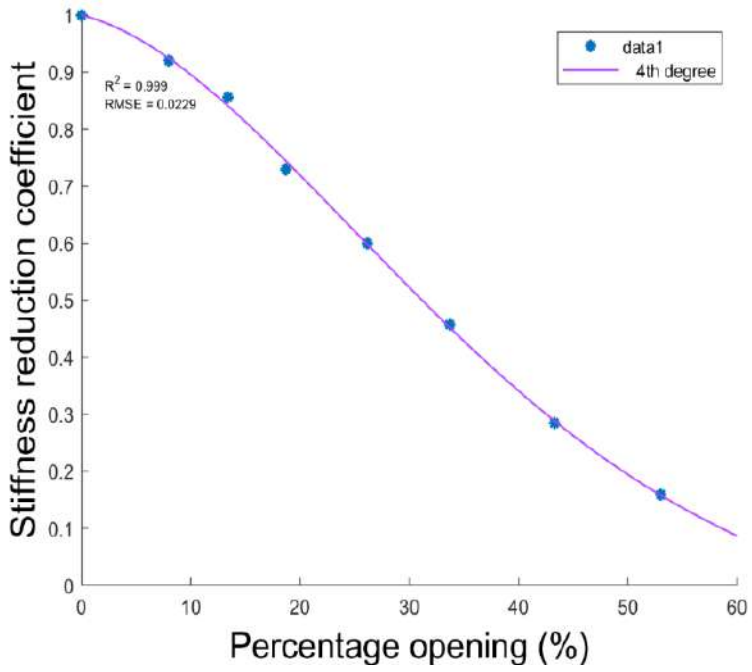

Fig. 32. The results of nonlinear regression for stiffness reduction coefficient.

The best fit line has been selected based on coefficient of determination (R^2). According to the dataset, the best fit line is 4th degree polynomial which has $R^2 = 0.993$ and finally an equation is extracted which fit this plot. This equation is used for stiffness reduction factor for any percentage of opening in the wall panel.

$$Stiffness\ Reduction\ Factor(SRF) = -6.58e^{-8}x^4 + 1.25e^{-5}x^3 - 0.00069x^2 - 0.00471x + 1$$

Where x in above equation is defined as opening percentage in infill panel in %.

4. Results and Discussions:

4.1. Parametric investigation:

This section utilizes the concept of parametric analysis on single story single bay infilled frame structure. For this purpose, a parametric analysis was carried out by altering the geometric and material characteristics of the proposed model's all components. The cross-sectional dimensions and material properties (elastic modulus) of the frame elements were tweaked for this reason. Similar to this, the effects of changing the joint stiffness (GAP) and its interaction with the panel under static and dynamic loading were also investigated. It turned out (as shown in **Table 13, 14 and 15**) that the model adequately captured all kinds of variations in the characteristics of the strut model's constituent pieces.50 KN static lateral load is applied at the top of both shell and strut model and their roof displacements are compared as shown in **Table 13** below for different variable parameters such as; in plane joint stiffness, material and geometric properties of infill and frame elements. For dynamic loading unscaled time history of YERMO ground motion (time history shown below) is selected to be applied on both shell and strut models and difference in their maximum roof displacements is show below in the **Table 13**for varying parameters same as for static loading.

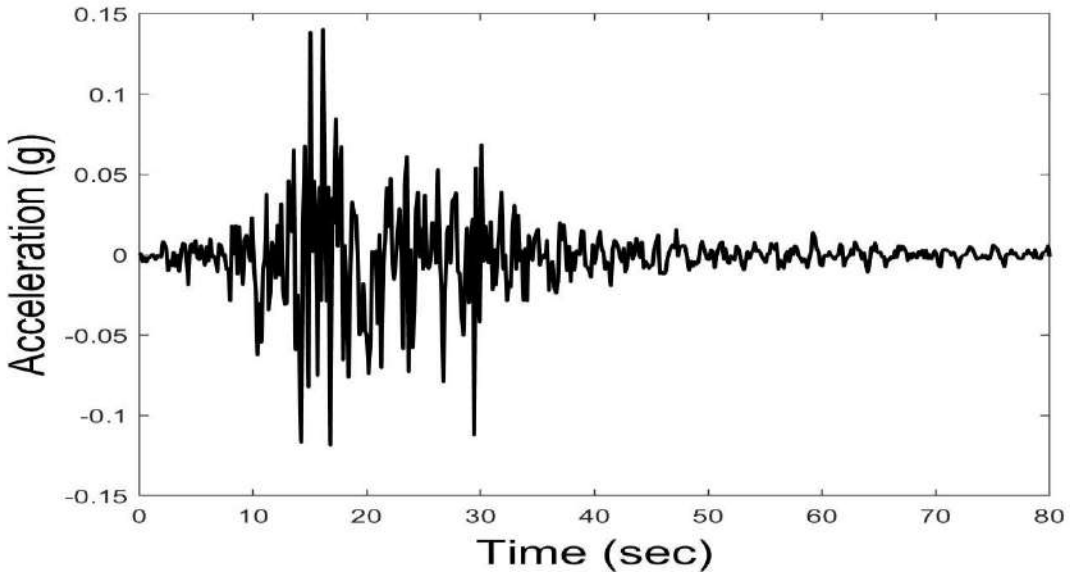

Fig. 33. Unscaled YERMO ground.

Table 13

The lateral displacements comparison by varying joint stiffness.

In plane joint stiffness (KN/m)	**Static response(mm)**				**Dynamic response(mm)**			
50000	**FEM**	0.48	**strut**	0.431	**FEM**	0.37	**strut**	0.34
124000	**FEM**	0.333	**strut**	0.329	**FEM**	0.25	**strut**	0.24
200000	**FEM**	0.28	**strut**	0.3	**FEM**	0.21	**strut**	0.2
	MAXIMUM DEVIATION=10%							

Table 14

The lateral displacements comparison by varying cross-sectional dimensions.

Colum and beam dimensions(b*h)	**Static response(mm)**				**Dynamic response(mm)**			
9 by 9 (in^2)	**FEM**	0.315	**strut**	0.284	**FEM**	0.22	**strut**	0.22
12 by 12(in^2)	**FEM**	0.249	**strut**	0.22	**FEM**	0.19	**strut**	0.18
20 by 20(in^2)	**FEM**	0.161	**strut**	0.153	**FEM**	0.27	**strut**	0.24

					MAXIMUM DEVIATION=9%			

Table 15

The lateral displacements comparison by varying elastic modulus.

Elastic modulus of frame (Mpa)	**Static response(mm)**				**Dynamic response(mm)**			
15000	**FEM**	0.29	**strut**	0.25	**FEM**	0.22	**strut**	0.19
30000	**FEM**	0.23	**strut**	0.21	**FEM**	0.18	**strut**	0.17
50000	**FEM**	0.2	**strut**	0.18	**FEM**	0.16	**strut**	0.14
				MAXIMUM DEVIATION=13%				

This parametric study shows how if we increase stiffness of the system by any mean, either by increasing material stiffness or by increasing cross sectional dimensions, displacements for same static and dynamic loads decreases both in dynamic and static load conditions. Results of this parametric studies also capture any type of change employing the proposed methodology.

4.2.Validation of the proposed model:

On the global level, validation of the proposed strut modeling approach was performed on 3 story -3bay ,5 story-3bay,10 story-3 bay, and 5 story-1 bay 2D frames. All the considered 2D frames were modeled with percentage openings not used in finding stiffness reduction factor using shell and struts model. The different testing values of openings (aside from the training data points) were modeled using shell and strut on the 2D frames of different stories and their global responses were compared. This was done to evaluate how accurately the stiffness factor reduces the strut width and how closely this modified strut width portrays the behavior of walls with openings. Geometric and material properties of all the frames considered for validation study is shown in **Table 16**. All these models were analyzed under dynamic loading conditions, shown above. and their peak global and local responses i.e., time period, story displacements, story drifts, overturning moments, and story shear were compared. The overall deviations were less than 10% which was satisfactory, results are shown in **Fig. 34, 35, 36 & 37**.

Table 16.

Geometric and material properties for all frames (3,5 and 10 stories)

3 story		**5 story**		**10 story**	
Bay width (m)	3.6576	Bay width (m)	3.6576	Bay width (m)	3.6576
Stories height(m)	3.6576	Stories height(m)	3.6576	Stories height(m)	3.6576
Beam cross section		**Beam cross section**		**Beam cross section**	
Height (m)	0.3048	Height (m)	0.3048	Height (m)	0.3048
Width (m)	0.3048	Width (m)	0.3048	Width (m)	0.3048
Column cross section		**Column cross section**		**Column cross section**	
Height (m)	0.3048	Height (m)	0.3048	Height (m)	0.3048
Width (m)	0.3048	Width (m)	0.3048	Width (m)	0.3048
Frame stiffness (Mpa)	20000	Frame stiffness (Mpa)	20000	Frame stiffness (Mpa)	20000
Infill stiffness (Mpa)	21666.7	Infill stiffness (Mpa)	21666.7	Infill stiffness (Mpa)	21666.7
Strut width (mm)	236	Strut width (mm)	236	Strut width (mm)	236
Infill geometry		**Infill geometry**		**Infill geometry**	
Thickness (mm)	152.4	Thickness (mm)	152.4	Thickness (mm)	152.4

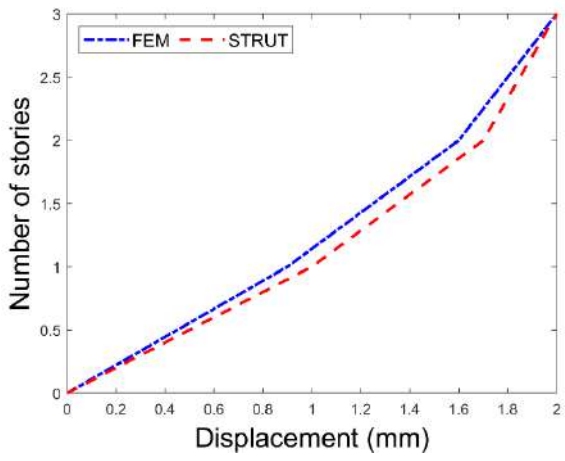

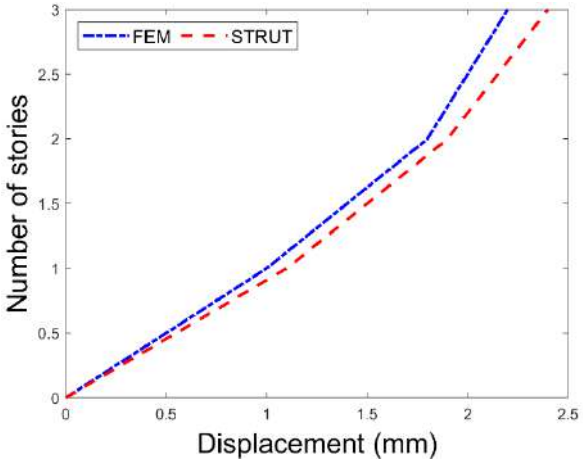

(a) (b)

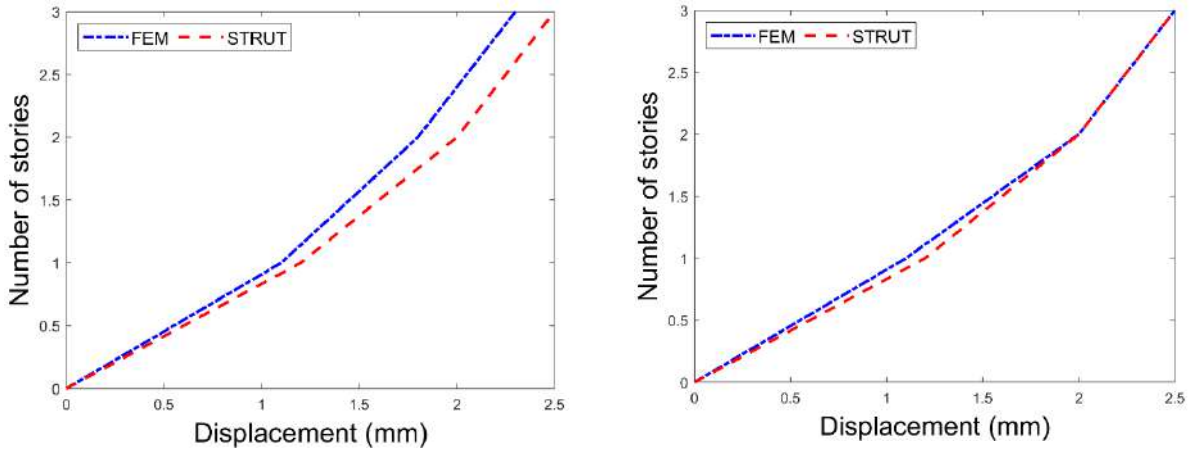

(c) (d)

Fig. 34. The story responses of 3 storey bay with (a) 0% opening (b) 10% opening (c) 15% opening (d) 20% opening.

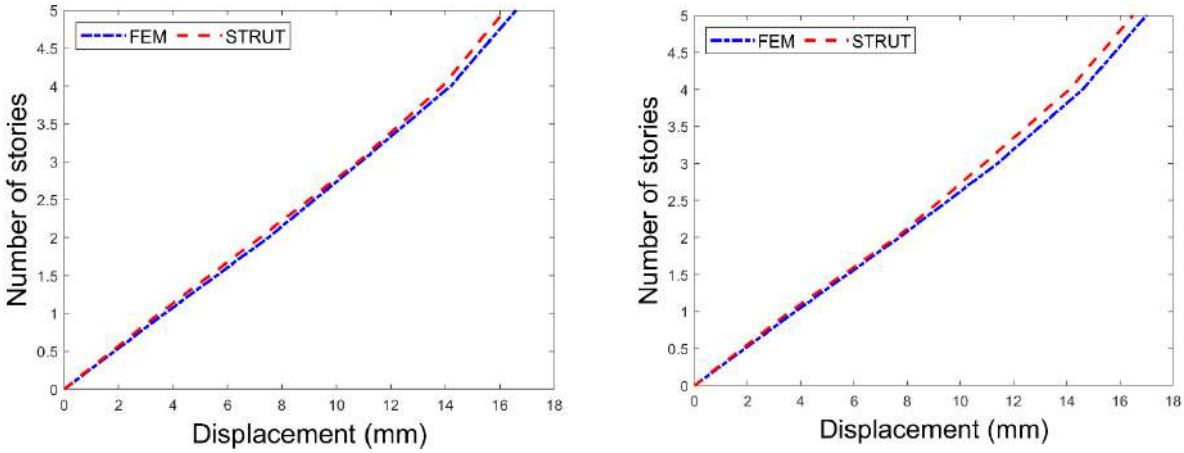

(a) (b)

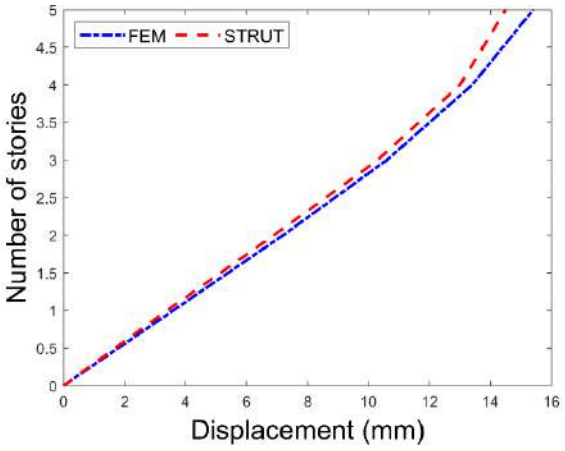

(c)

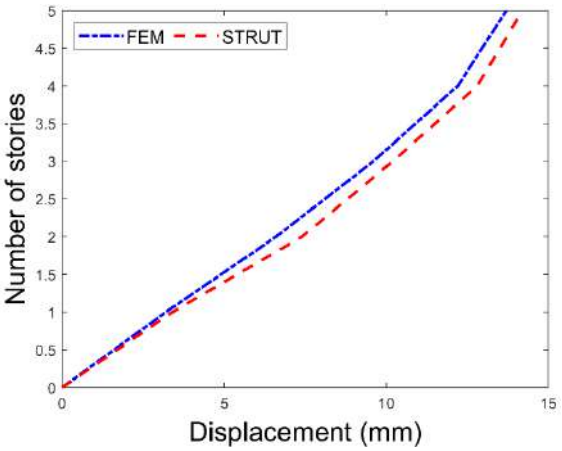

(d)

Fig. 35. The story responses of 5 story bay with (a) 0% opening (b) 10% opening (c) 15% opening (d) 20% opening.

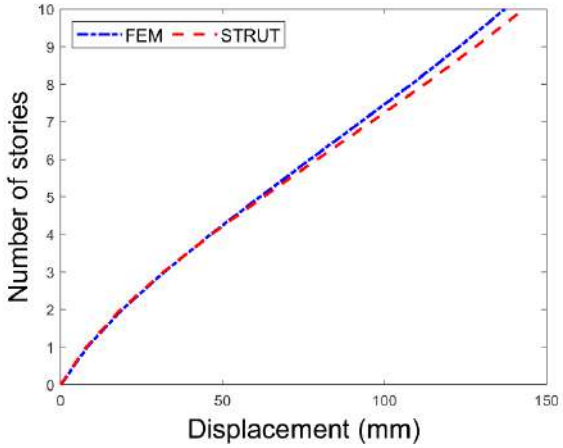

(a)

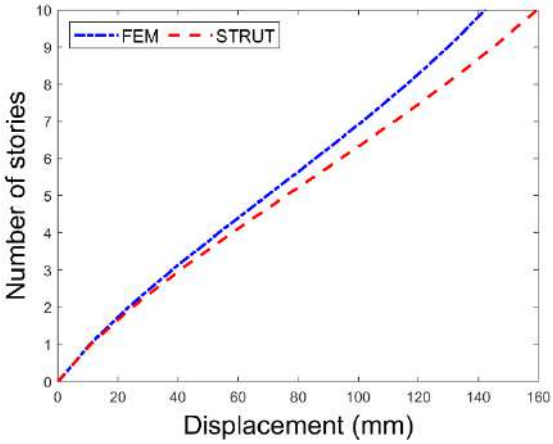

(b)

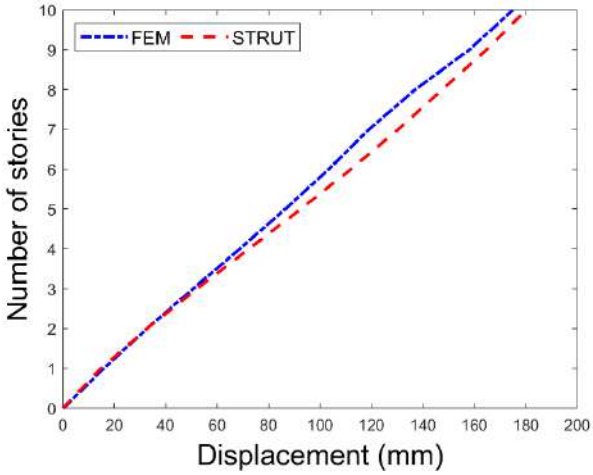

(C)

Fig. 36. The story displacements of 10 story bay with (a) 24% openings (b) 33% openings (C) 50%.

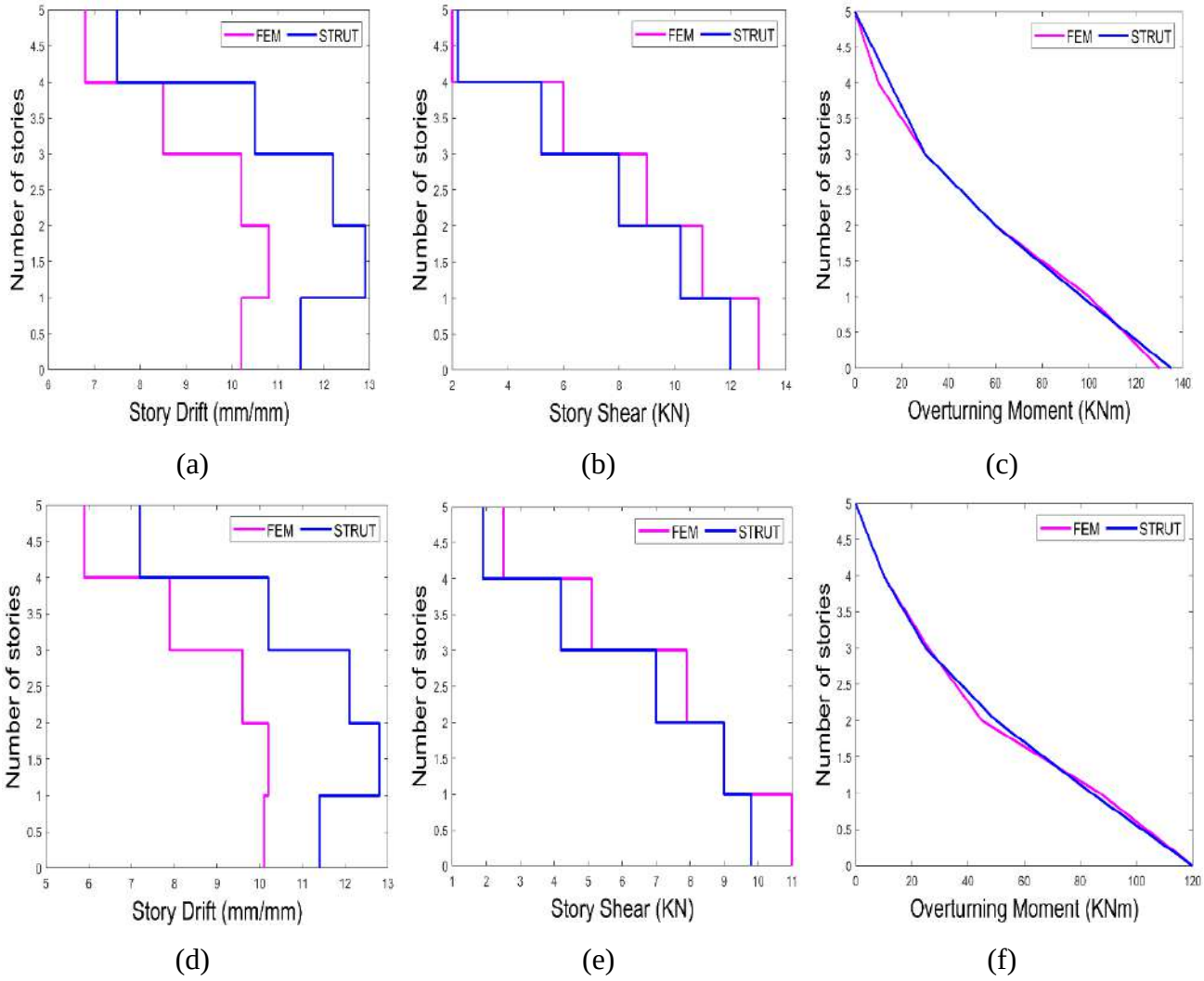

Fig. 37. The story responses against dynamic excitation (a) story drift for 0% opening (b) story shear for 0% opening (c) overturning moments for 0% openings (d) story drift for 15% opening (e) story shear for 15% opening (f) overturning moments for 15% openings

4.3.Validating in plane force transfer mechanism:

One of the major reasons for the failure of masonry structures is the rigidity of the frame infill connection. Due to the dynamic loadings induced by seismic excitations, stresses are concentrated on the contact zones, and this weakens the infill in the in-plane as well out-of-plane directions [23]. To overcome this issue, flexible joints are introduced in the frame infill contact area. The reduced stiffness of this joint reduces the amount of stress transferred. Therefore, a strut model which does not incorporate the variation in the stiffness of the interface between frame elements and infill panels cannot captures the close to true behavior. The proposed strut model has the capability to capture this effect as well.

An analytical demonstration has been shown in the **Fig. 37.** where the shell model used in the derivation of the strut formula is assigned with various joint stiffness values. The stress contours in **Fig. 38** shows increase in force transfer to the infill on increasing the in-plane stiffness of the interface.

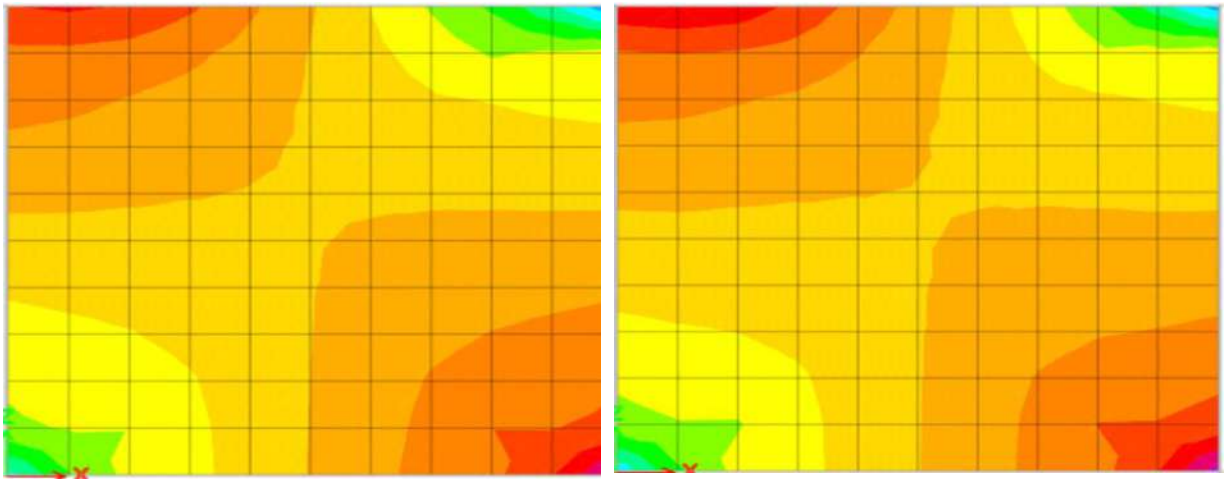

(a) (b)

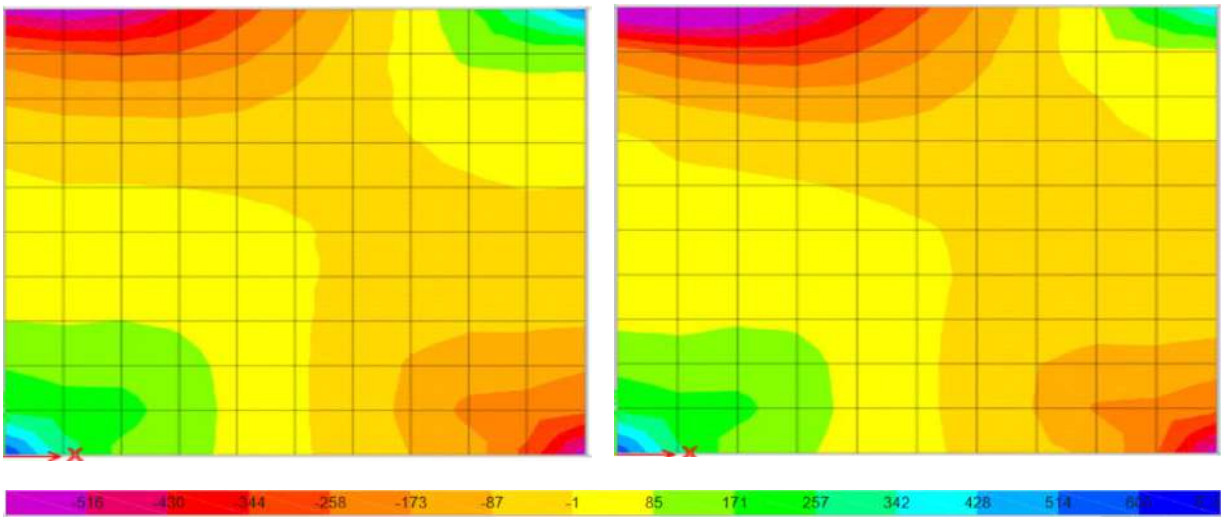

(c) (d)

Fig. 38. The stress (MPa) transfer phenomena between frame and infill panels for lateral loads at for joint stiffness (a) 11000 N/mm (b) 20000 N/mm (c) 100000 N/mm (d) 200000 N/mm.

4.4.Experimental Validation:

In this section, Mehrabi's [19] experimental investigations were utilized to compare the proposed method's results and results of eleven well-reputed approaches taken from the literature [24]–[34]. Mehrabi's experimental research is based on single bay single story prototype of a frame obtained from a structure with a scale of 1/2 and height to width ratio of 1/1.5.Input parameters are taken from Mehrabi's research and the equivalent width of the strut is calculated using the proposed model and the eleven other frequently used approaches.

Input parameters for frame and infill are shown in **Table 17** and for in-plane stiffness for the joint interface is calculated using expression stated in the literature, because in Mehrabi's research interface between frame and infill is made of plain concrete whose approximate stiffness is derived in [20], $0.0378E_i(t) +347$. In this study [20] stiffness of gap element was developed by utilizing single story single bay frame in which interface is modelled as link element. By trial and error procedure the stiffness of gap element was determined so that the results compared well with previous research results and thus validated the computer model. Finally, through regression analysis for various models, formula for interface is developed as a function of stiffness of infill.

The eleven other methods whose results are also compared against the same set of experimental data are as follows:

- Holmes method (24)
- Saneinejad-Hobbs (25)
- Stafford-Smith (26)
- Mainstones (27)
- Bazan-Meli (28)
- Liauw Kwan (29)
- FEMA 356(30)
- Durani Luo (31)
- Al-Chaar (32)
- Papia (33)
- Chen-Iranata (34)

Table 17

The details of experimental setup.

FRAME PARAMTERS	Numerical value	Infill parameters	numerical value
H’	1537 mm	H	1422 mm
L’	2312 mm	L	2134 mm
E_C	21910 MPa	D	2564 mm
B_C	178 mm	A	196328 mm^2
H_C	178 mm	Theta	34^0
I_C	83656321 mm^4	E_{IN}	9515 MPa
A_C	21684 mm^2	t_{in}	92 mm
B_B	153 mm	v_{in}	0.15
H_B	229 mm		
I_B	153114610 mm^4		
A_B	35037 mm^2		

Where

* H', L' and E_C are height length and elastic modulus of RC frame
* B_C, H_C, I_C and A_C are cross sectional dimensions, moment of inertia and cross-sectional area of columns
* B_B, H_B, I_B and A_B are cross sectional dimensions, moment of inertia and cross-sectional area of columns
* H, L, D, and A are height, length, diagonal length area of infill panels
* Theta is angle of diagonal length of infill panel with horizontal
* E_{IN}, t_{in} and v_{in} are elastic modulus, thickness poisons ratio of infill panel

Fig. 40 shows force vs displacement curves for all the models considered along with the proposed model, compared with the experimental force-displacement curve. Results show that the approach that gives the closest result to infill frame experimental results is the proposed model(w=923mm), followed by the Bazan-Meli approach(900mm) and the Holmes approach(854mm). On the other hand, the results of Al-Chaar, Mainstones-Weeks, Stafford-Smith, and Mainstones are stiffer than the experimental result. And results of, Sainedjad-Hoobs, Liauw-Kwan, Paulay-Priestley, Hendry, Papia, Chen-Iranata, Durani-Luo, and FEMA are conservative. The summary of strut width using all above mentioned approaches is shown in **Fig. 39**.

Bazan-Meli and Holmes approaches show results close to experimental but in Holmes method, strut width is only dependent on the diagonal length of the infill, and it is independent of frame and infill stiffnesses. As a result, it may not predict all types of infill frame structures behavior. Bazan-meli method is also based on empirical formula calculated from parametric FE studies of single-story single bay frame and it is independent of properties of interaction between infill and frame.

Resultantly we can conclude that proposed approach is best to apply in infill frames structures as it is dependent on most of the possible variables present in the field.

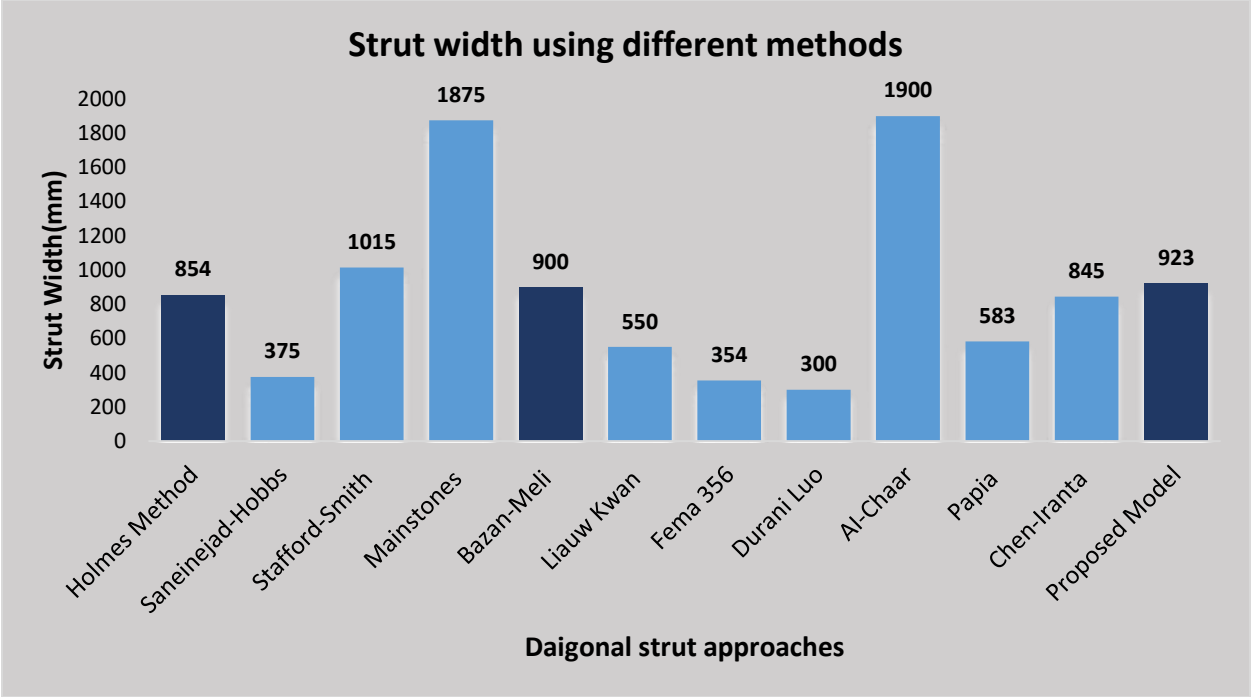

Fig. 39. The strut width using different approaches.

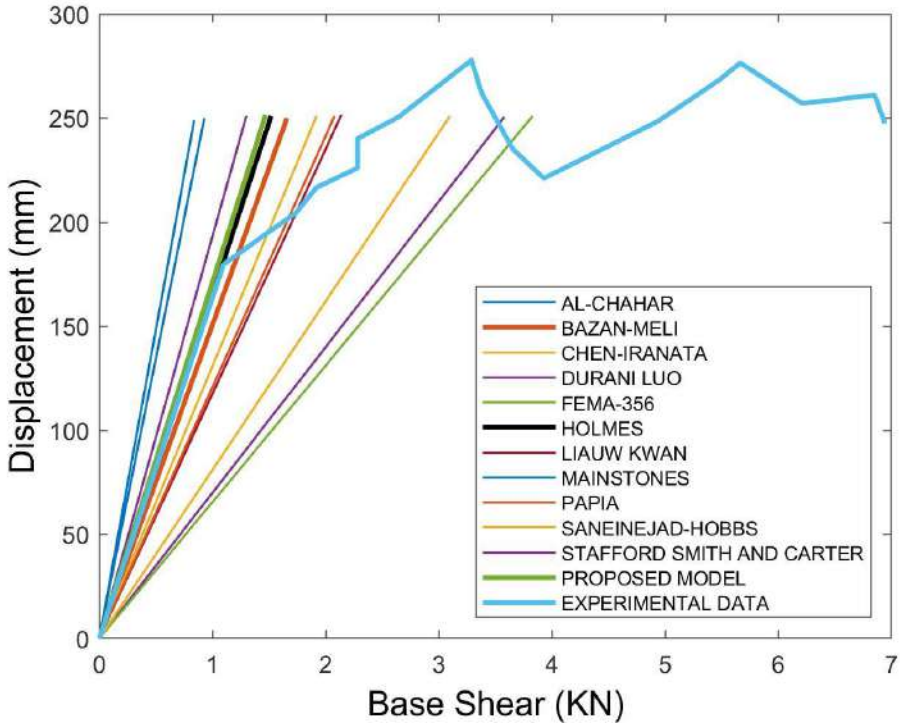

Fig. 40. The comparison of experimental results with various strut approaches.

4.5 Conclusions and Recommendations:

Infill panels have a significant influence in the building's response to dynamic excitation, revealing non-linear behavior since infill panels are the first to shatter during seismic excitation. As a result, designers require a practical, accurate, and explicit technique to simulate the nonlinear behavior of infill panels. Several techniques for modeling non-linear infill panels using pin-connected diagonal struts are now available in the literature. However, they are all either impracticable or do not adequately account for all the variables that may be present in various infill design scenarios. These variables include the design of the flexible connection between the infill panels and the frame elements, the reduction in stiffness caused by the percentage openings in the infill panels, and the geometry and material characteristics of the infill panels and the frame elements.

An adequate method for simulating the nonlinear behavior of infill panels was established in this study considering most of the factors variable in the field. The following are the key findings gathered from this study:

- The width of the strut is calculated using the classical initial stiffness formula with the following input parameters: Elastic modulus of the infill and frame components, the cross-sectional and member geometry of the infill and frame elements, and the flexibility of the connection between the frames. When these considered parameters vary, the structural responses such as the inter-story drift ratio, the displacement of the roof, and the stress in the infill walls also change significantly.
- Therefore, it's crucial to pick the finest infill panel material and the best technique for capturing the effects of these factors. The proposed model shows good comparison between shell and strut models for all types of variables considered.
- Along with the strut width formula, a stiffness reduction factor for the strut width was developed, allowing the strut width to be modified depending on if any openings were Present inside the wall. The infill opening has a substantial impact on the stiffness of the frame, fundamental period, inter-story drift ratios, infill stresses, and structural member pressures. They often rise as the opening size increases, demonstrating that the proposed technique correctly reproduced the reduction in stiffness.
- Presently, there are several techniques used in the industry to create flexible infill joints, reducing the forces that should pass to the infill panels under dynamic loading. Therefore,

a macro model should be able to capture this phenomenon as well. As demonstrated in figure 9, the suggested has the tendency to capture this phenomenon as well.

- To demonstrate the strut model's applicability, experimental data must be consistent with it. When validated over a set of experimental data the proposed model along with two other strut modeling approaches from the literature showed similar and accurate results. But the other two methods don't have any classical background and the number of input parameters to find the strut width is very less. The one proposed by Bazan and Meli [28] is independent of joint stiffness and based on empirical formulas. Holmes [24] has assumed strut with equal to diagonal length/3 which is only dependent variable for strut width. Therefore, the proposed model outperforms the approaches proposed by Holmes and Bazan as well.

Finally, it is concluded that the suggested strut modelling technique is the best for capturing many types of variations and is extremely practical to utilize during the structural design process and structural performance assessment on an existing structure.

4.6 Nonlinear modeling and performance assessment:

A nonlinear model for the case study building has been developed using Perform 3D. Fiber modeling has been used for columns and shear walls, while fiber hinge modeling has been employed for beams. The diagonal strut approach available in Perform 3D has been used for infill panels, and the strut width for these panels has been calculated using a previously developed approach. To analyze and compare the performance of both buildings, capacity curves have been generated and analyzed and following results comes as:

- ALECA buildings are less vulnerable to dynamic loadings as compare to building with masonry infill.
- ALECA panels fail at more drift than masonry panels.

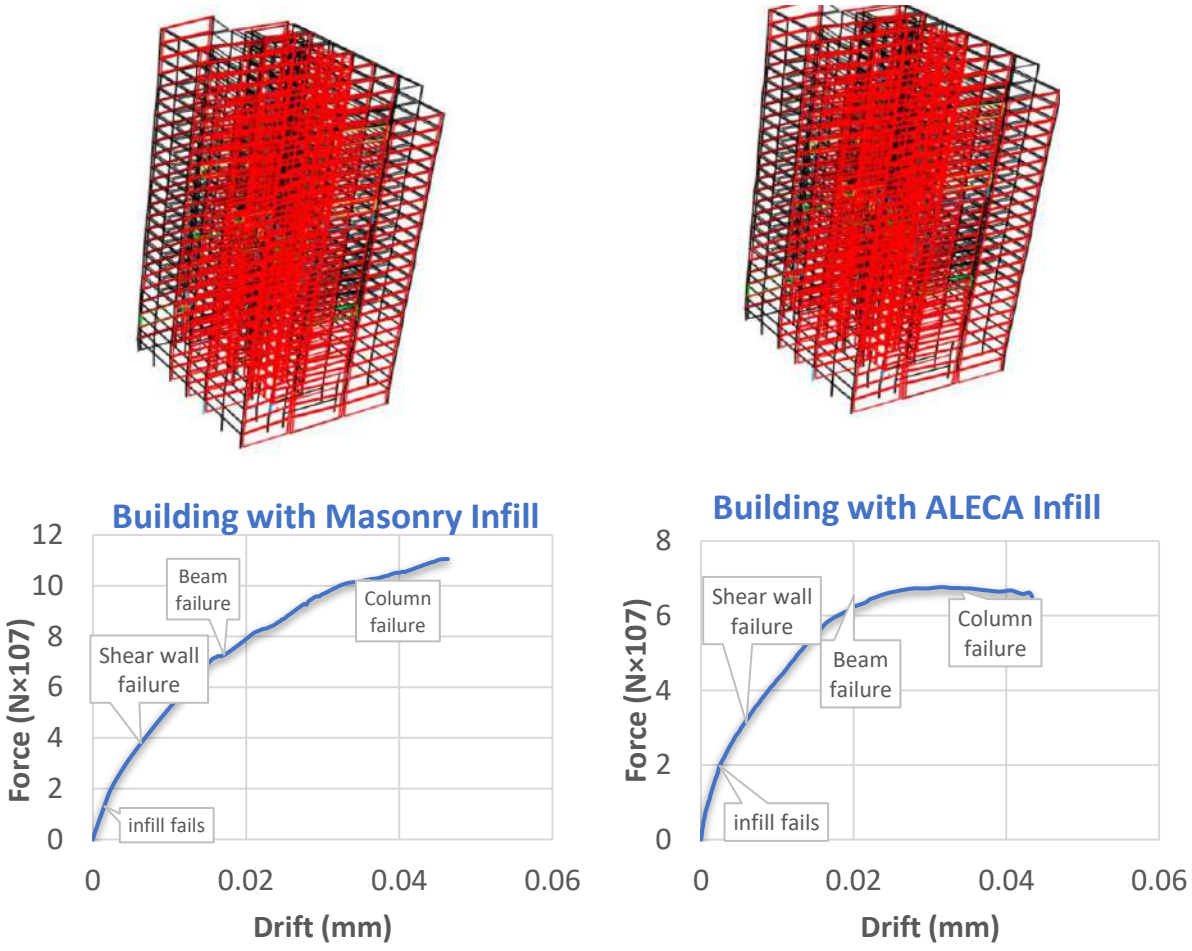

Masonry infill building **ALECA infill building**

Fig. 41. Capacity curves of building model with masonry and ALECA infill panels.

5. Conclusions and Recommendations:

Infill panels have a significant influence in the building's response to dynamic excitation, revealing non-linear behavior since infill panels are the first to shatter during seismic excitation. As a result, designers require a practical, accurate, and explicit technique to simulate the nonlinear behavior of infill panels. Several techniques for modeling non-linear infill panels using pin-connected diagonal struts are now available in the literature. However, they are all either impracticable or do not adequately account for all the variables that may be present in various infill design scenarios. These variables include the design of the flexible connection between the infill panels and the frame elements, the reduction in stiffness caused by the percentage openings in the infill panels, and the geometry and material characteristics of the infill panels and the frame elements.

An adequate method for simulating the nonlinear behavior of infill panels was established in this study considering most of the factors variable in the field. The following are the key findings gathered from this study:

- The width of the strut is calculated using the classical initial stiffness formula with the following input parameters: Elastic modulus of the infill and frame components, the cross-sectional and member geometry of the infill and frame elements, and the flexibility of the connection between the frames. When these considered parameters vary, the structural responses such as the inter-story drift ratio, the displacement of the roof, and the stress in the infill walls also change significantly.
- Therefore, it's crucial to pick the finest infill panel material and the best technique for capturing the effects of these factors. The proposed model shows good comparison between shell and strut models for all types of variables considered.
- Along with the strut width formula, a stiffness reduction factor for the strut width was developed, allowing the strut width to be modified depending on if any openings were Present inside the wall. The infill opening has a substantial impact on the stiffness of the frame, fundamental period, inter-story drift ratios, infill stresses, and structural member pressures. They often rise as the opening size increases, demonstrating that the proposed technique correctly reproduced the reduction in stiffness.
- Presently, there are several techniques used in the industry to create flexible infill joints, reducing the forces that should pass to the infill panels under dynamic loading. Therefore, a macro model should be able to capture this phenomenon as well. As demonstrated in figure 9, the suggested has the tendency to capture this phenomenon as well.
- To demonstrate the strut model's applicability, experimental data must be consistent with it. When validated over a set of experimental data the proposed model along with two other strut modeling approaches from the literature showed similar and accurate results. But the other two methods don’t have any classical background and the number of input parameters to find the strut width is very less. The one proposed by Bazan and Meli [28] is independent of joint stiffness and based on empirical formulas. Holmes [24] has assumed strut with equal to diagonal length/3 which is only dependent variable for strut width. Therefore, the proposed model outperforms the approaches proposed by Holmes and Bazan as well.

Finally, it is concluded that the suggested strut modelling technique is the best for capturing many types of variations and is extremely practical to utilize during the structural design process and structural performance assessment on an existing structure.

References:

[1] S. Roosta and Y. Liu, "Development of a Macro-Model for concrete masonry infilled frames," *Eng Struct*, vol. 257, Apr. 2022, doi: 10.1016/j.engstruct.2022.114075.

[2] S. Kömürcü and A. Gedikli, "Structural Analysis of Masonry Walls View project Advanced Plate and Shell Applications View project Macro and Micro Modeling of the Unreinforced Masonry Shear Walls," 2019. [Online]. Available: https://www.researchgate.net/publication/336472721

[3] P. Christou and C. Venizelou, "The Contribution of the Infill Walls to the Lateral Strength of Concrete Frames," *The Open Construction & Building Technology Journal*, vol. 13, no. 1, pp. 114–122, Jul. 2019, doi: 10.2174/1874836801913010114.

[4] U. Albayrak, E. Ünlüoğl, and M. Doğan, "An Overview of the Modelling of Infill Walls in Framed Structures," *International Journal of Structural and Civil Engineering Research*, pp. 24–29, 2017, doi: 10.18178/ijscer.6.1.24-29.

[5] https://masonrysociety.org/product/tms-402-602-2016/

[6] http://canadamasonrydesigncentre.com/download/10th_symposium/2c-6.pdf

[7] S.V. Polyakov, "Masonry in Framed Buildings," Gosudarstvennos izdate'stvo Literatury po stroitel'stvu i arkhitekture., Translated from the Russian by G.L. Cairns: Moscow, 1956.

[8] Holmes M 1961 Steel frames with brickwork and concrete infilling Institution of civil Engineers 19(4) 473–8

[9] Smith B S 1962 Lateral stiffness of infilled frames Journal of the Structural Division 88(6) 183–226

[10] Smith B S and Carter C 1969 A method of analysis for infilled frames Proceedings of the institution of civil engineers 44(1) 31–48.

[11] R. J. Mainstone and G. A. Weeks, "1e influence of a bounding frame on the racking stiffness and strength of brick walls," in Proceedings of the 2nd International Brick Masonry Conference, pp. 165–171, Stoke-on-Trent, UK, April 1970.

[12] K. M. Kareem and E. M. Güneyisi, "Effect of Masonry Infill Wall Configuration and Modelling Approach on the Behaviour of RC Frame Structures," *Arab J Sci Eng*, vol. 44, no. 5, pp. 4309–4324, May 2019, doi: 10.1007/s13369-018-3389-6.

[13] F. Khalid and S. Masood, "REVIEW OF INFILL WALL MODELLING TECHNIQUES: MACRO AND MICRO MODELS."

[14] L. Cavaleri, F. Di Trapani, P. G. Asteris, and V. Sarhosis,"Influence of column shear failure on pushover based assessment of masonry infilled reinforced concrete framed structures: a case study," Soil Dynamics and Earthquake Engineering, vol. 100, pp. 98–112, 2017.

[15] https://www.researchgate.net/publication/281281081_Evaluation_of_infilled_frames_an_updated_in-plane-stiffness_macro-model_considering_the_effects_of_vertical_loads

[16] F. J. Crisafulli and A. J. Carr, "Proposed macro-model for the analysis of infilled frame structures," *Bulletin of the New Zealand Society for Earthquake Engineering*, vol. 40, no. 2, pp. 69–77, 2007, doi: 10.5459/bnzsee.40.2.69-77.

[17] A. T. Akyıldız, A. Kowalska-Koczwara, and A. Kwiecień, “Stress distribution in masonry infills connected with stiff and flexible interface,” *Journal of Measurements in Engineering*, vol. 7, no. 1, pp. 40–46, Mar. 2019, doi: 10.21595/jme.2019.20449.

[18] M. Hohes, “STEEL FRAMES WITH BRICKWORK AND CONCRETE INFILLING.”

[19] “B. Mehrabi, P. B. Shing, M. P. Schuller and J. L. Noland. (1996),´ Experimental Evaluation of Masonry infilled RC frames

[20] https://www.researchgate.net/publication/27477890_Modelling_and_Analysis_of_Infilled_Frame_Structures_Under_Seismic_Loads

[21] G. Yang, E. Zhao, X. Li, E. Norouzzadeh Tochaei, K. Kan, and W. Zhang, “Research on Improved Equivalent Diagonal Strut Model for Masonry-Infilled RC Frame with Flexible Connection,” *Advances in Civil Engineering*, vol. 2019, 2019, doi: 10.1155/2019/3725373.

[22] L. Landi, P. P. Diotallevi, and A. Tardini, “Calibration of an Equivalent Strut Model for the Nonlinear Seismic Analysis of Infilled RC Frames.”

[23] A. T. Akyıldız, A. Kowalska-Koczwara, and A. Kwiecień, “Stress distribution in masonry infills connected with stiff and flexible interface,” *Journal of Measurements in Engineering*, vol. 7, no. 1, pp. 40–46, Mar. 2019, doi: 10.21595/jme.2019.20449.

[24] Holmes M 1961 Steel frames with brickwork and concrete infilling Institution of civil Engineers 19(4) 473–8

[25] A. Saneinejad and B. Hobbs, “INELASTIC DESIGN OF INFILLED FRAMES.”

[26] B. S. Smith, B. Phd, and C. Carter, “A method of analysis for infilled frames.”

[27] Mainstone R J 1971 Summary of paper 7360- On the stiffness and strengths of infilled frames The Institution of Civil Engineers 49(2) 230w

[28] bazan and R. Meli ,”seismic analysis of structures with masonary walls”in 7th world conf.on earthquake Engineering, Vol. 5, International Association of Earthquake Engineering (IAEE), Tokyo, 1980, pp. 633±640.

[29] Liauw and K.H.Kwan,”non linear behavior of nonlinear behavior of NON-integral infilled frames ,”computer and structures,vol.18,pp.551-560,1984.

[30] “FEDERAL EMERGENCY MANAGEMENT AGENCY FEMA 356 / November 2000 PRESTANDARD AND COMMENTARY FOR THE SEISMIC REHABILITATION OF BUILDINGS.”

[31] durrani and Y.H.LUO,”seismic retrofit of flat slab buildings with masonry infills ,”NCEER workshop on seismic response in masonry infills,1994

[32] G. Al-Chaar, “Evaluating Strength and Stiffness of Unreinforced Masonry Infill Structures Foreword,” 2002.

[33] G. Amato, L. Cavaleri, M. Fossetti, and M. Papia, “INFILLED FRAMES: INFLUENCE OF VERTICAL LOAD ON THE EQUIVALENT DIAGONAL STRUT MODEL.”

[34] H.M Chen and iranata,”realistic simulation of reinforced concrete structural systems with combine of simplified and rigorous component model “,structural engineering and mechanics , vol .30 ,No .5 ,pp. 619-645,2005

Chapter 8

MODULE - 5

BIM based conceptual framework to conduct LCC and LCA for infill materials in order to optimize the construction of Sustainable Buildings

Abstract:

This research paper presents a conceptual framework for the overall lifecycle assessments of different infill materials using Building Information Modeling (BIM). The proposed framework provides a standard operating procedure to conduct economic analyses through lifecycle cost assessment (LCCA) and environmental lifecycle assessments (LCA) swiftly to evaluate the best infill materials from the perspective of sustainability. The LCCA of materials was used to determine the most cost-effective infill material, whereas LCA gave us the most suitable material in terms of environmental performance. The LCA was conducted using a BIM model developed through Revit ®, which was then used to acquire the costs associated with the acquisition, construction, and operations associated with the material to conduct LCCA. Further, for LCA, the material's carbon emissions, eutrophication potential, and acidification potential were captured using a cloud-based software, “One click LCA ®”. The developed frameworkhelps select theoptimal infill material that carters both the environmental and economic needs of constructing sustainable buildings. selected scenario. This paper provides a comprehensive overview of the potential of using BIM for conducting LCA and LCC during feasibility studies to evaluate the performance of different infill materials over the lifecycle of projects.of different design options. This study will be beneficial for optimizing the construction of sustainable buildings as it evaluates infill materials to suggest the most economical and environment friendly option according to a project’s specific conditions.

8.1. Introduction

The world has seen a rapid transformation in the construction field due to extensive digitalization over the last two decades. The construction industry is not an exception in this regard. The AEC industry (architecture, engineering, and construction) has made good progress owing to digitization and Building Information Modelling (BIM) is one of the most promising developments in this field [1].The BIM models are intuitive, rich in information, and digital representatives of their real-world counterparts. The intuitive nature of BIM models has made it the natural progression from Computer Aided Technology (CAD) which did not provide such deep insights into the projects undertaken.

Construction has always been a complex industry with a lot of variables and factors associated with it. Traditional methods of construction planning and management lack accurately projecting the effect of design options on the overall performance of project. Clashes among architectural, structural, and HVAC plans often result in change orders and variations that add to the challenges associated with construction. However, BIM has resolved these issues by presenting coordinated models and clash detections to rectify such problems timely [2]. Thus, BIM has enabled planners and designers to make better decisions during the conceptual stages to optimize the performance of the entire building construction process. Besides developing tools for construction documentation and clash detection, BIM has a dedicated dimension to "Sustainability" which deals with energy studies and environmental impact assessments of construction projects in the form of Life Cycle Assessment (LCA). The LCA is a group of assessment techniques that quantify construction projects' economic and environmental sustainability [3]–[5].These assessments include Life Cycle Cost Assessment (LCCA) and LCA and deal with the environmental impacts of a project.

LCCA is a way of assessing the overall cost of a construction project at the end of its lifecycle. It is a powerful and effective way of analyzing the performance of a construction project from an economic perspective. It involves costs associated with different construction phases, such as manufacturing, execution, operation, and demolition [6]. However, LCCA is a complicated and lengthy process; hence it has not been standardized in the construction industry on a commercial scale. BIM solves this problem by incorporating intuitive and fast costing features such as Revit's

material take off schedules and by intuitively calculating quantities for each building element such as walls and floors etc.

Previous studies have attempted to illustrate and quantify the ability of BIM in quantity take offs and estimation of building construction cost [7]. Noor Akmal *et al.* argues that BIM has great potential in accurately calculating the construction cost of projects [8]. BIM has extended its cost estimating capabilities from construction to operational cost, which primarily involves energy costs, i.e., fuel and electricity. Sumedha Kumar *et al.* assessed the energy simulation capabilities of BIM-based software applications such as Green Building Studio ® (GBS) and Insight ® which the United States Department of Energy (DOE) and American Society of Heating, Refrigerating and Air-Conditioning Engineers (ASHRAE) backs [9]. The demolition cost of a project is also an integral component of LCCA as it provides potential salvage value and end-of-life savings captured through pertinent BIM tools [10]. Dermot and Jason underscored the necessity of BIM-based frameworks to integrate LCCA and BIM effectively to standardize the design process [11].

In addition to cost-saving benefits, BIM has expanded its services in the domain of environmental assessment by developing tools, such as Tally® and EC3® (Embodied Carbon in Construction Calculator), which estimate the environmental impacts of building projects. Efforts have been made to integrate the process of LCA with BIM to utilize their potential benefits[12]. One of the earlier frameworks used to evaluate BIMmodels' environmental performance was inventory analysis [13]. Further researchers conducted LCA with BIM using the globally renowned International Organization for Standardization *ISO 14040* standard [14]. Lately, smart, and effective plugins have been developed to make this process easy so that environmental assessment using BIM may be adopted widely on a commercial scale. One such plugin is the Tally ® which has a fine material library and analyzes the environmental performance of buildings over their lifecycle [15]. Tally®, however, had a limited material library, so LCA could not have been performed for dynamic materials. This issue has been addressed by One Click LCA ®, which is a cloud-based application and plugin. The integration of LCA with BIM through One Click LCA® was found to be immensely beneficial due to its diverse material library that supports more than 90,000 material databases and seamless interoperability with the BIM platform (Revit) [16].

LCCA is a method of measuring and managing the cost of a project over its lifecycle. Performing LCCA at the initial stages of the project gives a better understanding of the parameters that affect

the project's cost over its lifetime [16]. LCCA helps in getting a better outlook on design options by indicating their economic performance. It suggests the best option based on lowest cost over the project's lifecycle. However, manual LCCA is challenging and hectic due to many variables involved in it. Using BIM, designers could perform LCCA without spending much time and effort [17].Thus, BIM provides an opportunity to benefit from the prospects of LCCA without the worries and implications of spending much time and energy on the process. LCA assesses a product's environmental impact over its lifecycle, including building materials. Performing LCA during the conceptual stage provides insight into the materials' environmental impacts, which is crucial in the context of climate change. Traditional methods result in time overruns, but BIM's "One Click LCA ®" tool is a swift and reliable way to conduct detailed environmental impact studies.

Efforts have been made to conduct LCCA and LCA with BIM independently [18], [19]. However, no substantial contributions have been made to provide any means to evaluate different infill materials in order to come up with the most sustainable alternative. Previous studies lack contributions in providing any framework to project the lifetime performance of infill materials that would help planners chose better materials during the feasibility studies. This study aimed to develop a conceptual framework that would employ the tools and platforms of BIM to comprehensively conduct LCCA and LCA during the conceptual phase of a project in order to find out the most economical and environment friendly infill material over the lifecycle of project. Accordingly, the objectives of the study are (1) To provide a conceptual framework for evaluating infill materials for their economic and environmental performance. (2) To optimize the use of economic and environmental resources by choosing better infill materials based on their performance over the entire lifecycle of building.

The proposed framework aims to standardize and simplify assessments on a commercial level. The study applies the framework to evaluate established and emerging infill materials such as Bricks, Concrete Masonry, Auto Aerated Blocks (AAC), and Lightweight Expanded Clay aggregate (LECA) blocks, providing recommendations for the best design option based on economic and environmental considerations during project's conceptualization. This framework should allow the planners and designers to select best infill materials that provides value to the owners of buildings by decreasing their lifecycle cost. Also, it would suggest the infill material having least environmental impact in the form of Global Warming, Acidification and Eutrophication. These

factors were chosen due to their prominence as environmental threats. The chosen factors for LCA include carbon emissions, which are greenhouse gases emitted into the atmosphere mainly due to human activities like burning fossil fuels. These emissions pose a major threat to sustainable construction and have significant global warming potential, resulting in climate change impacts such as floods and melting glaciers. Similarly, Acidification is the release of protons into the atmosphere. As a result, the pH of soil and specifically water decreases, causing ecosystem acidification [20]. It gives rise to one of the most frequent environmental problems: acid rain. It is also called "Climate Change's Equally Evil Twin". It is of great significance in the regions adjoining oceans and seas. It is a highly hazardous phenomenon that must be considered for the well-being of our environment [21]. Whereas Eutrophication is when the environment becomes enriched with nutrients or growth factors necessary to the plants and algae, resulting in excessive growth [22]. Most prominent of these nutrients include compounds of **Phosphorous** and **Nitrogen** [23]. Excess nutrients in water cause unwanted plant and algae growth, so it's important to consider this when choosing construction materials near water bodies. It's essential to evaluate and understand the environmental impact of the materials based on this factor.

The methodology section describes the proposed framework and its components. BIM models were created for each infill material studied, and a case study of a hospital in Lahore was conducted to apply the framework. The results for LCA (Carbon Emission, Acidification, and Eutrophication) and LCCA (Material, Construction, Operation, and Demolition Cost) are presented, and an optimal infill material is chosen based on performance. The study concludes with recommendations for future research.

8.2. Methodology and Proposed Framework:

The current study adopted a multi-stepped approach in which the framework was devised at first for conducting LCC and LCA using BIM. This was followed by developing BIM models and adding materials to the material library of Revit. Then LCCA was performed for each phase of construction project followed by LCA studies taking into account major environmental concerns such as Carbon Emissions etc. (infographic)

8.2.1 Proposed Framework:

This approach is based on evaluating the key components of LCCA and LCA early on the project's lifecycle. A visual representation of the process is provided in **Fig. 42.**

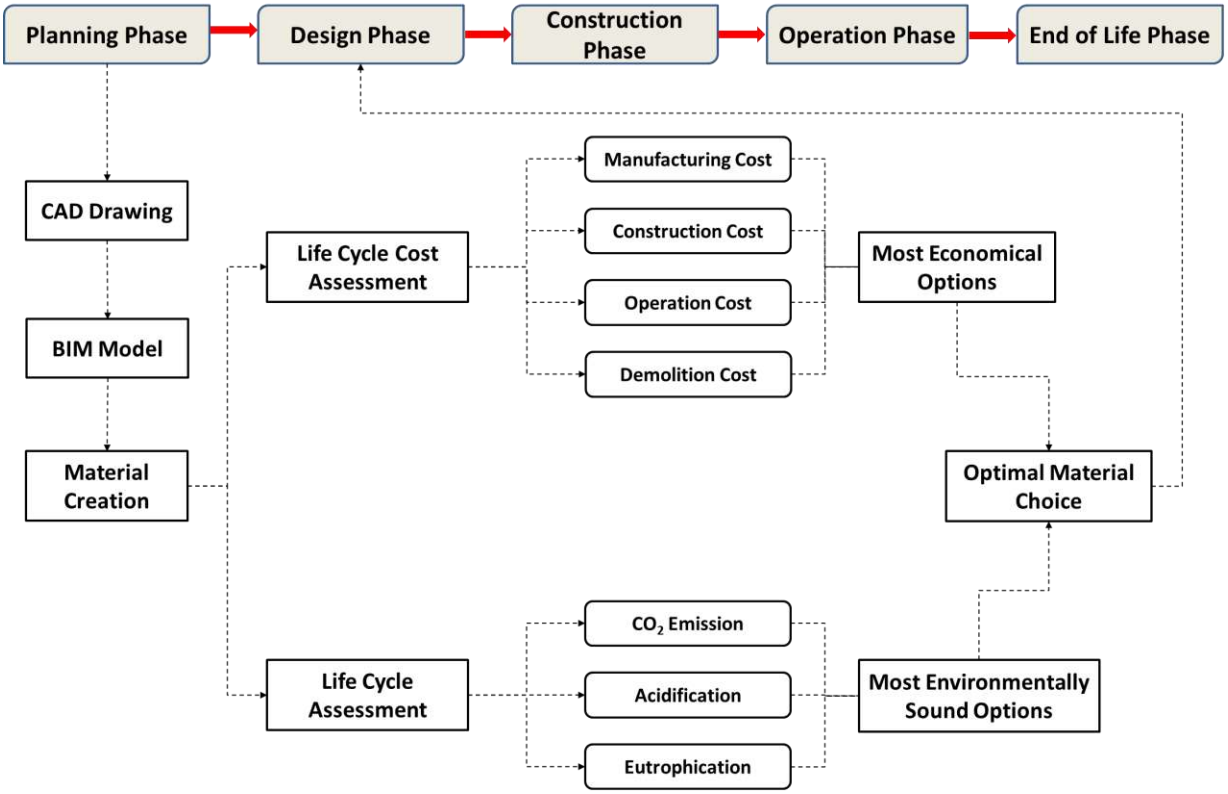

Fig. 42. BIM based conceptual framework for LCC-LCA.

Preliminary design documents are acquired by the BIM team along with a possible set of infill materials that might be used later on in the project. The BIM team adds the materials of interest to the Revit ® Material library followed by preparing identical BIM models for each design option. Then a part of the team works on LCCA while the other works on LCA. The team working on LCCA calculates the cost of material based on the Market Rate System specific the locality of the project, construction cost based upon the amount of material and labor cost, operation cost based upon the energy efficiency of building owing to the thermal properties of infill materials and finally the demolition cost for the project. This is mainly performed by using Revit ® for quantity surveying of materials along with Green Building Studio ® and Insight 360 ® for energy studies. The material having the least lifetime cost is regarded as the "Best option as per LCCA". Simultaneously, the team performing LCA calculates the Carbon emission, Acidification potential and Eutrophication for each infill material. These environmental impacts are selected as they are

some of the most prominent issues induced by the construction industry onto the environment. A cloud-based platform called “One Click LCA ®’’ would be used to perform LCA. The material having the least environmental implications is selected as “Best option as per LCA”. Based upon the results of LCCA and LCA, an optimal material is chosen which serves both economic and environmental concerns as the most suitable design option. In case there is a conflict between the materials suggested by both teams, then the choice of infill material will be taken according to the specific needs of the project based upon its location as different parts of the world face different challenges. For example, the most economical option will be chosen by developing countries over environmentally friendly options as finance is a bigger issue in such countries. However, in developed countries, where economic resources are not strained, as well those regions facing harsh effects of climate depletion will prioritize LCA over LCC. Therefore, the decision in such cases will be best left upon the discretion of Project Managers and on the individual needs of the locality of the project. The information about the best infill materials will be then used in the Design phase of the project when preparing specifications and schedules during the detailed design process. As a result, the planners and designers will get an idea of the performance of different materials during the conceptual/design stage and will choose the most appropriate design options based on their performance.

8.2.2 BIM Model Creation:

BIM model was prepared according to the CAD drawings acquired for a project of our interest. Multiple copies of the model were produced for each infill material under study to assess their effects on cost and environment. The BIM models created for this study were developed up to LOD 300 to comprehensively carry out assessments such as Energy Simulations for operational costs and to acquire quantities of material required in infill panels. This involved creating coordinated models for each infill material having Architectural plan, Structural plan, Energy model and HVAC plan along with the properties of infill materials used in its walls. The models were used to carry out LCCA and LCA assessments for infill materials based upon the quantity of materials obtained from Revit’s Material Takeoff schedules and Energy simulations to quantify heating and cooling costs.

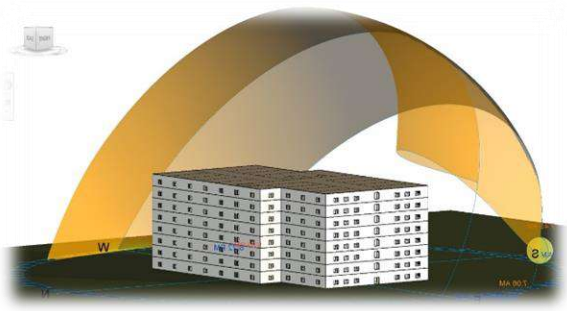

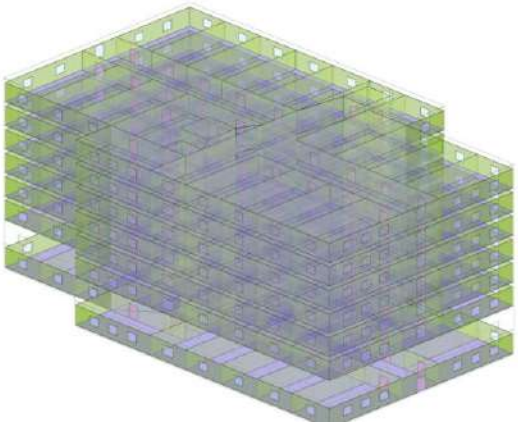

(a)

Gross Floor Area = 34950 ft^2

Number of Floor = 8

Total Wall Area = 224179 ft^2

Total Wall Volume = 153930.46 ft^3

(c)

Fig. 43. Components of the BIM model,0 (a) Coordinated Revit Model, (b)Energy Model, (c)CAD Drawings Imported in Revit, (d) General Properties of the Building.

8.2.3 Material library:

Once the models were developed, the next process was to add materials in the Revit's Materials Library. In this study, four materials have been considered:

1. Brick
2. Concrete block masonry
3. Aerated autoclaved concrete.
4. Lightweight expanded clay aggregate concrete panels.

These materials were chosen to have a good blend of both traditional and non-traditional materials used for construction. Having Bricks and Concrete Blocks as key materials were necessary as they

make up the bulk of the construction material's market shares and are widely used on a commercial scale in the case study region [24]. Further, lightweight aggregate concrete block (LECA) and autoclaved cellular concrete (AAC) blocks were incorporated into the study as these are novel materials that have shown great potential for their widespread use is projected to grow rapidly in the near future [25], [26]. AAC and LECA were added to in Revit's material library, whereas brick and concrete block were already present. After adding their respective properties, they were separately applied to the model's walls we had created previously. Afterward, these models were utilized to perform LCC and LCA for each material to determine their performance from the perspective of Sustainable Building. The properties of infill materials that were added to the material library of Revit ® included Thermal conductivity, Specific Heat and Density as shown in **Table 18**. Thermal conductivity is defined as "the rate at which heat is transferred by conduction through a unit cross-section area of a material, when a temperature gradient exits perpendicular to the area" [27]. This property shows how readily a material transfers heat through a unit area when a temperature difference occurs between its ends. This property is important in determining the transfer of heat through infill materials to evaluate their insulating capacity. Good insulating materials yield low thermal conductivities. Whereas Specific heat is defined as "the amount of heat that is required to increase the temperature of unit mass of that particular substance through one degree" [27]. This is a measure of the amount of heat stored in a material to create a temperature change. The higher the Specific Heat, the better is the insulation. Lastly, density is the mass per unit volume of materials. Usually, materials with higher density have better thermal properties. However, different materials have been discovered that have lower densities yet good insulation properties such as EPS [28].

Table 18

Materials chosen for analysis and their properties.

Materials	Thermal Conductivity (W/mK)	Specific Heat (J/kg.K)	Density(kg/m3)
AAC	0.7	1050	510
Brick	0.34	840	1800
Concrete Block	1.30	860	1500
LECA	0.208	1100	650

AAC = [29] Brick = [30] Concrete Masonry Block = [30], [31], LECA= [32]

Next step was applying the workflow that was devised to perform LCCA and LCA. There are numerous steps devised in the framework and each of them were performed for all infill materials under study. After applying the framework for each infill material, their economic and environmental performance was evaluated and compared to assess the best design option available in the study sample. A Case Study Building: Well Care Hospital Lahore, Pakistan

For the case study, Well Care Hospital situated in Lahore (Pakistan) was considered. It is an actual hospital that is currently operational. The construction drawings wrere obtained from the INN Consulting which rendered the design for the hospitial during its construction. Based on the CAD drawings provided, BIM models were created for each infill material under study. Details about the BIM models developed are given in **Table 19**.

Table 19

Details about Revit models.

Gross Internal Floor Area	34950 ft^2
Number of Floors	8
Operational Hours of Model	24/7
Energy Model	According to Volumes and Spaces

8.3.1 Life Cycle Cost Assessment:

LCCA was conducted using Revit for quantity survey and cost estimation of building components for each material. Also, the energy use and its respective cost were estimated using Insight 360 ®

to calculate the operational cost of the BIM model. Detailed explanation and illustration of the LCCA process is as follows:

8.3.1.1 Definition of Scope

Our study encompasses the Material cost, Construction cost, Operation cost, and Demolition cost for the BIM models having the infill materials of our interests.

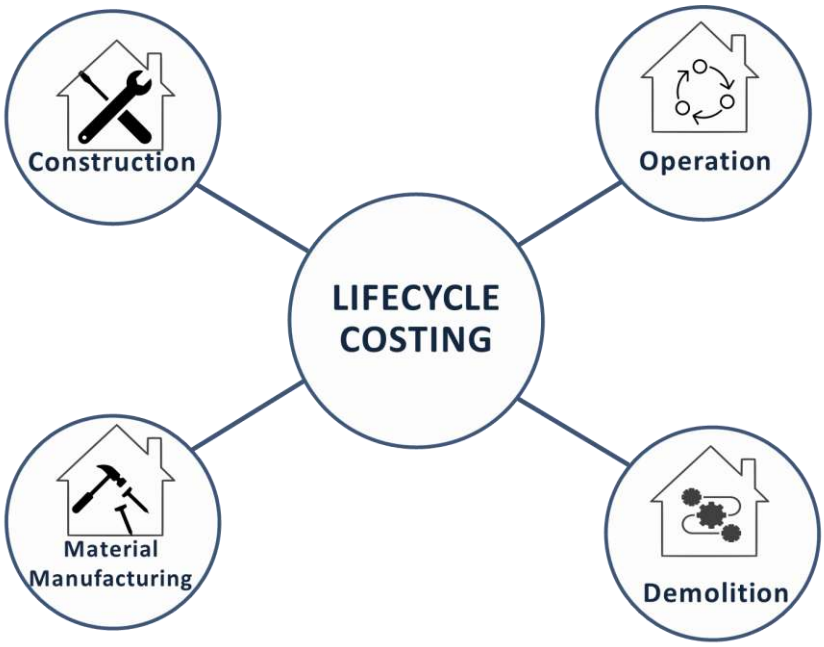

Fig. 44. Scope of Life Cycle Cost assessment.

8.3.1.2 Material Cost

Material cost is a term used to define the unit cost of any material. Material cost is quantified after considering different stages of making the product. The first step in LCCA is determining the infill materials' cost. The cost of Concrete masonry block, LECA, AAC and Bricks was acquired from Punjab Pakistan's 2023 market rates system (MRS) and was illustrated in **Table 20**. The MRS is a document that serves as a reference for cost estimates of construction projects, maintenance, and repair work. Next, the composite material cost was extracted, including the cost for the unit quantity of material and unit labor cost.

Table 20

Material cost of the infill materials under study.

Materials	Price USD
LECA	1.89
AAC	2.34
Brick	1.80
Concrete Masonry Block	1.50

LECA [32]; Brick, Concrete Blocks [33]; AAC [34]

8.3.1.3 Construction Cost

Construction cost is the cost incurred during the construction of a project. Construction cost consists of the costs of materials needed to build the project according to the desired specifications. It also includes the labor cost needed to perform different tasks to realize the project's intended outcome, i.e., the construction of a building or infrastructure, etc. Calculating the construction cost of a project is important as it gives insights into the amount of resources (human and material) that will be used to construct the project. An entire dimension of BIM is dedicated to calculating the construction cost of buildings, i.e., the 5^{th} Dimension of BIM or 5D BIM. 5D BIM deals with cost estimation, analysis, and budgetary tracking.

For this research, the 5D characteristics of BIM were employed to estimate the construction cost of case study building. First, the total quantity of material required in the walls of the entire project was calculated using Revit. Revit is an intuitive software that keeps track of the quantity of each material used in the building elements of the entire project. This saves a lot of time and effort which would be consumed if this process was to be done manually. In the next step, the material prices were added to the Revit library using the values from **Table 19**. Then the "Add Calculated Parameter" function of the Revit schedules was used to create a custom formula. The pertinent formula, given in equation1, was used to calculate the cost of the material for the case study project.

Cost of the material = (unit price of material and labor cost) x **(**Quantity of material in infill panels)

This process was done for each infill material under study. Construction cost for each material was calculated from their pertinent model and compared with each other. The analysis indicated that Concrete Blocks had the lowest price in terms of construction cost which gives us an indication of the cost that will be incurred during the initial phase of the project.

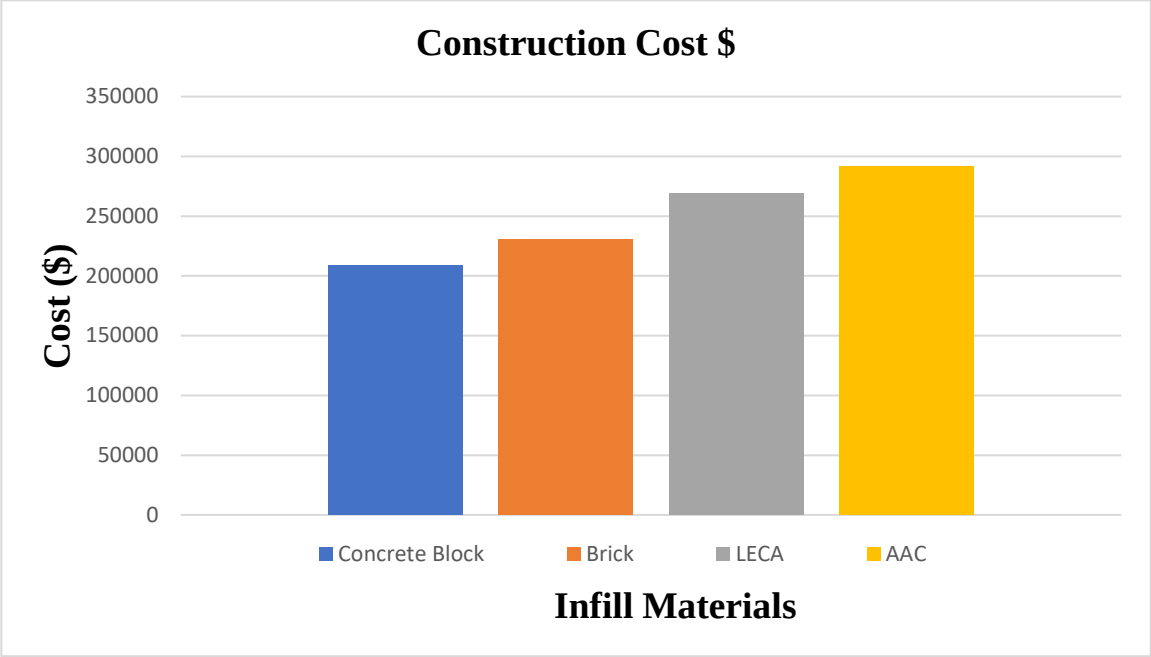

Fig. 45. Construction cost comparison of infill materials.

8.3.1.4 Operation Cost

Operation cost of a building consists of all the expenses incurred during the functioning or operation of the building for its intended purpose or use. It is mainly composed of costs of building utilities and the cost spent on the heating and cooling of the building's spaces. Operation cost is mainly an indicator of the building's energy efficiency (heating and cooling loads) [35]. It gives the performance of a building regarding the amount of energy it requires to maintain a certain range of temperature within its rooms and envelope throughout the year. And infill materials greatly influence the energy consumption of buildings as they can provide good insulation thus reducing the amount of energy needed to maintain room temperature. However, the choice of a poor infill material having bad insulation properties can lead to increased energy consumption for heating and cooling, which increases the operational cost. Building operation cost makes up most of the cost of the building's lifecycle. Therefore, it is an important factor to be computed to visualize the overall performance of different materials.

BIM provides two powerful tools to calculate energy efficiency. They are Insight 360® and GBS. Both are cloud-based applications that import the energy model created in Revit in gbXML format. The energy model is created in a specific location for which the weather data is obtained from the

nearest World Meteorological Organizations (WMO) weather stations integrated into Autodesk Revit. A design temperature is provided for Revit's energy model to be maintained inside the building's spaces. Then, analysis is performed through Insight 360® and GBS to calculate the energy required to maintain the design temperature within the building's spaces.

In this study the locations chosen to test the performance of materials were Lahore, Islamabad, Karachi, Peshawar, and Quetta. The reason for performing energy simulations for multiple locations was that different materials perform variably under different climate conditions. So, to comprehensively evaluate the performance of the design options under study, analysis was performed for different locations having diverse weather conditions. Moreover, these five locations were chosen specifically because these major cities of Pakistan are located in different climate regions. Therefore, all these locations have different characteristic weather conditions. Performing energy analysis for these locations helped us evaluate the performance of our design options in almost all climate zones of Pakistan, thus giving us a more comprehensive outlook of the design options. The building type selected was a hospital and the operation type was set as 24/7 because it is a health care facility. The heating and cooling set point where the facility was set at room temperature of 20-22 Degree Celsius [36]. After creating the energy models of the building for each material according to the specifications, the energy models were uploaded to Insight 360® for analysis. The energy use intensity of our models were computed accordingly; the results are given in **Fig. 46**.

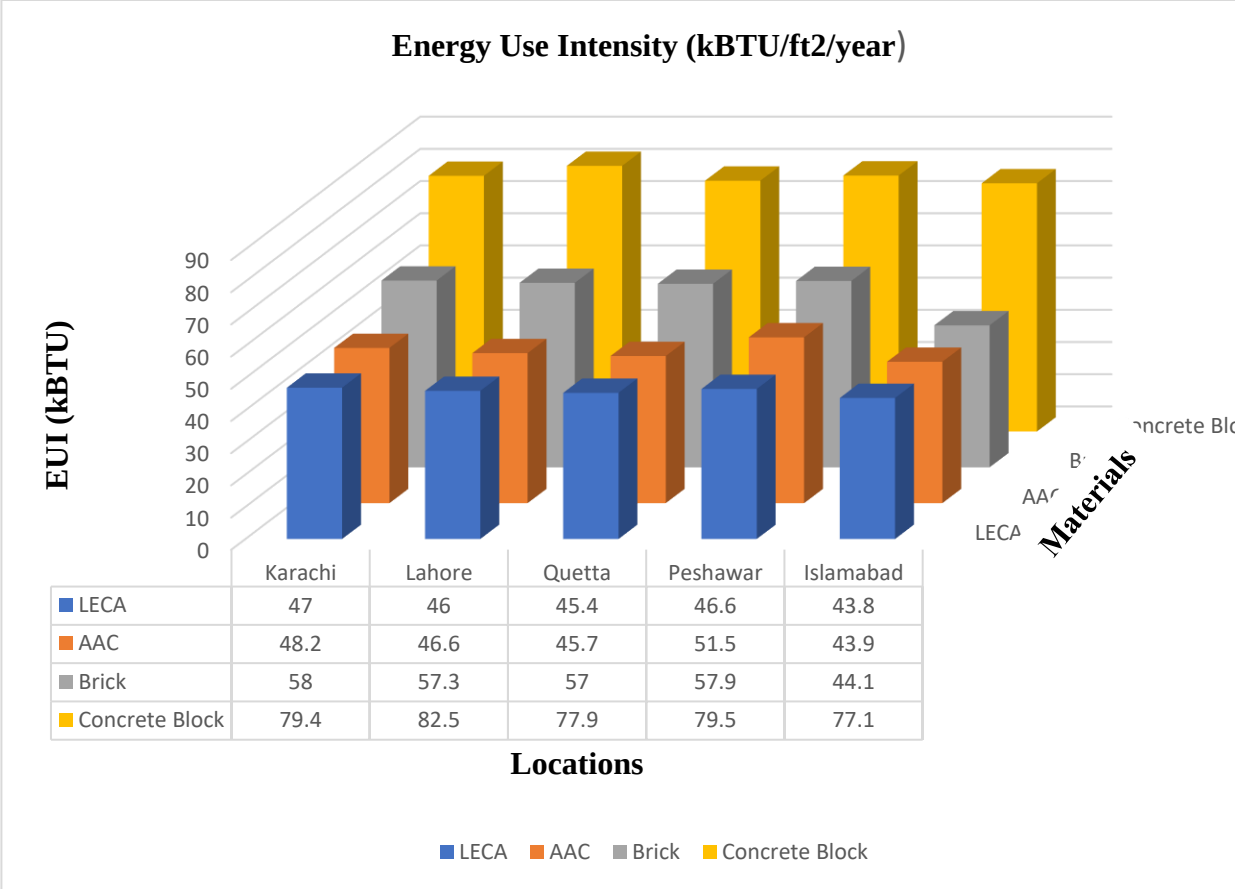

	Karachi	Lahore	Quetta	Peshawar	Islamabad
LECA	47	46	45.4	46.6	43.8
AAC	48.2	46.6	45.7	51.5	43.9
Brick	58	57.3	57	57.9	44.1
Concrete Block	79.4	82.5	77.9	79.5	77.1

Fig. 46. Chart for comparison of energy use intensity for infill materials.

The data in **Fig. 46.** is representative of how much energy is required to heat and cool a unit square foot of building throughout the year. These values are affected by the thermal properties of the materials used in the model. The materials having high specific heat tend to maintain a specific temperature without dissipating or absorbing excess heat to or from the atmosphere. Thus, the energy efficiency of the models is a function of their intrinsic thermal properties.

Similarly, Insight 360 ® provides the operational cost to maintain the temperature within the spaces of the case study building based on the energy used for maintaining the temperature within our model throughout the year. First, the unit cost for cooling (electricity) and heating (gas), provided in **Table 21**, were given to Insight 360® as utility rates following [37], [38].

Table 21

Utility Rates for Cost of Energy.

Type	Unit Cost
Electricity	0.125$ per KWh
Gas	0.2257 per Therm

Then, Insight 360® was used to calculate the average annual cost spent on energy, as given in **Fig. 47.** The following chart shows the average annual cost that would be incurred on yearly basis for the BIM models set in 5 different cities of Pakistan. These cities are falling in different climate conditions. The cost incurred is a function of the infill materials and their thermal properties. The costs incurred indicate the energy efficiency and corresponding economic performance of the infill materials.

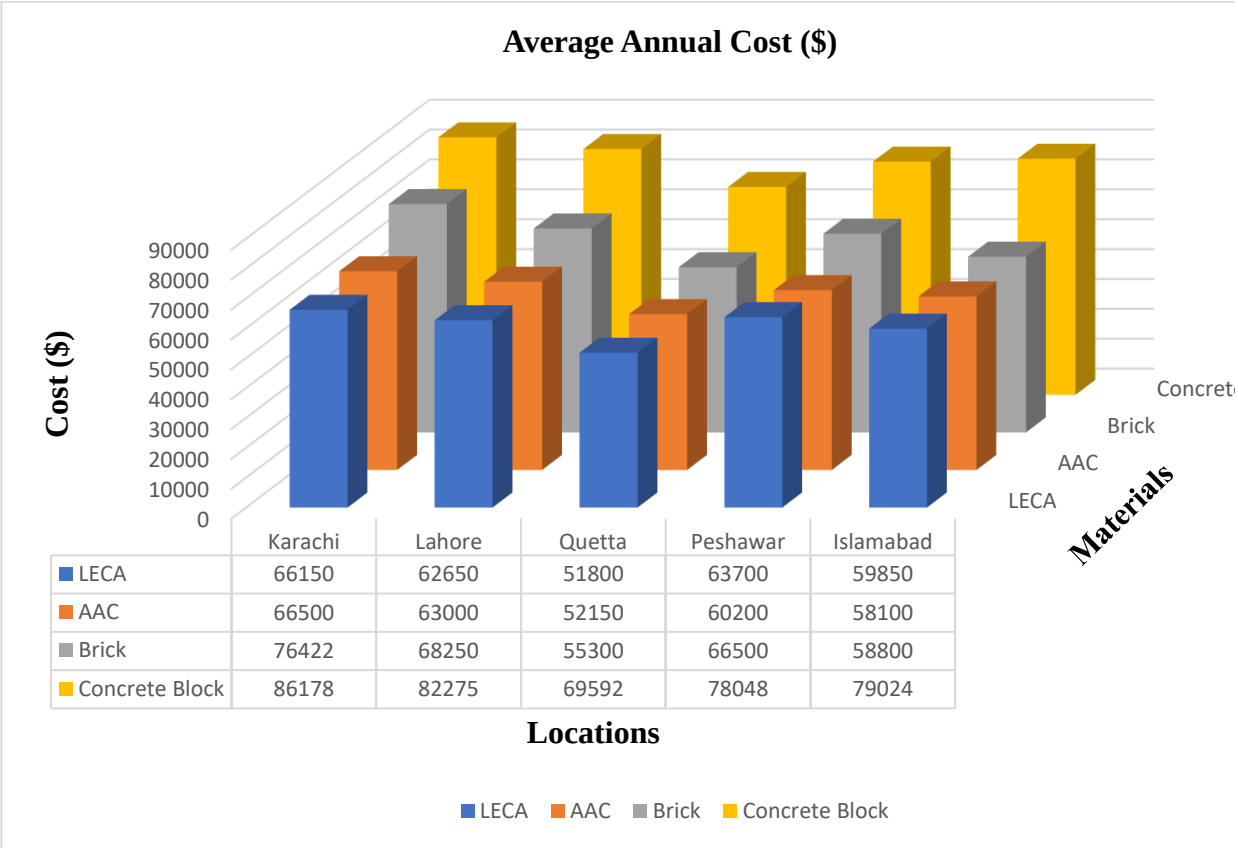

Fig. 47. Average annual cost comparison.

To validate the results, average annual electric use for hospitals as given by DSO Electric Cooperative (2009) was used that is around 27.4 kWh/ft^2. For the case study building, having 34950 sq ft area, the value equals 961125 kWh/sq ft of energy use per year. Multiplying it with the unit cost for kWh of energy (**USD** 0.125**$),** it becomes 120140.6$ per year. However, this figure

is for the entire expenses of the hospital. In reality, HVAC takes up 33 percent of hospital's energy, equivalent to 39646.4$/year [39]. After incorporating an average inflation rate of 2.69% per year, this amount rounds up to around USD 60000$ per year [40]. Hence, it can be concluded that the calculation is a good estimate of the real operational cost of the hospital. Similarly, the results generated in GBS were used to validate the analysis results extracted from Insight 360®. The results for energy use intensity obtained from GBS are visualized in **Fig. 48**. These results show how much energy is needed to heat or cool a unit area of the building. This is affected by the infill materials used and their thermal properties such as insulation which naturally regulate the temperature of the building.

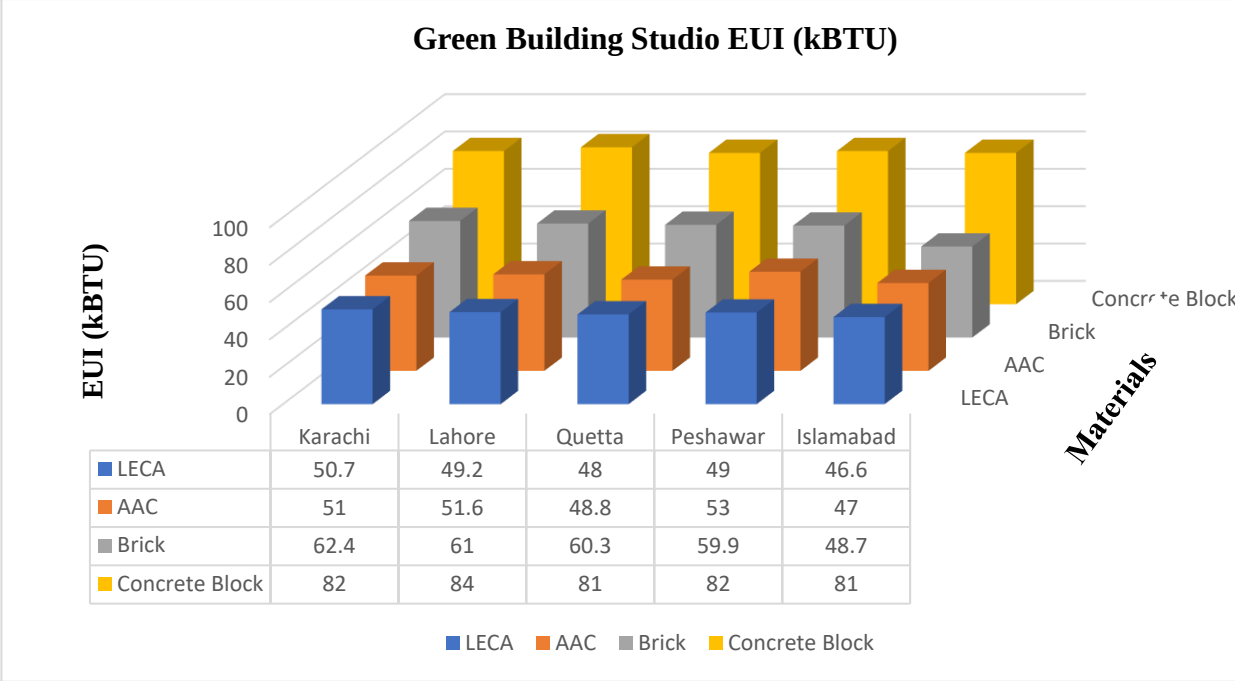

Fig. 48. Green building studio energy use intensity comparison chart for validation of results.

The results for Energy Use intensity and its corresponding Average Annual Cost obtained from Insight and GBS comply with each other with minor variations which comprehensively illustrates the accuracy of energy analysis performed in this study. The precision of results acquired from both platforms is illustrated by **Table 22**. For simplicity, this table shows only the results for LECA.

Table 22

Comparison of Results for Energy Use Intensity given by GBS and Insight 360.

Infill Materials	Insight 360	Green Building Studio
Karachi	47	50.7
Lahore	46	49.2
Quetta	45.4	48
Peshawar	46.6	49
Islamabad	43.8	46.6

From the above analyses, it is evident that LECA is the best-performing material in case of operational cost as it has the lowest energy expense of all materials under study.

8.3.1.5 Demolition Cost

The final parameter in LCCA is the demolition cost, also known as the end-of-lifecycle cost. It is the amount of money employed to demolish the project after it has run the course of its lifecycle [41]. It mainly consists of the labor cost that will be used to dismantle the building's elements. Therefore, it is important to calculate the demolition cost for a project at its planning stage as it can greatly influence the overall lifecycle cost of the project. Estimating the demolition cost provides the amount of money used to dismantle a project at the end of its lifecycle for a specific material used during its construction. Different infill materials have to be dismantled in different manners which results in different demolition costs. Therefore, it is necessary to calculate the demolition cost for infill materials available during conceptual stage to get an idea about how different materials will effect the overall cost of project at the end of their lifecycle.

The demolition cost for our models was calculated using Revit's Schedules. First, the quantity of material to be demolished was determined using schedules of Revit. Only those materials were considered which were used in walls were used since our design options are limited to infill materials for this study. After that, the "Add Calculated Parameter" function of Revit was used to create a custom formula, in which we multiplied the Quantity of material to be demolished by the Unit Cost of Demolition for that material. The formula is presented in equation 2 below.

Demolition Cost= (Unit price of Labor cost for dismantling works) x (Quantity of infill material/panels to be Demolished)

The unit demolition cost for respective materials was picked from MRS Punjab 2022 (July). Therefore, the unit price for each material under study is provided in **Table 23**.

Table 23.

Unit Cost for Demolition of Materials.

MATERIAL	DEMOLITION COST ($) AND ITEM NUMBER IN MRS
LECA	0.10 (item 17)
AAC	0.14 (item 14)
BRICKS	0.16 (item13)
CONCRETE BLOCK	0.14 (item 14)

Reference for MRS = [33]

After performing the calculations using equation 2 via Revit's schedule, the results for the demolition costs of various materials were obtained, as shown in **Fig. 49**. The following chart consists of infill materials under study plotted on x-axis and their demolition cost calculated is plotted on the y-axis. This shows the cost incurred to dismantle the walls based upon the type of infill material used.

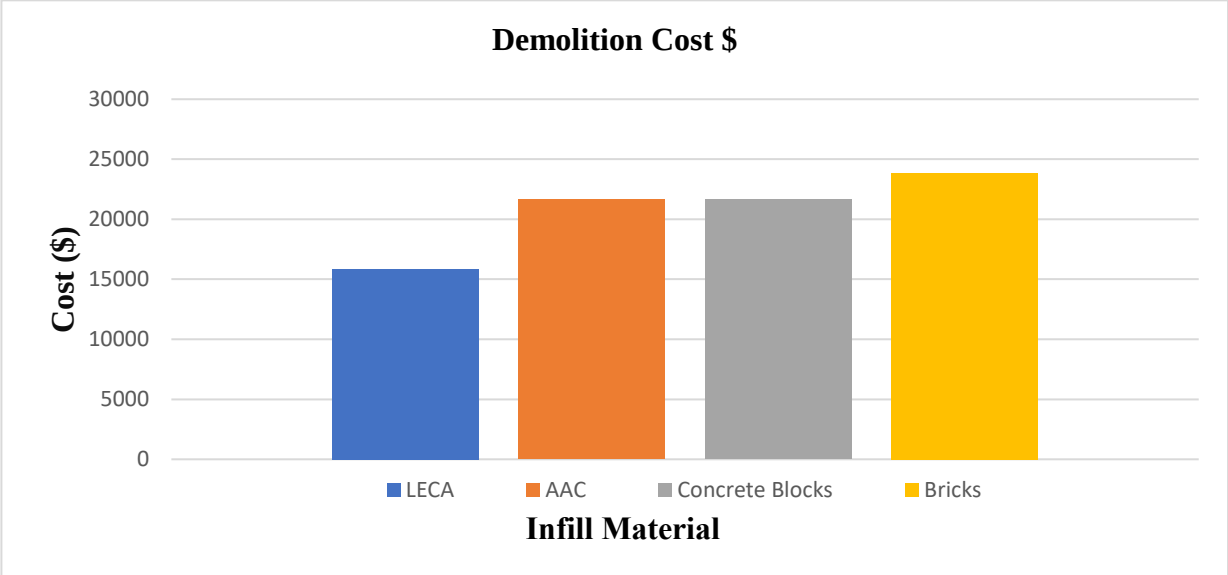

Fig. 49. Comparison chart for demolition cost of in fill materials.

It is important to mention that not only is the demolition cost the lowest for LECA, but it is also made up of natural aggregates with a huge potential for reusability, thus helping with sustainability and circularity endeavors. Furthermore, this elevates the salvage value of LECA among its counterparts.

8.3.1.6 Total Cost of Project and Best Option as per LCCA

As per LCCA using BIM (Revit), it was found that LECA was the best design option to be used on the walls of the building under study for our conditions. Using LECA would save USD 221242 at the end of its life cycle (60 years) [42] compared to the second-best performer, AAC. Thus, even though the construction cost for LECA was high, using it would provide a great return on investment due to its lowest lifetime cost as a result of energy efficiency and salvage value. Therefore, using BIM to assess the cost-effectiveness of design options will enable the designers to go for a better option in terms of building materials. **Fig. 50.** shows the lifetime cost of all infill materials incurred during various stages of the project.

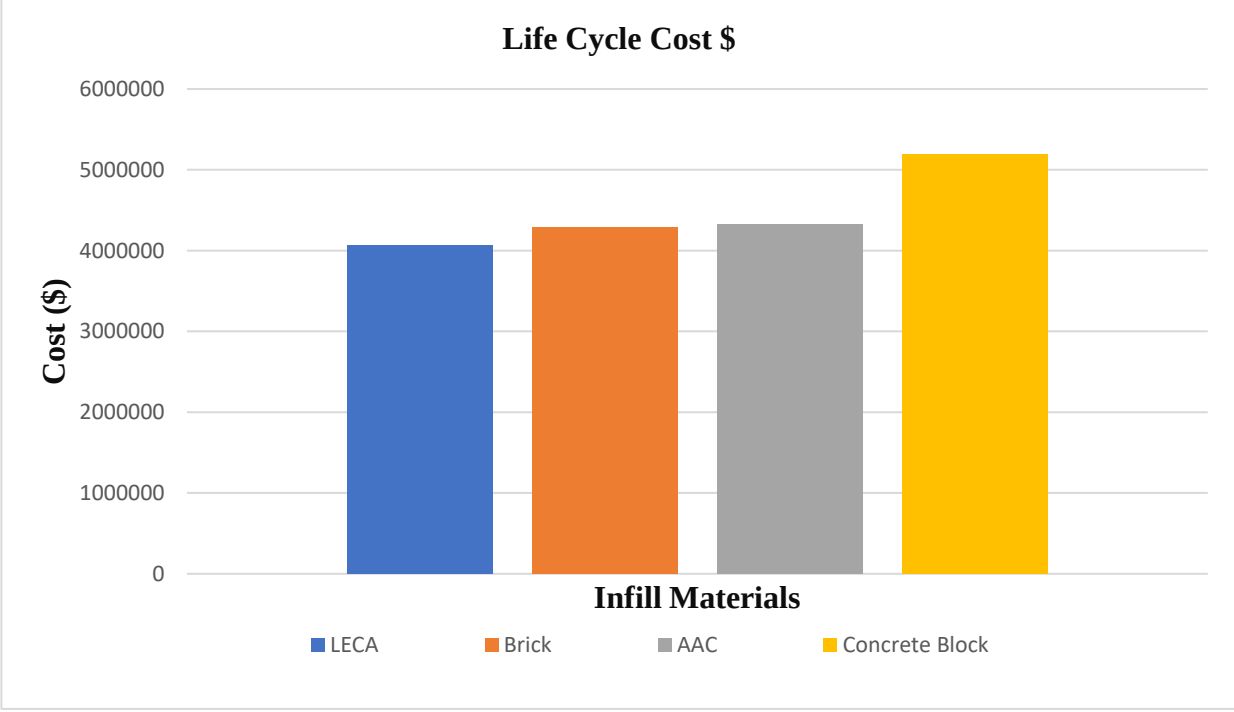

Fig. 50. Life cycle cost comparison of selected infill materials.

ItsThe importance of performing LCCA studies is undeniable in case of developing countries where projects have limited financial resources. Moreover, performing LCCA during the conceptual stage of a project can be the decisive factor in choosing economic or uneconomic design options for the project. Thus, LCCA is a great prospect that has to be employed while planning a project to make it as economically sound as possible, especially in developing countries.

8.3.2 Life Cycle Assessment

This study used the BIM-based tool called "One Click LCA®" to conduct LCA which includes the calculation of Carbon emission, Acidification potential and Eutrophication potential. The infill materials used in our models were traced to the library of One Click LCA ® as shown by **Table 24**, and detailed analysis was performed for each of them according to the Leadership in Energy and Environmental Design (LEED) standards embedded into the One Click LCA's inventory.

Table 24.

Materials Traced in the Material library of One Click LCA. (EPD Numbers).

Materials	**One Click LCA library References**
LECA	Lightweight concrete block, with expanded clay aggregate, 650 kg/m3
AAC	Aerated concrete block, 600 kg/m^3
Brick	Clay bricks, red, 1800 kg/m^3
Concrete Blocks	Concrete masonry brick, 2000 kg/m^3

LECA= EPD HUB-146 [43], AAC= [44], Brick= [45], Concrete Masonry Block= [46]

While transferring materials from Revit's material library to One Click LCA's material library, minor variations such as difference in the density of materials between the material libraries of the two platforms must be incorporated into the material properties as there are still gaps to fill in terms of creating identical shared material libraries between the two platforms. Therefore, minor changes have to be incorporated in terms of material properties to project the behavior of infill

materials as precisely as possible. However, One Click LCA ® still remains a useful tool for swift LCA analysis and is highly advantageous over manual procedures as shown by **Fig. 51**.

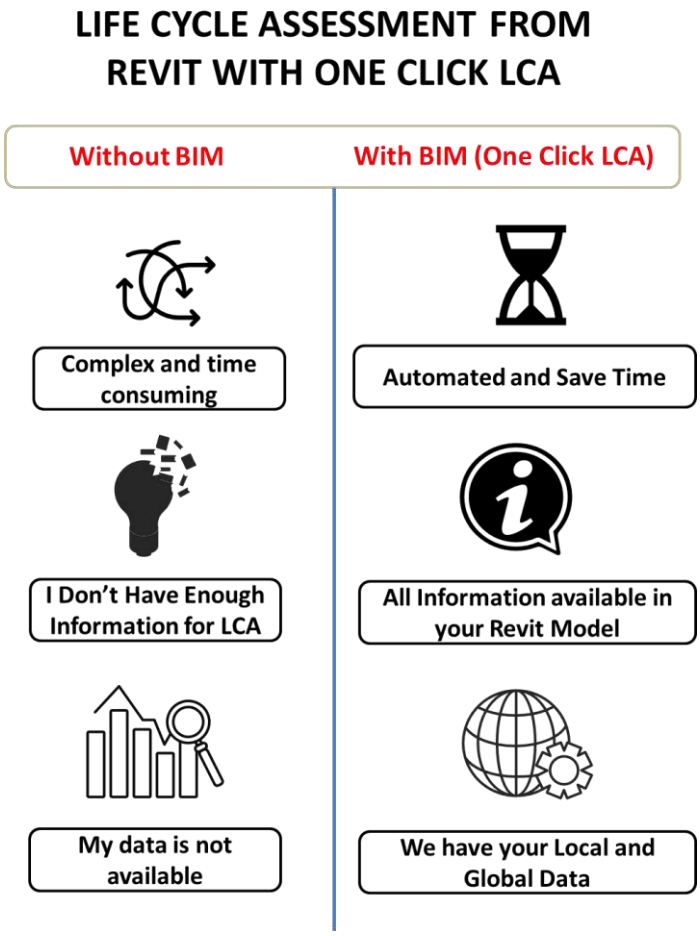

Fig. 51. Advantages of using one click LCA for environmental impact study.

8.3.2.1 Carbon Emissions

In this study, One Click LCA® was used to quantify the carbon emission for the lifecycle of the building. One Click LCA® was used to perform analysis for the building's entire lifecycle, i.e., 60 years. It calculated the carbon emissions based on the type and quantity of material used in construction. The results obtained for each material after analysis are visualized in **Fig. 52.** which shows the CO_2 emission for each infill material that occurs over the entire lifecycle of the material.

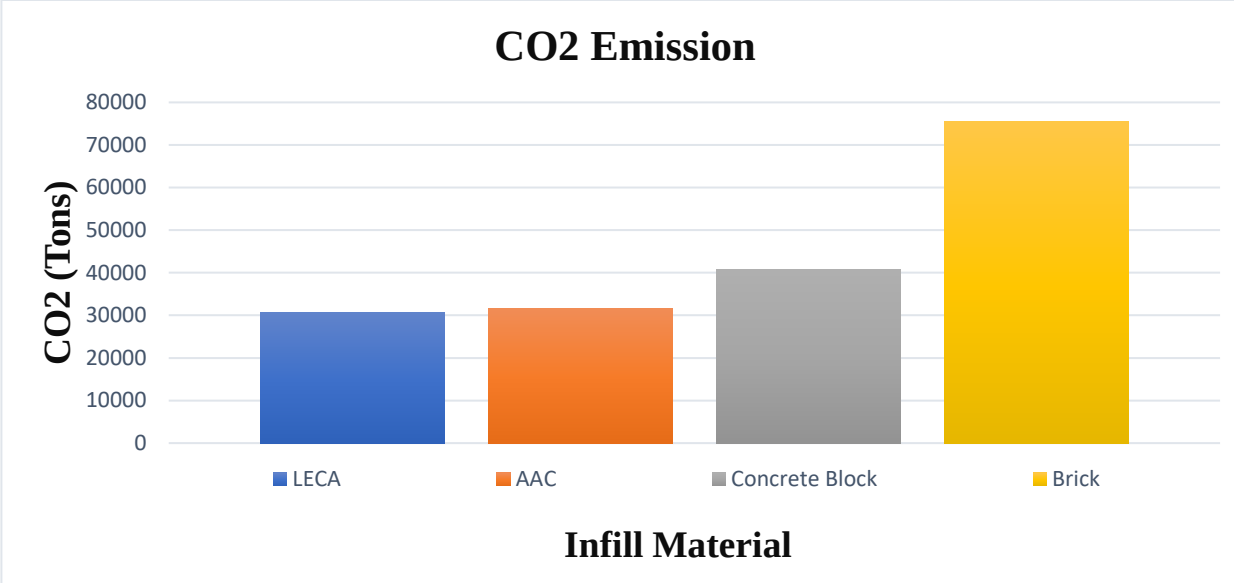

Fig. 52. Comparison of CO_2 emission of materials.

It is evident from Fig. 52 that the material with the least Carbon emission and, thus, the least global warming potential is LECA. This is mainly due to the manufacturing products of LECA which constitute of expanded clay and fly ash. These materials have low carbon footprint unlike concrete based materials which have high carbon emission due to excessive hydration reactions. The production of bricks is highly carbon intensive due to burning of a lot of fossil fuels in their production.

8.3.2.2 Acidification

One Click LCA® was also used to quantify the acidification potential for the materials under study. It accurately indicates how much a material contributes to increasing the pH of the soil, water and atmosphere etc. One Click LCA® measures acidification potential as a function of CO_2 emission and its equivalent contributing compounds. The procedure is the same as that for CO_2 emission calculation. One Click LCA® was provided with the quantity of respective materials to be used in the project. Then the materials were transferred from Revit's material library to the material library of One Click LCA®. After providing these inputs to One Click LCA®, the analysis was conducted. The results for acidification for each infill material are presented in **Fig. 53**. This figure shows the acidification induced by each infill material by virtue of lowering the pH of the environment.

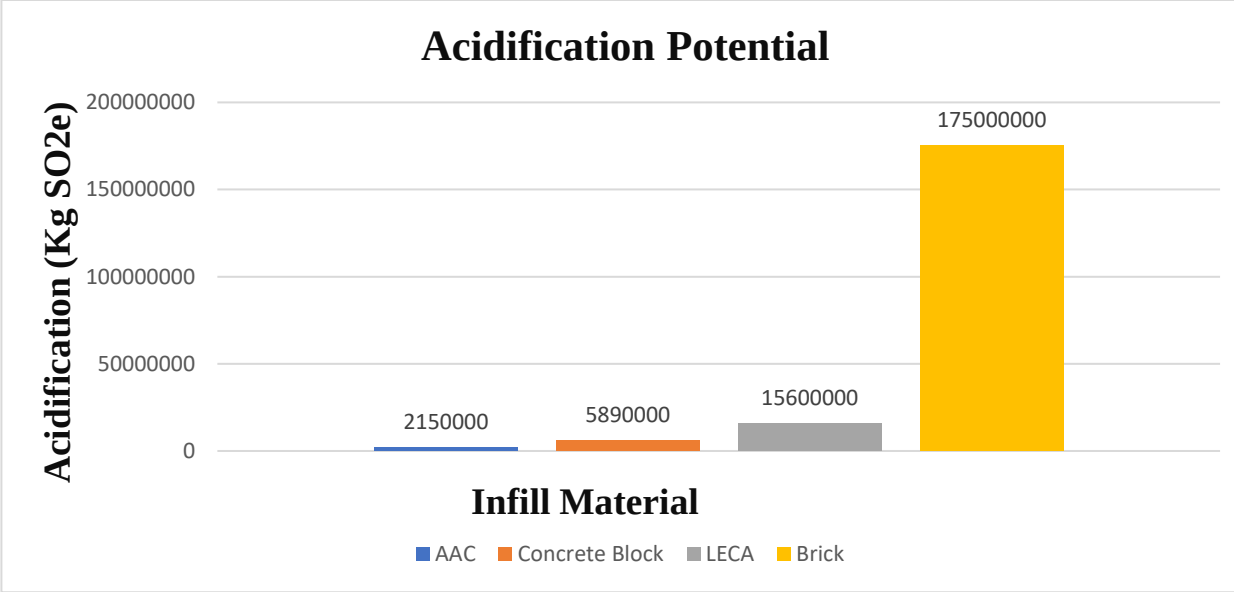

Fig. 53. Comparison of acidification potential of materials.

In terms of acidification potential, AAC blocks are the best performer as they have lowest contribution to acidification. The low acidification potential of AAC blocks is a result of their high pH value and the chemical composition of the material, which makes them resistant to acid attacks.

8.3.2.3 Eutrophication

Eutrophication is also one of the outputs of One Click LCA®. The same procedure was performed to calculate eutrophication as acidification. The quantity of material was fed from Revit into One Click LCA® and analysis was performed for the materials under study. The analysis result given by One Click LCA® is a function of Phosphate (PO_4) emission and other contributing compounds. The results of the eutrophication analysis for the current study are presented in **Fig. 54**.

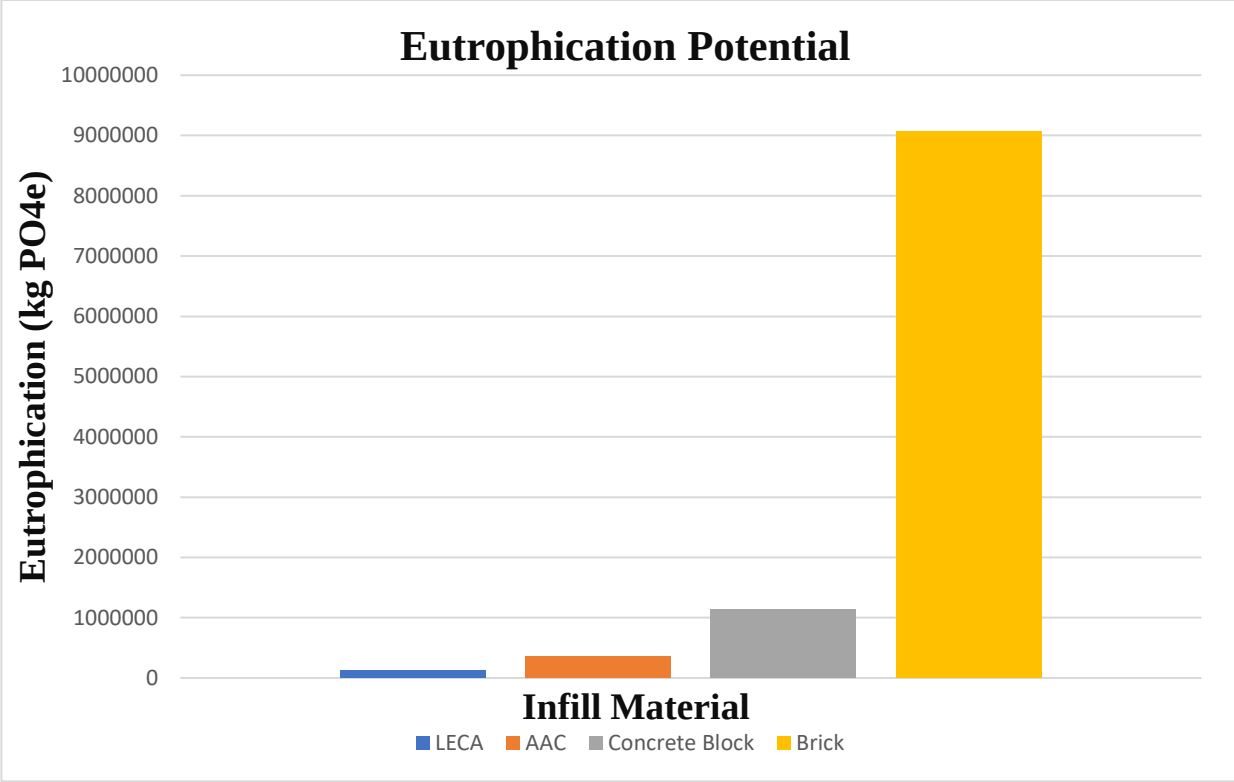

Fig. 54. Comparison of eutrophication potential of infill materials.

In terms of eutrophication potential, LECA is the best performer among all materials. LECA is made from clay that is heated to a high temperature, causing it to expand and form lightweight, porous pellets. The production process does not involve the addition of any nutrients, and the final product is chemically stable and does not release significant amounts of nutrients into the environment.

8.3.2.4 Best Option as Per LCA

Many different variables must be considered to decide which material is the best option in terms of LCA. It depends on the situation at hand for each project, and a generic solution cannot be devised for every project. For example, a project located on a coastal region or near a water body like a lake. The factor of acidification becomes very significant, and it must be treated as design criteria for the situation. This is because acidification actively affects water bodies, a major environmental concern besides global warming.

This research paper considers Carbon Emission as the benchmark for judging the best design option. LCA has different indicators that are important. However, of all these indicators, Global Warming potential is the most alarming and is not localized like acidification. Rather it is a global issue arising from and affecting every part of the world. Its implications are also more drastic and dynamic as it contributes to atmospheric warming, melting of ice sheets and Precipitation changes, etc. International treaties aim to reduce carbon emissions to zero by 2030 to prevent the horrifying implications of climate change [47]. Therefore, we chose it as the decisive factor for LCA in this study due to the global nature of the challenge presented by Carbon Emissions. The analysis illustrated that LECA has the lowest carbon emission of all materials, making it the best design option for enabling sustainable and greener buildings. LECA also was the top performer regarding eutrophication. However, in the case of acidification, AAC blocks outperformed all other infill materials, and they would be the preferred design option when constructing a project in a coastal region.

Using the proposed BIM-based conceptual framework in the planning stage could be vital in foreseeing the environmental impact of the materials used in construction so that the decision makers can make better choices to reduce the environmental effects of construction and buildings leading to more sustainable buildings in line with the United Nations' Sustainable Development Goals (UN-SDGs).

8.4. Conclusion

This research paper proposed a conceptual framework to conduct LCAs of different infill materials using BIM. Furthermore, it presents a way of choosing cost- and environment-friendly design options (infill materials).

- The proposed LCCA framework analyses examined the cost-effectiveness of various infill materials over their life cycle. LCCA involved the manufacturing cost, construction cost, operation cost, and demolition cost of the project in this study. As a result, the LCCA of LECA over 60 years is USD 4066108$ which is 5.4% less than Bricks, 6.4% less than AAC blocks and 27% better than Concrete Masonry Blocks. These results illustrate that LECA was the best performer among other contenders mainly due to its energy efficiency and optimum operation costs.

- LCA (environmental) performed for the materials under study aimed to illustrate the performance of materials using carbon emissions, acidification, and eutrophication. The study suggested that LECA was the most environmentally friendly infill material among other options. We choose carbon emissions as the prime indicator of environmental performance because it is a major global concern compared to acidification and eutrophication, which are relatively localized issues. The carbon and emission of equivalent global warming gases for the entire lifecycle of case study projects were 30770 Tones. This is 2.8% less than AAC blocks, 32% less than concrete masonry blocks and 53% less than bricks.

The proposed conceptual framework can help develop a decision-making platform to choose the best design options in terms of infill materials from the perspective of cost and environment. Furthermore, it is a reliable and swift way of assessing the life cycle performance of materials through BIM. The next step in this regard would be to automate these assessments to become faster and more efficient.

8.5 Recommendations, limitations, and future directions:

- To improve the efficacy of this process, an automated version of LCC and LCA integration with BIM must be developed. This will save time consumed during studies and apply LCC and LCA with ease during the conceptual phases of project. As a result, big steps could be taken toward commercializing sustainable buildings worldwide.
- Fragility curves must be developed for novel materials like LECA and AAC so that maintenance costs can be estimated for them due to damages incurred over their lifecycle due to various hazards such as earthquakes etc.

Further studies should be conducted to quantify the results of LCC and LCA for other design options such as building orientation, structural design, HVAC systems, slabs, and floor composition, etc.

As far as the limitations of this study go, A point to be considered regarding the maintenance cost of project is that no research has been conducted on the damage incurred by LECA and AAC blocks because of earthquake, fire and other hazards. These factors are important to cosnsider in LCCA studies as damages to the building acquired due to these factors require repairing which impact the lifetime cost of the buildings. Due to lack of studies, there aren’t any probabilistic

damage curves derived for these novel materials till now. Without these curves, we cannot calculate how much damages will be incurred as a result of different hazards. Consequently, it becomes impossible to accurately determine the repairing and maintenance cost because of having no data about probabilistic damages that might occur. Therefore, due to the lack of research on these non-traditional infill materials (LECA and AAC), their maintenance cost has not been included in our research project scope. However, future researchers should work on developing the probabilistic damage curves for novel materials such as LECA and AAC so that their maintenance cost could be added to further studies regarding their LCCA.

References

[1] D. Bryde, M. Broquetas, and J. M. Volm, "The project benefits of building information modelling (BIM)," *International Journal of Project Management*, vol. 31, no. 7, pp. 971–980, 2013, doi: 10.1016/J.IJPROMAN.2012.12.001.

[2] R. Chahrour *et al.*, "Cost-benefit analysis of BIM-enabled design clash detection and resolution," *Construction Management and Economics*, vol. 39, no. 1, pp. 55–72, 2021, doi: 10.1080/01446193.2020.1802768.

[3] J. Xu and L. Xu, "Affordability and Life-Cycle Costs Analysis," *Integrated System Health Management*, pp. 433–450, Jan. 2017, doi: 10.1016/B978-0-12-812207-5.00009-2.

[4] L. Sun, "LCCA-based design method for asphalt pavement," *Structural Behavior of Asphalt Pavements*, pp. 549–600, Jan. 2016, doi: 10.1016/B978-0-12-849908-5.00008-0.

[5] S. Kubba, "Economics of Green Design," *LEED Practices, Certification, and Accreditation Handbook*, pp. 379–415, Jan. 2010, doi: 10.1016/B978-1-85617-691-0.00010-2.

[6] C. Ingrao, A. Messineo, R. Beltramo, T. Yigitcanlar, and G. Ioppolo, "How can life cycle thinking support sustainability of buildings? Investigating life cycle assessment applications for energy efficiency and environmental performance," *Journal of Cleaner Production*, vol. 201. Elsevier Ltd, pp. 556–569, Nov. 10, 2018. doi: 10.1016/j.jclepro.2018.08.080.

[7] E. Plebankiewicz, K. Zima, and M. Skibniewski, "Analysis of the First Polish BIM-Based Cost Estimation Application," in *Procedia Engineering*, Elsevier Ltd, 2015, pp. 405–414. doi: 10.1016/j.proeng.2015.10.064.

[8] N. A. Adillah Ismail, E. Utiome, R. Owen, and R. Drogemuller, "Exploring Accuracy Factors in Cost Estimating Practice towards Implementing Building Information Modelling (BIM)," in *Proceedings of the 2015 (6th) International Conference on Engineering, Project, and Production Management*, Association of Engineering, Project, and Production Management, Sep. 2015, pp. 364–373. doi: 10.32738/CEPPM.201509.0036.

[9] S. Kumar, "INTEROPERABILITY BETWEEN BUILDING INFORMATION MODELS (BIM) AND ENERGY ANALYSIS PROGRAMS," 2008.

[10] "ESTIMATION OF COST AND DEMOLITION COST OF SMITHA MEMORIAL CANCER, THODUPUZHA CENTER USING BIM TECHNOLOGY 1 Irin Ann Isac, 2 Ittoop R Ancheril, 3 Rohith Jerry, 4 Rohit Graduates in Civil Engineering," 2022. [Online]. Available: www.ijcrt.org

[11] D. Kehily and J. Underwood, "Embedding life cycle costing in 5D BIM," 2017. [Online]. Available: http://www.itcon.org/2017/8

[12] C. Jiayu, "Integration of Life Cycle Assessment within Building Information Modeling Environment JIAYU CUI KTH ROYAL INSTITUTE OF TECHNOLOGY SCHOOL OF ARCHITECTURE AND THE BUILT ENVIRONMENT."

[13] M. Najjar, K. Figueiredo, M. Palumbo, and A. Haddad, “Integration of BIM and LCA: Evaluating the environmental impacts of building materials at an early stage of designing a typical office building,” *Journal of Building Engineering*, vol. 14, pp. 115–126, Nov. 2017, doi: 10.1016/j.jobe.2017.10.005.

[14] V. W. Tam, Y. Zhou, C. Illankoon, and K. N. Le, “A critical review on BIM and LCA integration using the ISO 14040 framework,” *Building and Environment*, vol. 213. Elsevier Ltd, Apr. 01, 2022. doi: 10.1016/j.buildenv.2022.108865.

[15] T. D. Mora, E. Bolzonello, C. Cavalliere, and F. Peron, “Key parameters featuring bim-lca integration in buildings: A practical review of the current trends,” *Sustainability (Switzerland)*, vol. 12, no. 17, Sep. 2020, doi: 10.3390/su12177182.

[16] D. M. A. Morsi, W. S. E. Ismaeel, A. Ehab, and A. A. E. Othman, “BIM-based life cycle assessment for different structural system scenarios of a residential building,” *Ain Shams Engineering Journal*, vol. 13, no. 6, Nov. 2022, doi: 10.1016/j.asej.2022.101802.

[17] “Does BIM really save money on capital projects? - Landform Surveys.” https://www.landform-surveys.co.uk/news/thoughts/bim-really-save-money-capital-projects/ (accessed Apr. 15, 2023).

[18] J. Díaz and L. Á. Antön, “Sustainable construction approach through integration of LCA and BIM tools,” in *Computing in Civil and Building Engineering - Proceedings of the 2014 International Conference on Computing in Civil and Building Engineering*, American Society of Civil Engineers (ASCE), 2014, pp. 283–290. doi: 10.1061/9780784413616.036.

[19] Y. M. Rashed, I. A. R. Nosair, K. Nassar, I. A. Mashaly, and M. Ghanem, “A BIM-based life cycle cost (LCC) method to reduce the operation energy costs in buildings,” in *Building Simulation Conference Proceedings*, International Building Performance Simulation Association, 2019, pp. 151–158. doi: 10.26868/25222708.2019.210616.

[20] M. D. Danyluk, M. E. Parish, R. M. Goodrich-Schneider, and R. W. Worobo, “Microbial decontamination of juices,” *Microbial Decontamination in the Food Industry: Novel Methods and Applications*, pp. 163–189, Jan. 2012, doi: 10.1533/9780857095756.1.163.

[21] “Ocean Acidification: Understanding the Threats, and Reducing the Impacts.” https://en.unesco.org/events/ocean-acidification-understanding-threats-and-reducing-impacts (accessed Apr. 15, 2023).

[22] N. O. and A. A. US Department of Commerce, “What is eutrophication?”.

[23] “Nutrients and Eutrophication | U.S. Geological Survey.” https://www.usgs.gov/mission-areas/water-resources/science/nutrients-and-eutrophication (accessed Apr. 15, 2023).

[24] “Global Concrete Block and Brick Manufacturing Market Size By Product Type, By Geographic Scope And Forecast.” https://www.researchandmarkets.com/reports/5440575/global-concrete-block-and-brick-manufacturing (accessed Apr. 15, 2023).

[25] “Lightweight Expanded Clay Aggregate (LECA) Market Latest Research Report 2023-2028, MGR - MarketWatch.” https://www.marketwatch.com/press-release/lightweight-expanded-clay-aggregate-leca-market-latest-research-report-2023-2028-mgr-2023-02-26 (accessed Apr. 15, 2023).

[26] “AAC Blocks And Panels Market Size,Share,Growth forecast 2031.” https://www.alliedmarketresearch.com/aac-blocks-and-panels-market-A31594 (accessed Apr. 15, 2023).

[27] S. M. Mirnezami, A. Hassani, and A. Bayat, “Evaluation of the effect of metallurgical aggregates (steel and copper slag) on the thermal conductivity and mechanical properties of concrete in jointed plain concrete pavements (JPCP),” *Constr Build Mater*, vol. 367, p. 129532, Feb. 2023, doi: 10.1016/J.CONBUILDMAT.2022.129532.

[28] “Expanded Polystyrene (EPS) EPS.”

[29] X. Gu *et al.*, “Effect of hydroxypropyl methyl cellulose (HPMC) as foam stabilizer on the workability and pore structure of iron tailings sand autoclaved aerated concrete,” *Constr Build Mater*, vol. 376, p. 130979, May 2023, doi: 10.1016/J.CONBUILDMAT.2023.130979.

[30] “Specific heat capacity - Designing Buildings.” https://www.designingbuildings.co.uk/wiki/Specific_heat_capacity (accessed Apr. 15, 2023).

[31] “Blockwork - A Short Guide on Block & Blockwork Specification.” https://knowledge.specifiedby.com/blocks-blockwork/ (accessed Apr. 15, 2023).

[32] “Properties – Leca AE.” https://leca.ae/properties/ (accessed Apr. 15, 2023).

[33] “Market Rates of Materials, Labours and Machinery | Finance Department.” https://finance.punjab.gov.pk/mlm (accessed Apr. 16, 2023).

[34] “What Is AAC Block? | AAC block size and Cost | Disadvantages & Advantages.” https://www.perlcon.com/what-is-aac-block/ (accessed Apr. 16, 2023).

[35] “RIBA 2030 Climate Challenge: How can we reduce operational energy demand by at least 75%?” https://www.mesh-energy.com/insights/riba-2030-climate-challenge-how-can-we-reduce-operational-energy-demand-by-at-least-75 (accessed Apr. 16, 2023).

[36] “Robot Challenge Screen.” https://sciencenotes.org/.well-known/captcha/?r=%2Fwhat-is-room-temperature%2F (accessed Apr. 16, 2023).

[37] “Pakistan electricity prices, September 2022 | GlobalPetrolPrices.com.” https://www.globalpetrolprices.com/Pakistan/electricity_prices/ (accessed Apr. 16, 2023).

[38] “Domestic Rates | Sui Southern Gas Company Limited.” https://www.ssgc.com.pk/web/?page_id=103 (accessed Apr. 16, 2023).

[39] C. Hodge, “How Hospitals Use Energy Turning Things Off,” 2010. [Online]. Available: www.energystar.gov/index.cfm?c=evaluate_performance.

[40] “Best Inflation Calculator (2023) - Historical & Future Value By Year.” https://smartasset.com/investing/inflation-calculator#tRm15iBzjL (accessed Apr. 16, 2023).

[41] “Demolition Cost Definition | Law Insider.” https://www.lawinsider.com/dictionary/demolition-cost (accessed Apr. 16, 2023).

[42] “Which Factors Determine the Lifespan of a Building?” https://bciconstruction.us/which-factors-determine-the-lifespan-of-a-building/ (accessed Apr. 16, 2023).

[43] “Environmental Product Declaration created with One Click LCA ENVIRONMENTAL PRODUCT DECLARATION.” [Online]. Available: www.tiileri.fi

[44] “ENVIRONMENTAL PRODUCT DECLARATION.” [Online]. Available: www.lignacite.co.uk

[45] “Environmental Product Declaration.” [Online]. Available: https://bauroc.eu/products/

[46] “ENVIRONMENTAL PRODUCT DECLARATION.”

[47] “The Paris Agreement | UNFCCC.” https://unfccc.int/process-and-meetings/the-paris-agreement (accessed Apr. 16, 2023).

Chapter 9

CONCLUSION & RECOMMENDATIONS

9.1 Conclusion:

The primary focus of this thesis was to develop a cost-effective lightweight concrete using domestic raw materials. The aim was to provide a sustainable solution that can be implemented in the construction industry in Pakistan. The research involved exploring the use of locally available materials for the production of lightweight concrete, while also ensuring that the resulting product met the necessary standards for strength and durability. The intention was to develop a practical solution that can be easily implemented in the construction industry, with the potential to reduce costs and improve sustainability.

- A total of 120 ALECA mixes were designed for producing both structural and non-structural lightweight concrete. The particle density of the ALECA ranged from 0.42 to 1.79 g/cm3, with a single aggregate crushing strength of 1.5 to 25.5 MPa. The water absorption of the ALECA was found to be in the range of 1.3% to 13.4%. The bloating index of the ALECA ranged from 0.82% to 28%, while the loss on ignition was in the range of 4.81% to 25%. These findings are important for identifying the optimal ALECA mix for producing lightweight concrete with desired properties, such as strength, water absorption, and bloating index.
- A novel application based on machine learning was designed to address the challenge of complex lightweight concrete design. The application leverages the power of machine learning algorithms to analyze data and make predictions, allowing for faster and more accurate design decisions. By automating the design process, the application helps to reduce the time and effort required to produce optimal lightweight concrete mixes. This technology has the potential to transform the way lightweight concrete is designed, making it easier and more efficient for engineers and designers to create high-performance lightweight concrete with specific properties.
- The study proposed three highly effective lightweight concrete mixes, each with unique properties. The compressive strength of the mixes ranged from 7 to 14 MPa, while the density ranged from 870 to 1150 kg/m3. The flexural strength of the mixes was found to be between 0.35 and 0.84 MPa, with a water absorption rate of 8% to 10.5%. The combustion performance of all mixes was rated Grade-A, while the thermal conductivity was measured at 0.19 W/m.K.

Additionally, the acoustic performance of the mixes was found to range from 39 to 42 dB. These findings highlight the potential of these lightweight concrete mixes for various construction applications, including lightweight panels, blocks, for non-structural concrete members with low density, and excellent acoustic and thermal insulation properties.

- A cost comparison study was conducted on a selected building using ALECA infill panels versus brick infill. The results showed that using ALECA infill panels reduced overall construction costs by 16% compared to a building constructed with brick infill. Furthermore, BIM-based modeling was performed to evaluate the heating and cooling load demands and environmental performance of the building. The results revealed that the use of ALECA infill panels not only provided a cost-effective solution but also resulted in sustainable environmental performance. The study findings suggest that incorporating ALECA infill panels in building construction can result in significant cost savings and improved sustainability performance.

9.2 Recommendations:

- Investigate the influence of artificial lightweight expanded clay aggregate (ALECA) shape on the mechanical properties of lightweight concrete: Conduct experiments to evaluate the effect of ALECA shape, such as spherical, cylindrical, or irregular, on the mechanical properties of lightweight concrete. This research can help identify the optimal shape of ALECA for producing high-strength lightweight concrete.
- Utilize ALECA for structural lightweight concrete: Explore the potential of ALECA as a structural material for producing lightweight concrete. Investigate the compressive, tensile, and flexural strength of concrete made with ALECA, and compare it with traditional concrete.
- Find alternative bloating agents to increase ALECA bloating: Investigate alternative materials to expand ALECA, such as kerosene, petrol, waste engine oil or other waste materials, to improve the bloating properties of ALECA. This research can help reduce the cost of ALECA production and increase its availability.
- Experimental investigation of in-plan and out-of-plan behavior of ALECA infill panels: Conduct experimental tests to investigate the behavior of ALECA infill panels under in-plan and out-of-plan loading conditions. This research can provide insight into the structural behavior of ALECA infill panels and help optimize their design for different applications.

- Investigate the durability of ALECA infill concrete in different environments: Evaluate the durability of ALECA infill concrete in different environments, such as wet, dry, or freeze-thaw cycles. This research can help identify the optimal mix design for ALECA infill concrete to ensure its long-term performance in different environments.